THE EUROPEAN
PHYSICAL JOURNAL C

Regular Article - Experimental Physics

Search for heavy resonances decaying into a pair of Z bosons in the $\ell^+\ell^-\ell'^+\ell'^-$ and $\ell^+\ell^-\nu\bar{\nu}$ final states using 139 fb^{-1} of proton–proton collisions at $\sqrt{s} = 13$ TeV with the ATLAS detector

ATLAS Collaboration[*]

CERN, 1211 Geneva 23, Switzerland

Abstract   A search for heavy resonances decaying into a pair of Z bosons leading to $\ell^+\ell^-\ell'^+\ell'^-$ and $\ell^+\ell^-\nu\bar{\nu}$ final states, where ℓ stands for either an electron or a muon, is presented. The search uses proton–proton collision data at a centre-of-mass energy of 13 TeV collected from 2015 to 2018 that corresponds to the integrated luminosity of 139 fb^{-1} recorded by the ATLAS detector during Run 2 of the Large Hadron Collider. Different mass ranges spanning 200 GeV to 2000 GeV for the hypothetical resonances are considered, depending on the final state and model. In the absence of a significant observed excess, the results are interpreted as upper limits on the production cross section of a spin-0 or spin-2 resonance. The upper limits for the spin-0 resonance are translated to exclusion contours in the context of Type-I and Type-II two-Higgs-doublet models, and the limits for the spin-2 resonance are used to constrain the Randall–Sundrum model with an extra dimension giving rise to spin-2 graviton excitations.

Contents

1 Introduction

The discovery of a scalar particle by the ATLAS and CMS collaborations [1,2] in 2012, with measured properties [3–7] consistent with those of the Standard Model (SM) [8–10] Higgs boson, was a major milestone in the understanding of electroweak symmetry breaking [11–13]. One important question is whether the discovered particle is part of an extended scalar sector as postulated by various extensions to the Standard Model such as the two-Higgs-doublet model (2HDM) [14]. These extensions predict additional Higgs bosons, motivating searches in an extended mass range.

This paper reports on two searches for heavy resonances decaying into two SM Z bosons, encompassing the final states produced from the subsequent $ZZ \to \ell^+\ell^-\ell'^+\ell'^-$ and $ZZ \to \ell^+\ell^-\nu\bar{\nu}$ decays, where ℓ stands for either an electron or a muon and ν stands for all three neutrino flavours.

[*] e-mail: atlas.publications@cern.ch

Springer

The data employed were recorded by the ATLAS detector between 2015 and 2018 in proton–proton collisions at $\sqrt{s} = 13$ TeV and correspond to an integrated luminosity of 139 fb^{-1}. The additional Higgs boson (spin-0 resonance), denoted by H throughout this paper, is assumed to be produced mainly via gluon–gluon fusion (ggF) and vector-boson fusion (VBF) processes with the ratio of the two production mechanisms unknown in the absence of a specific model. The results are interpreted separately for the ggF and VBF production modes, with events being classified into ggF- and VBF-enriched categories in both final states, as discussed in Sects. 5 and 6. The searches cover a wide mass range from 200 GeV up to 2000 GeV and look for an excess in the distribution of the the four-lepton invariant mass, $m_{4\ell}$, for the $\ell^+\ell^-\ell'^+\ell'^-$ final state, and the transverse mass, m_T, for the $\ell^+\ell^-\nu\bar{\nu}$ final state, as the escaping neutrinos do not allow the full reconstruction of the final state. This mass range is chosen based on the sensitivity of the analysis as determined by the selection criteria and the size of the data sample.

The transverse mass is defined as:

$$m_{\mathrm{T}} \equiv \sqrt{\left[\sqrt{m_Z^2 + \left(p_{\mathrm{T}}^{\ell\ell}\right)^2} + \sqrt{m_Z^2 + \left(E_{\mathrm{T}}^{\mathrm{miss}}\right)^2}\right]^2 - \left|\vec{p_{\mathrm{T}}}^{\ell\ell} + \vec{E}_{\mathrm{T}}^{\mathrm{miss}}\right|^2},$$

where m_Z is the mass of the Z boson [15], $\vec{p_{\mathrm{T}}}^{\ell\ell}$ and $\vec{E}_{\mathrm{T}}^{\mathrm{miss}}$ are the transverse momentum of the lepton pair and the missing transverse momentum with magnitudes of $p_{\mathrm{T}}^{\ell\ell}$ and $E_{\mathrm{T}}^{\mathrm{miss}}$, respectively. In the absence of such an excess, limits on the production rate of different signal hypotheses are obtained from a simultaneous likelihood fit in the two final states. The hypothesis of a heavy Higgs boson in the narrow-width approximation (NWA) is studied. The upper limits on the production rate of a heavy Higgs boson are also translated into exclusion contours in the context of the two-Higgs-doublet model. As several theoretical models favour non-negligible natural widths, large-width assumption (LWA) models [14], assuming widths of 1%, 5%, 10% and 15% of the resonance mass, are examined only for ggF production, which dominates in many scenarios over the next-largest contribution (VBF) in the search range. Results are also interpreted assuming the bulk Randall–Sundrum (RS) model [16,17] with a warped extra dimension giving rise to a spin-2 Kaluza–Klein (KK) excitation of the graviton G_{KK}.

The main improvements relative to the previous search [18] are the following: (i) full LHC Run 2 integrated luminosity is used; (ii) both analyses profit from improved lepton reconstruction and isolation selection to mitigate the impact of additional pp interactions in the same or neighbouring bunch crossing (pile-up); (iii) the reconstruction of jets uses a particle-flow algorithm which combines measurements from the tracker and the calorimeter; (iv) the normalisation of the SM ZZ background is derived from data

rather than being estimated from SM predictions; (v) event classification targeting different production processes is optimised using machine learning (ML) algorithms in the case of $ZZ \to \ell^+\ell^-\ell'^+\ell'^-$ final state; (vi) the m_T distribution is used to search for signals in the VBF-enriched category in the case of the $ZZ \to \ell^+\ell^-\nu\bar{\nu}$ final state, in addition to the use of m_T in the ggF-enriched category; and (vii) the search range is extended to 2000 GeV in signal mass. The improved analyses reduce the expected upper limit on the production cross section of an additional heavy resonance by up to 40% in comparison with the previous published result scaled to the full Run 2 luminosity. Results of a similar search from a subset of data collected at the LHC with $\sqrt{s} = 13$ TeV have been reported by the CMS Collaboration in Ref. [19].

The paper is organised as follows. A brief description of the ATLAS detector is given in Sect. 2. In Sect. 3 the data and simulated samples are described. The object reconstruction is described in Sect. 4. The analysis strategies for the $\ell^+\ell^-\ell'^+\ell'^-$ and $\ell^+\ell^-\nu\bar{\nu}$ final states are described in Sects. 5 and 6, respectively. Section 7 describes the systematic uncertainties, Sect. 8 the final results, and Sect. 9 the interpretation of these results in the various models.

2 ATLAS detector

The ATLAS experiment is described in detail in Ref. [20]. ATLAS is a multipurpose detector with a forward–backward symmetric cylindrical geometry and a solid-angle[1] coverage of nearly 4π. The inner tracking detector (ID), covering the region $|\eta| < 2.5$, consists of a silicon pixel detector, a silicon microstrip detector, and a transition-radiation tracker. The innermost layer of the pixel detector, the insertable B-layer [21], was installed between Run 1 and Run 2 of the LHC. The inner detector is surrounded by a thin superconducting solenoid providing a 2 T magnetic field, and by a finely segmented lead/liquid-argon (LAr) electromagnetic calorimeter covering the region $|\eta| < 3.2$. A steel/scintillator-tile hadron calorimeter provides coverage in the central region $|\eta| < 1.7$. The endcap and forward regions, covering the pseudo-rapidity range $1.5 < |\eta| < 4.9$, are instrumented with LAr electromagnetic and hadron calorimeters, with steel, copper, or tungsten as the absorber material. A muon spectrometer (MS) system incorporating large superconducting toroidal air-core magnets surrounds the calorimeters. Three layers of precision wire chambers provide muon tracking in the range

---

[1] The ATLAS experiment uses a right-handed coordinate system with its origin at the nominal interaction point (IP) in the centre of the detector and the z-axis along the beam pipe. The x-axis points from the IP to the centre of the LHC ring, and the y-axis points upward. Cylindrical coordinates (r, ϕ) are used in the transverse plane, ϕ being the azimuthal angle around the z-axis. The pseudorapidity is defined in terms of the polar angle θ as $\eta = -\ln\tan(\theta/2)$.

$|\eta| < 2.7$, while dedicated fast chambers are used for triggering in the region $|\eta| < 2.4$. The trigger system, composed of two stages, was upgraded [22] before Run 2. The first stage, implemented with custom hardware, uses information from the calorimeters and muon chambers to select events from the 40 MHz bunch crossings at a maximum rate of 100 kHz. The second stage, called the high-level trigger (HLT), reduces the data acquisition rate to about 1 kHz on average. The HLT is software-based and runs reconstruction algorithms similar to those used in the offline reconstruction.

3 Data and simulation

The proton–proton (pp) collision data used in these searches were collected by the ATLAS detector at a centre-of-mass energy of 13 TeV with a 25 ns bunch-spacing configuration from 2015 to 2018. The data are subjected to quality requirements: if any relevant detector component was not operating correctly during the period in which an event was recorded, the event is rejected. The efficiency for recording good-quality data during Run 2 is 95.6% [23].

Simulated events are used to determine the signal acceptance and some of the background contributions. The events produced by each Monte Carlo (MC) event generator were processed through the ATLAS detector simulation [24] within the GEANT4 framework [25]. Additional inelastic pp interactions were overlaid on the simulated signal and background events. The MC event generator used for pile-up is PYTHIA 8.186 [26] with the A2 set of tuned parameters [27] and the MSTW2008LO [28] parton distribution function (PDF) set. The simulated events are weighted to reproduce the observed distribution of the mean number of interactions per bunch crossing in data (pile-up reweighting).

Heavy spin-0 resonance production was simulated using the POWHEG- BOX v2 [29] MC event generator. The gluon–gluon fusion and vector-boson fusion production modes were simulated separately, with matrix elements calculated to next-to-leading-order (NLO) accuracy in quantum chromodynamics (QCD). POWHEG- BOX was interfaced to PYTHIA 8.212 [30] for parton showering and hadronisation with the AZNLO set of tuned parameters [31], and for decaying the Higgs boson into the $H \rightarrow ZZ \rightarrow \ell^+\ell^-\ell'^+\ell'^-$ or $H \rightarrow ZZ \rightarrow \ell^+\ell^-\nu\bar{\nu}$ final states. The event generator was interfaced to the EVTGEN v1.2.0 program [32] for the simulation of bottom and charm hadron decays. The leading-order (LO) CT10 PDF set [33] was used for the hard-scattering process. Events from ggF and VBF production were generated in the resonance mass range of 300–2000 GeV in the NWA, using a step size of 100 GeV up to 1000 GeV and 200 GeV above. For the $\ell^+\ell^-\ell'^+\ell'^-$ final state, due to the sensitivity of the analysis at lower masses, events were also generated for $m_H = 200$ GeV. In addition, events from ggF heavy Higgs

production with a width of 15% of the Higgs boson mass m_H were generated at NLO accuracy in QCD with MADGRAPH5_aMC@NLO v2.3.2 [34], which was interfaced to PYTHIA 8.210 for parton showering and hadronisation with the A14 set of tuned parameters (A14 tune) [35], and for decaying the Higgs boson into the two leptonic final states. The properties of bottom and charm hadron decays were simulated by EVTGEN v1.2.0. Events were generated in the resonance mass range of 400–2000 GeV using a step size of 100 (200) GeV up to (above) 1000 GeV. Similarly, events with a width of 5% or 10% of $m_H = 900$ GeV were generated for validating the analytic parametrisation of the $m_{4\ell}$ distribution used in the $\ell^+\ell^-\ell'^+\ell'^-$ final state as described in Sect. 5.3. For the $\ell^+\ell^-\nu\bar{\nu}$ final state, a reweighting procedure as described in Sect. 6.3 is used on fully simulated events to obtain the reconstructed m_T distribution at any value of mass and width tested.

Spin-2 Kaluza–Klein gravitons from the bulk Randall–Sundrum model [17,36] were generated with MADGRAPH5_aMC@NLO at LO accuracy in QCD with the NNPDF2.3 LO PDF set with $\alpha_s = 0.130$ [37], which is then interfaced to PYTHIA 8.210 for parton showering and hadronisation with the A14 tune and for decaying the heavy ZZ resonance into the two leptonic final states. The properties of bottom and charm hadron decays were simulated by EVTGEN v1.2.0. The dimensionless coupling $k/\overline{M}_{Pl}$, where $\overline{M}_{Pl} = M_{Pl}/\sqrt{8\pi}$ is the reduced Planck scale and k is the curvature scale of the extra dimension, is set to 1. The width of the resonance is correlated with the coupling $k/\overline{M}_{Pl}$ and in this configuration it is around $\sim 6\%$ of its mass. Mass points between 600 GeV and 2 TeV with 200 GeV spacing were generated for both final states.

The $q\bar{q} \rightarrow ZZ$ background was simulated by the SHERPA v2.2.2 [38] generator, in which the NNPDF3.0 NNLO PDF set [37] was used for the hard-scattering process, achieving NLO accuracy in the matrix-element calculation for 0- and 1-jet final states and LO accuracy for 2- and 3-jet final states with the COMIX [39] and OPENLOOPS [40–42] matrix-element generators. The merging with the SHERPA parton shower [43] was performed using the MEPS@NLO prescription [44]. NLO electroweak (EW) corrections were applied as a function of $m_{4\ell}$ for the $\ell^+\ell^-\ell'^+\ell'^-$ final state [45,46], and as a function of the transverse momentum of the Z boson that decays into two neutrinos for the $\ell^+\ell^-\nu\bar{\nu}$ final state [40,47–50]. The EW production of a ZZ pair and two additional jets via vector-boson scattering up to $O(\alpha_{EW}^6)$ was generated using SHERPA v2.2.2 for both the $\ell^+\ell^-\ell'^+\ell'^-$ and $\ell^+\ell^-\nu\bar{\nu}$ final states, where the process $ZZZ \rightarrow 4\ell qq$ is also taken into account. In addition, the WZ diboson events from both QCD and EW production, with the subsequent leptonic decays of both the W and Z bosons, were simulated by SHERPA with a similar set-up. The WZ events with Z boson

decaying leptonically and W boson decaying hadronically were modelled with SHERPA v2.2.1.

The $gg \rightarrow ZZ$ process was modelled by SHERPA v2.2.2 at LO accuracy in QCD for both final states, including the off-shell SM h boson contribution and the interference between the h and ZZ processes. The higher-order correction factor accounting for up to NLO accuracy in QCD for the $gg \rightarrow ZZ$ continuum production was calculated for massless quark loops [51–53] in the heavy-top-quark approximation [54], including the $gg \rightarrow h^* \rightarrow ZZ$ process [55]. Based on these studies, a constant factor of 1.7 is used, and a relative uncertainty of 60% is assigned to the normalisation in both searches.

For the $\ell^+\ell^-\nu\bar{\nu}$ final state, the contribution from WW production was removed in the SHERPA simulation of the $q\bar{q} \rightarrow ZZ$ and $gg \rightarrow ZZ$ processes by requiring the charged leptons and the neutrinos to have different lepton flavours. The $q\bar{q} \rightarrow WW$ and $gg \rightarrow WW$ processes were then modelled with POWHEG- BOX v2 and SHERPA v2.2.2, respectively. The interference between WW and ZZ production is expected to be negligible [48] and is therefore not considered.

Events containing a single Z boson with associated jets were simulated using the SHERPA v2.2.1 event generator. Matrix elements were calculated for up to two partons at NLO and four partons at LO using the COMIX and OPENLOOPS matrix-element generators and merged with the SHERPA parton shower using the MEPS@NLO prescription. The NNPDF3.0 NNLO PDF set was used in conjunction with dedicated parton-shower tuning developed by the SHERPA authors. The $Z +$ jets events are normalised using the NNLO cross sections [56].

The triboson backgrounds ZZZ, WZZ, and WWZ with fully leptonic decays and at least four prompt charged leptons were modelled using SHERPA v2.2.2 with LO accuracy of the QCD calculations and the CT10 PDF set. The simulation of $t\bar{t} + V$ production ($V = W$ or Z) with both top quarks decaying semileptonically and the vector boson decaying inclusively was performed with MADGRAPH5_aMC@NLO interfaced to PYTHIA 8.210 for parton showering and hadronisation with the A14 tune and to EVTGEN v1.2.0 for the simulation of bottom and charm hadron decays. The total cross section is normalised to the prediction of Ref. [57], which includes the two dominant terms at both LO and NLO in a mixed perturbative expansion in the QCD and EW couplings. The $t\bar{t}$ background, as well as single-top and Wt production, were modelled using POWHEG- BOX v2 interfaced to PYTHIA 8.230 with the A14 tune and to EVTGEN v1.6.0 for the simulation of bottom and charm hadron decays.

In order to study the interference treatment for the LWA case, samples containing the $gg \rightarrow ZZ$ continuum background (B) as well as its interference (I) with a hypothetical heavy Higgs signal (S) were used and are referred to as SBI

samples hereafter. In the $\ell^+\ell^-\ell'^+\ell'^-$ final state the MCFM NLO event generator [58], interfaced to PYTHIA 8.212, was used to produce SBI samples where the width of the heavy scalar is set to 15% of its mass, for masses of 200, 300, 400, 500, 600, 800, 1000, 1200, and 1400 GeV. Background-only samples were also generated with the MCFM event generator, and are used to extract the signal-plus-interference term (SI) by subtracting them from the aforementioned SBI samples. For the $\ell^+\ell^-\nu\bar{\nu}$ final state, the SBI samples were generated with the GG2VV event generator [59,60]. The samples include signal events with a scalar mass of 400, 700, 900, 1200, and 1500 GeV.

4 Event reconstruction

Electron reconstruction uses a dynamic, topological calorimeter-cell clustering-based approach which allows improved measurement of the electron energy, particularly in situations where an electron radiates a bremsstrahlung photon; details can be found in Ref. [61]. Electron candidates are clusters of energy deposits in the calorimeter associated with ID tracks, where the final track–cluster matching is performed after the tracks have been fitted with a Gaussian-sum filter (GSF) [62] to account for bremsstrahlung energy losses. The electron's transverse momentum is computed from the cluster energy and the track direction at the interaction point. Background rejection relies on the longitudinal and transverse shapes of the electromagnetic showers in the calorimeters, track–cluster matching, and properties of tracks in the ID. All of this information, except for that related to track hits, is combined into a likelihood discriminant. The selection combines the likelihood with the number of track hits and defines several working points (WP). Selected electrons have $p_T > 4.5$ GeV and $|\eta| < 2.47$. The $\ell^+\ell^-\ell'^+\ell'^-$ analysis uses a 'loose' WP, with an efficiency of at least 90% for electrons with $p_T > 30$ GeV [63]. The 'medium' WP (with an efficiency about 85% for electrons with $p_T > 30$ GeV) is adopted to select candidate electrons in the $\ell^+\ell^-\nu\bar{\nu}$ analysis.

Muons are formed from tracks reconstructed in the ID and MS, and their identification is primarily based on the presence of the track or track segment in the MS [64]. If a complete track is present in both the ID and the MS, a combined muon track is formed by a global fit using the hit information from both the ID and MS detectors (combined muon); otherwise the momentum is measured using the ID, and the MS track segment serves as identification (segment-tagged muon). The segment-tagged muon is limited to the centre of the barrel region ($|\eta| < 0.1$) which has reduced MS geometrical coverage. Furthermore, in this central region an ID track with $p_T > 15$ GeV is identified as a muon if its calorimetric energy deposition is consistent with a minimum-ionising particle (calorimeter-tagged muon). In

the forward region ($2.5 < |\eta| < 2.7$) with limited or no ID coverage, the MS track formed out of three MS layers is either used alone (stand-alone muon) or combined with silicon-detector hits, if found in the forward ID (combined muon). The ID tracks associated with the muons are required to have at least a minimum number of associated hits in each of the ID subdetectors to ensure good track reconstruction. The minimum p_T for muon candidates is 5 GeV, while the maximum $|\eta|$ is 2.7. A 'loose' muon identification WP, which uses all muon types, is adopted by the $\ell^+\ell^-\ell'^+\ell'^-$ analysis. This criterion has an efficiency of at least 98% [64] for isolated muons with $p_T = 5$ GeV and rises to 99.5% at higher p_T. For the $\ell^+\ell^-\nu\bar{\nu}$ analysis a 'medium' WP is used, which only includes combined muons and has an efficiency of 98%.

The reconstruction of jets uses a particle-flow algorithm [65] which combines measurements from both the tracker and the calorimeter. The energy deposited in the calorimeter by all charged particles is removed, and the jet reconstruction is performed on an ensemble of 'particle-flow objects' consisting of the remaining calorimeter energy and tracks which are matched to the hard interaction. This improves the accuracy of the charged-hadron measurement, while retaining the calorimeter measurements of neutral-particle energies. Compared to only using topological clusters [66], jets reconstructed with the particle-flow algorithm with p_T of about 30 GeV have approximately 10% better transverse momentum resolution. The two different algorithms have similar resolutions for p_T above 100 GeV. Particle-flow jets are reconstructed using the anti-k_t algorithm [67] with a radius parameter $R = 0.4$. The jet four-momentum is corrected for the calorimeter's non-compensating response, signal losses due to noise threshold effects, energy lost in non-instrumented regions, and contributions from pile-up [68]. The jets used are required to satisfy $p_T > 30$ GeV and $|\eta| < 4.5$. Jets from pile-up with $|\eta| < 2.5$ are suppressed using a jet-vertex-tagger multivariate discriminant [69,70].

Jets containing b-hadrons, referred to as b-jets, are identified by the long lifetime, high mass, and decay multiplicity of b-hadrons, as well as the hard b-quark fragmentation function. The $\ell^+\ell^-\nu\bar{\nu}$ analysis identifies b-jets of $p_T > 20$ GeV and $|\eta| < 2.5$ using an algorithm that achieves an identification efficiency of about 85% in simulated $t\bar{t}$ events, with a rejection factor for light-flavour jets of about 30 [71].

Selected events are required to have at least one vertex having at least two associated tracks with $p_T > 500$ MeV, and the primary vertex is chosen to be the vertex reconstructed with the largest $\sum p_T^2$ of its associated tracks. As lepton and jet candidates can be reconstructed from the same detector information, a procedure to resolve overlap ambiguities is applied. In the $\ell^+\ell^-\ell'^+\ell'^-$ case, the overlap ambiguities are resolved as follows. If two electrons have overlapping energy deposits, the electron with the higher p_T is retained. If a reconstructed electron and muon share the same ID track,

the muon is rejected if it is calorimeter-tagged; otherwise the electron is rejected. Reconstructed jets geometrically overlapping in a cone of size $\Delta R = 0.2$ with electrons or muons are also removed. The overlap removal in the $\ell^+\ell^-\nu\bar{\nu}$ case is similar to that in the $\ell^+\ell^-\ell'^+\ell'^-$ case, except for an additional criterion that removes any leptons close to the remaining jets with $0.2 < \Delta R < 0.4$. This additional criterion is not imposed in the $\ell^+\ell^-\ell'^+\ell'^-$ case due to the cleaner environment of this final state and in order to maximise the signal efficiency.

The missing transverse momentum $\vec{E}_T^{\text{miss}}$, which accounts for the imbalance of visible momenta in the plane transverse to the beam axis, is computed as the negative vector sum of the transverse momenta of all identified electrons, muons and jets, as well as a 'soft term', accounting for unclassified soft tracks and energy clusters in the calorimeters [72]. This analysis uses a track-based soft term, which is built by combining the information provided by the ID and the calorimeter, in order to minimise the effect of pile-up, which degrades the E_T^{miss} resolution.

5 Analysis of $\ell^+\ell^-\ell'^+\ell'^-$ final state

5.1 Event selection and categorisation

In Sect. 5.1.1 the four-lepton event selection is described. After this selection, events are further split into several categories, in order to probe different signal production modes, such as VBF production and ggF production. To enhance the search sensitivity to the NWA signals, multivariate classifiers are optimised for the event categorisation as described in Sect. 5.1.2. In order to also obtain results that are more model-independent (since the training of the multivariate classifiers is usually based on a specific signal model), a cut-based event categorisation that enhances the sensitivity in the VBF production mode is also considered and is described in Sect. 5.1.3.

In the search for LWA signals, due to the complexity of modelling the categorisation of the interference between heavy Higgs boson and SM Higgs boson processes, only the ggF-enriched categories of the cut-based analysis (CBA) are used. The same strategy is adopted in the search for a Kaluza–Klein graviton excitation.

5.1.1 Common event selection

Four-lepton events are selected and initially classified according to the lepton flavours: 4μ, $2e2\mu$, $4e$, called 'channels' hereafter. They are selected using a combination of single-lepton, dilepton and trilepton triggers with different transverse momentum thresholds. The single-lepton triggers with the lowest p_T thresholds had tighter requirements than the

high p_T threshold single-lepton triggers and the multilepton triggers. Due to an increasing peak luminosity, these p_T thresholds increased during the data-taking periods [73,74]. For single-muon triggers, the p_T threshold increased from 20 to 26 GeV, while for single-electron triggers, the p_T threshold increased from 24 to 26 GeV. The overall trigger efficiency for signal events passing the final selection requirements is about 98%.

In each channel, four-lepton candidates are formed by selecting a lepton-quadruplet made out of two same-flavour, opposite-sign lepton pairs, selected as described in Sect. 4. Each electron (muon) must satisfy $p_T > 7$ (5) GeV and be measured in the pseudorapidity range of $|\eta| < 2.47$ (2.7). The highest-p_T lepton in the quadruplet must satisfy $p_T > 20$ GeV, and the second (third) lepton in p_T order must satisfy $p_T > 15$ GeV (10 GeV). In the case of muons, at most one calorimeter-tagged, segment-tagged or stand-alone ($2.5 < |\eta| < 2.7$) muon is allowed per quadruplet.

If there is ambiguity in assigning leptons to a pair, only one quadruplet per channel is selected by keeping the quadruplet with the invariant mass of the lepton pairs closest (leading pair) and second closest (subleading pair) to the Z boson mass [15], with invariant masses referred to as m_{12} and m_{34} respectively. In the selected quadruplet, m_{12} must satisfy 50 GeV $< m_{12} < 106$ GeV and m_{34} must satisfy 50 GeV $< m_{34} < 115$ GeV.

Selected quadruplets are required to have their leptons separated from each other by $\Delta R > 0.1$. For 4μ and $4e$ quadruplets, if an opposite-charge same-flavour lepton pair is found with $m_{\ell\ell}$ below 5 GeV, the quadruplet is removed to suppress the contamination from J/ψ mesons. If multiple quadruplets from different channels are selected at this point, only the quadruplet from the channel with the highest signal acceptance is retained, in the order: 4μ, $2e2\mu$, $4e$.

The Z + jets and $t\bar{t}$ background contributions are reduced by imposing impact-parameter requirements as well as track- and calorimeter-based isolation requirements on the leptons. The transverse impact-parameter significance, defined as the impact parameter calculated relative to the measured beam-line position in the transverse plane divided by its uncertainty, $|d_0|/\sigma_{d_0}$, for all muons (electrons), is required to be lower than 3 (5). The track-isolation discriminant is calculated from the tracks with $p_T > 500$ MeV that lie within a cone of $\Delta R = 0.3$ around the muon or electron and that either originate from the primary vertex or have a longitudinal impact parameter z_0 satisfying $|z_0 \sin(\theta)| < 3$ mm if not associated with any vertex. Above a lepton p_T of 33 GeV, the cone size falls linearly with p_T to a minimum cone size of 0.2 at 50 GeV. Similarly, the calorimeter isolation is calculated from the positive-energy topological clusters that are not associated with a lepton track in a cone of $\Delta R = 0.2$ around the muon or electron. The sum of the track isolation and 40% of the calorimeter isolation is required to be less than

16% of the lepton p_T. The calorimeter isolation is corrected for electron shower leakage, pile-up, and underlying-event contributions. Both isolations are corrected for track and topological cluster contributions from the remaining three leptons. The pile-up dependence of this isolation selection is reduced compared with that of the previous search by optimising the criteria used for exclusion of tracks associated with a vertex other than the primary vertex and by the removal of topological clusters associated with tracks.

An additional requirement based on a vertex-reconstruction algorithm, which fits the four-lepton candidates with the constraint that they originate from a common vertex, is applied in order to further reduce the Z + jets and $t\bar{t}$ background contributions. A cut of $\chi^2/\mathrm{ndof} < 6$ for 4μ and < 9 for the other channels is applied, with an efficiency larger than 99% for signal in all channels.

The QED process of radiative photon production in Z boson decays is well modelled by simulation. Some of the final-state-radiation (FSR) photons can be identified in the calorimeter and incorporated into the $\ell^+\ell^-\ell'^+\ell'^-$ analysis. The strategy to include FSR photons into the reconstruction of Z bosons is the same as in Run 1 [75]. It consists of a search for collinear (for muons) and non-collinear FSR photons (for muons and electrons) with only one FSR photon allowed per event. After the FSR correction, the four-momenta of both dilepton pairs are recomputed by means of a Z-mass-constrained kinematic fit [76]. The fit uses a Breit–Wigner Z boson lineshape and a single Gaussian function per lepton to model the momentum response function with the Gaussian width set to the expected resolution for each lepton. The Z-mass constraint is applied to both Z candidates.

Events that pass the common event selection (as described above) which are not yet split according to lepton flavours, form a category which is called 'inclusive' hereafter.

5.1.2 Event categorisation: multivariate analysis

In order to improve the sensitivity in the search for an NWA Higgs boson signal produced either in the VBF or the ggF production mode, two multivariate classifiers, namely a 'VBF classifier' and a 'ggF classifier', are used. These classifiers are built with deep neural networks (DNN) and use a architecture similar to that in Ref. [77], combining a multilayer perceptron (MLP) and one or two recurrent neural networks (rNN) [78]. For both classifiers, the outputs of the MLP and rNN(s) are concatenated and fed into an additional MLP that produces an event score.

The 'VBF classifier' uses two rNNs and an MLP. The two rNNs have as inputs the p_T-ordered transverse momenta and the pseudorapidities of the two leading jets and the transverse momenta and the pseudorapidities of the four leptons in the event. The MLP uses as inputs the invariant mass of the four-lepton system, the invariant mass and the transverse

momentum of the two-leading-jets system, the difference in pseudorapidity between the $\ell^+\ell^-\ell'^+\ell'^-$ system and the leading jet, and the minimum angular separation between the $\ell^+\ell^-$ or $\ell'^+\ell'^-$ pair and a jet.

The 'ggF classifier' uses one rNN and an MLP. The rNN has as inputs the p_{T}-ordered transverse momenta and the pseudorapidities of the four leptons in the event. The MLP uses as inputs the following variables: (1) the four-lepton invariant mass; (2) the transverse momentum and the pseudorapidity of the four-lepton system; (3) the production angle of the leading Z defined in the four-lepton rest frame, $\cos\theta^*$; (4) the angle between the negative final-state lepton and the direction of flight of leading (subleading) Z in the Z rest frame, $\cos\theta_1$ ($\cos\theta_2$); (5) the angle between the decay planes of the four final-state leptons expressed in the four-lepton rest frame, Φ; and (6) the transverse momentum and the pseudorapidity of the leading jet.

The two classifiers are trained separately using the above-listed discriminating variables on all simulated NWA signal events from their corresponding production mode, and the SM ZZ background events. The 'VBF classifier' is trained on events with at least two jets while the 'ggF classifier' is trained on events with fewer than two jets. In order to represent the relative importance of the signal and background events, weights that scale the events to the same luminosity according to their production cross sections are used in the training. Furthermore, in order to achieve good discriminating power of the classifiers over a large range of signal mass hypotheses, the signal events are reweighted such that their overall four-lepton invariant mass spectrum matches that of the SM background events. As a result of this reweighting method the classifiers do not produce a bias towards a specific mass point. Extensive checks are performed to ensure such treatment does not create a local excess of background events that would fake a signal. Figure 1 shows the 'ggF classifier' and 'VBF classifier' output for the data, the SM background and an example signal with $m_H = 600$ GeV.

After the common event selection, as described in Sect. 5.1.1, events with at least two jets ($n_{\mathrm{jets}} \geq 2$) and a 'VBF classifier' score value greater than 0.8 form the VBF-MVA-enriched category. Events failing to enter the VBF-MVA-enriched category are classified into the ggF-MVA-high category if the 'ggF classifier' score value is greater than 0.5; these events are further split into three distinct categories according to the lepton flavour of the $\ell^+\ell^-\ell'^+\ell'^-$ system. Finally, events failing both classifiers form the ggF-low category. Overall, five mutually exclusive categories are formed: VBF-MVA-enriched, ggF-MVA-high-4μ, ggF-MVA-high-$2e2\mu$, ggF-MVA-high-$4e$, ggF-MVA-low. This categorisation is used in the search for a heavy scalar with the NWA and in the search in the context of a CP-conserving 2HDM.

The signal acceptance, defined as the ratio of the number of reconstructed events after all selection requirements to the total number of simulated events, is found to be between 30% (15%) and 46% (22%) in the ggF (VBF)-enriched category for the ggF (VBF) production mode depending on the signal mass hypothesis.

5.1.3 Event categorisation: cut-based analysis

As in the previous publication [18], a cut-based analysis is also performed to probe the sensitivity in the VBF production mode. If an event has two or more jets with p_{T} greater than 30 GeV, with the two leading jets being well separated in η, $\Delta\eta_{\mathrm{jj}} > 3.3$, and having an invariant mass $m_{\mathrm{jj}} > 400$ GeV, this event is classified into the VBF-enriched category; otherwise the event is classified into one of the ggF-enriched categories further split according to the lepton flavour of the $\ell^+\ell^-\ell'^+\ell'^-$ system. Four distinct categories are formed, namely VBF-CBA-enriched, ggF-CBA-4μ, ggF-CBA-$2e2\mu$, and ggF-CBA-$4e$. The ggF-enriched categories are used in the search for a heavy large-width scalar and the search for a Kaluza–Klein graviton excitation. In addition, as for the multivariate-based analysis, such categorisation is used in the search for a heavy scalar with the NWA and the corresponding results are described in the Appendix.

5.2 Background estimation

The main background source in the $H \to ZZ \to \ell^+\ell^-\ell'^+\ell'^-$ final state is non-resonant SM ZZ production, accounting for 97% of the total background events in the inclusive category. It arises from quark–antiquark annihilation $q\bar{q} \to ZZ$ (86%), gluon-initiated production $gg \to ZZ$ (10%), and a small contribution from EW vector-boson scattering (1%). The last of these is more important in the VBF-enriched category using the DNN-based categorisation, where it accounts for 20% of the total background events. While in the previous publication [18] the SM ZZ background was exclusively estimated from simulation for both the shape and the normalisation, in this analysis its normalisation is derived from the data in the likelihood fit used in the statistical treatment of the data as explained in Sect. 8. The shapes of the $q\bar{q} \to ZZ$ and $gg \to ZZ$ invariant mass distributions are parameterised with analytic functions as described in Sect. 5.3. Additional background comes from the Z + jets and $t\bar{t}$ processes. These contribute to the total background yields at the percent level and decrease more rapidly than the non-resonant ZZ contribution as a function of $m_{4\ell}$. These backgrounds are estimated using data where possible, following slightly different approaches for final states with a dimuon ($\ell\ell + \mu\mu$) or a dielectron ($\ell\ell + ee$) subleading pair [79,80].

The $\ell\ell + \mu\mu$ non-ZZ background comprises mostly $t\bar{t}$ and Z + jets events, where in the latter case the muons arise mostly from heavy-flavour semileptonic decays and to a lesser extent from π/K in-flight decays. The normalisations of the Z +

(a)

(b)
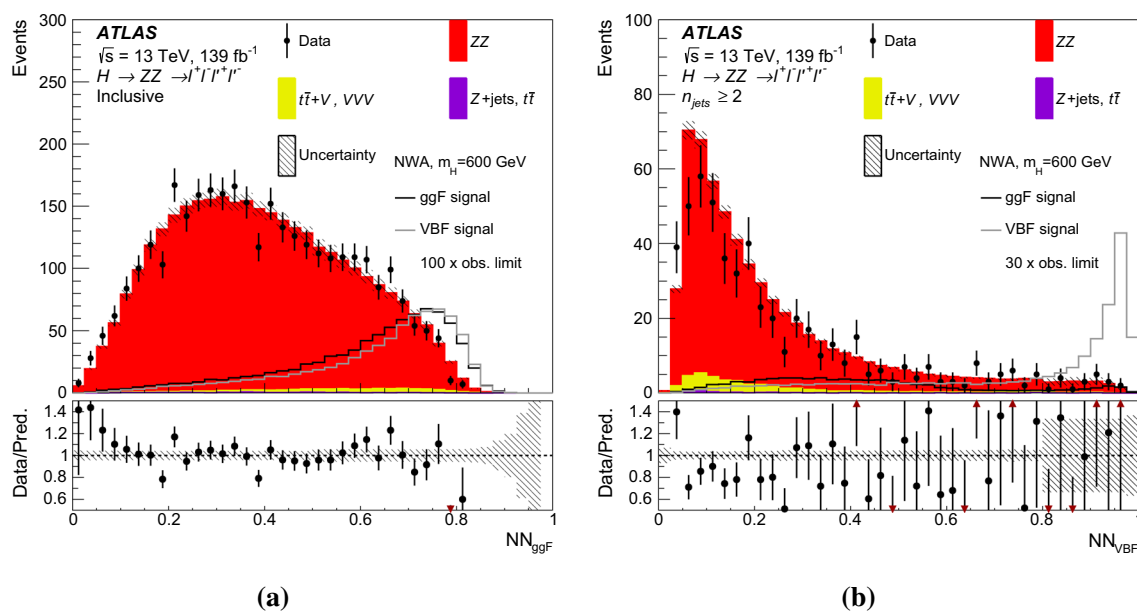
Fig. 1 The output of **a** the 'ggF classifier' (NN_{ggF}) and **b** the 'VBF classifier' (NN_{VBF}) for the events passing the common event selections for the data, the SM background and NWA signal events with a mass of 600 GeV. For **b** the 'VBF classifier' output, an additional requirement of at least two jets in the event, is applied. The signal cross section is set to 100 times the observed limit for the 'ggF classifier' and 30 times the observed limit for the 'VBF classifier'. The ZZ background is scaled by the normalisation factors shown in Table 2. The lower panels show the ratio of data to prediction. Only statistical and experimental systematic uncertainties are included

jets and $t\bar{t}$ backgrounds are determined by fitting the invariant mass of the leading lepton pair in dedicated data control regions. The control regions are formed by relaxing the χ^2 requirement on the four-lepton vertex fit, and by inverting and relaxing isolation and/or impact-parameter requirements on the subleading muon pair. An additional control region ($e\mu\mu\mu$) is used to improve the $t\bar{t}$ background estimate. The contribution of transfer factors, defined as the number of events in the signal region divided by the number of events in the control region, are obtained separately for $t\bar{t}$ and $Z +$ jets using simulated events to extrapolate the yields from the control regions to the signal regions.

The main non-prompt background for the $\ell\ell + ee$ process arises from three sources: light-flavour jets misidentified as electrons; photon conversions; and semileptonic decays of heavy-flavour hadrons. The $\ell\ell + ee$ control-region selection requires the electrons in the subleading lepton pair to have the same charge, and relaxes the identification and isolation requirements on the electron candidate, denoted X, with the lower transverse momentum. The heavy-flavour background is found to be negligible, whereas the light-flavour and photon-conversion background is obtained with the sPlot [81] method, based on a fit to the number of hits in the innermost ID layer in the data control region. Transfer factors for the light-flavour jets and converted photons, obtained from simulated samples, are corrected using a $Z + X$ control region and then used to extrapolate the extracted yields to the sig-

nal region. Both the yield extraction and the extrapolation are performed in bins of the transverse momentum of the electron candidate and the jet multiplicity.

The WZ production process is included in the data-driven estimates for the $\ell\ell + ee$ final states, while it is added from simulation for the $\ell\ell + \mu\mu$ final states even though its contribution to the total background is at the per-mille level. The contributions from $t\bar{t}V$ (where V stands for either a W or a Z boson) and triboson processes are minor and taken from simulated samples.

5.3 Signal and background modelling

The reconstructed four-lepton invariant mass $m_{4\ell}$ distribution is used as the discriminating variable for the $\ell^+\ell^-\ell'^+\ell'^-$ final state. It is extracted from simulation for signal events and for most background components ($t\bar{t}V$, VVV, $\ell\ell + \mu\mu$ and heavy-flavour hadron component of $\ell\ell + ee$), except for the light-flavour jets and photon conversions in the case of $\ell\ell + ee$ background, which are taken from the control region as described in Sect. 5.2.

To obtain statistical interpretations for each mass hypothesis, the $m_{4\ell}$ distribution for signal is parameterised as a function of the mass hypothesis m_H. In the case of a narrow resonance, the width in $m_{4\ell}$ is determined by the detector resolution, which is modelled by the sum of a Crystal Ball ($\mathcal{C}$) function [82,83] and a Gaussian ($\mathcal{G}$) function:

$$P_s(m_{4\ell}) = f_{\mathcal{C}} \times \mathcal{C}(m_{4\ell}; \mu, \sigma_{\mathcal{C}}, \alpha_{\mathcal{C}}, n_{\mathcal{C}})$$
$$+ (1 - f_{\mathcal{C}}) \times \mathcal{G}(m_{4\ell}; \mu, \sigma_{\mathcal{G}}).$$

The Crystal Ball and Gaussian functions share the same peak value of $m_{4\ell}$ (μ), but have different resolution parameters, $\sigma_{\mathcal{C}}$ and $\sigma_{\mathcal{G}}$. The $\alpha_{\mathcal{C}}$ and $n_{\mathcal{C}}$ parameters control the shape and position of the non-Gaussian tail, and the parameter $f_{\mathcal{C}}$ ensures the relative normalisation of the two probability density functions. To improve the stability of the parameterisation in the full mass range considered, the parameter $n_{\mathcal{C}}$ is set to a fixed value. The bias in the extraction of signal yields introduced by using the analytic function is below 2% and treated as a systematic uncertainty of the signal parameterisation. The function parameters are determined separately for each final state using the simulated events for each generated mass m_H, and then fitted with a polynomial in m_H to interpolate between the generated mass points. The order of the polynomial is determined by first fitting with a third-order polynomial and then decreasing its order until the χ^2 is three times larger than the number of degrees of freedom. The use of this parameterisation for the function parameters introduces a bias in the signal yield and m_H extraction of about 1%. The extra bias is included in the systematic uncertainties of the signal acceptance.

In the case of the LWA and the graviton model, a parton-level lineshape of $m_{4\ell}$ is derived from a theoretical calculation and multiplied by the signal acceptance obtained from the simulated events; it is then convolved with the detector resolution, using the same functions as those for modelling the narrow resonance. The parton-level lineshape of $m_{4\ell}$ is taken from Ref. [84] for the LWA, and from Ref. [85] for the graviton model.

For the ZZ continuum background, the $m_{4\ell}$ distribution is parameterised by an empirical function for both the quark- and gluon-initiated processes in order to reduce the statistical uncertainties stemming from the limited number of simulated events. The empirical function is described by the following:

$$f_{q\bar{q}ZZ/ggZZ}(m_{4\ell}) = C_0 \times H(m_0 - m_{4\ell}) \times f_1(m_{4\ell})$$
$$+ H(m_{4\ell} - m_0) \times f_2(m_{4\ell}),$$

where,

$$f_1(m_{4\ell}) = \left(\frac{m_{4\ell} - a_4}{a_3}\right)^{a_1 - 1} \left(1 + \frac{m_{4\ell} - a_4}{a_3}\right)^{-a_1 - a_2},$$
$$f_2(m_{4\ell}) = \exp\left[b_0\left(\frac{m_{4\ell} - b_4}{b_3}\right)^{b_1 - 1}\left(1 + \frac{m_{4\ell} - b_4}{b_3}\right)^{-b_1 - b_2}\right],$$
$$C_0 = \frac{f_2(m_0)}{f_1(m_0)}.$$

The function's first part, f_1, covers the low-mass part of the spectrum until the ZZ threshold around $2 \cdot m_Z$, and the second part, f_2, describes the high-mass tail. The transition between low- and high-mass parts is modelled with the Heaviside step function $H(x)$ around $m_0 = 260$ GeV for $q\bar{q} \to ZZ$ and

around 350 GeV for $gg \to ZZ$. The continuity of the function around m_0 is ensured by the normalisation factor C_0 that is applied to the low-mass part. Finally, a_i and b_i are shape parameters which are obtained by fitting the $m_{4\ell}$ distribution in simulation for each category. A large number of $m_{4\ell}$ distributions are calculated from the analytic function with variations of the a_i and b_i values sampled from a multivariate Gaussian distribution that is constructed from their covariance matrix. The uncertainty in the $m_{4\ell}$ distribution is determined by calculating a central interval that captures 68% of the variations, and is treated as a nuisance parameter in the likelihood fit, namely a ZZ parameterisation uncertainty. The ZZ parameterisation uncertainty is one of the leading systematic uncertainties for a low-mass signal, as shown in Table 1.

Interference modelling

The gluon-initiated production of a heavy scalar H, the SM Higgs h and the $gg \to ZZ$ continuum background all share the same initial and final state, and thus lead to interference terms in the total amplitude. Theoretical calculations described in Ref. [86] have shown that the effect of interference could modify the integrated cross section by up to $\mathcal{O}(10\%)$, and this effect is enhanced as the width of the heavy scalar increases. Therefore, a search for a heavy scalar Higgs boson in the LWA case must properly account for two interference effects: the interference between the heavy scalar and the SM Higgs boson (denoted by H–h) and between the heavy scalar and the $gg \to ZZ$ continuum (denoted by H–B). However, because the width of the KK excitation resonance is relatively small, the interference effect is assumed to be negligible in the graviton interpretation for both final states.

If the H and h bosons have similar properties, they have the same production and decay amplitudes and therefore the only difference between the signal and interference terms in the production cross section comes from the propagator. Hence, the acceptance and resolution of the signal and interference terms are expected to be the same. The H–h interference is obtained by reweighting the particle-level lineshape of generated signal events using the following formula:

$$w(m_{4\ell}) = \frac{2 \cdot Re\left[\frac{1}{s - s_H} \cdot \frac{1}{(s - s_h)^*}\right]}{\frac{1}{|s - s_H|^2}},$$

where $1/(s - s_{H(h)})$ is the propagator for a scalar (H or h). The particle-level lineshape is then convolved with the detector resolution function, and the signal and interference acceptances are assumed to be the same.

In order to extract the H–B interference contribution, signal-only and background-only samples are subtracted from the generated *SBI* samples. The extracted particle-level

$m_{4\ell}$ distribution for the H–B interference term is then convolved with the detector resolution.

6 Analysis of $\ell^+\ell^-\nu\bar{\nu}$ final state

6.1 Event selection and categorisation

The $\ell^+\ell^-\nu\bar{\nu}$ final state consists of a pair of high-p_T isolated leptons (electrons or muons) and large E_T^{miss}, and is subject to larger background contamination than the $\ell^+\ell^-\ell'^+\ell'^-$ channel. Candidate events are recorded with a combination of multiple single-lepton triggers, which gives a high efficiency of about 98% for typical signal processes in the signal region defined in the following.

Candidate events are preselected by requiring exactly two electrons or muons with opposite charges and $p_T > 20$ GeV, where the electrons (muons) must have $|\eta| < 2.47$ (2.5). The leading lepton is further required to have $p_T > 30$ GeV, well above the threshold of the single-lepton triggers. The selected electrons or muons must have a longitudinal impact parameter satisfying $|z_0 \sin(\theta)| < 0.5$ mm. The lepton candidates are required to satisfy the same isolation criteria and the same requirement on the transverse impact-parameter significance as used in the $\ell^+\ell^-\ell'^+\ell'^-$ channel (see Sect. 5.1.1), which leads to an efficiency above 98% for typical prompt leptons with $p_T > 30$ GeV. To suppress the WZ background, events containing any additional lepton satisfying the 'loose' identification requirement with $p_T > 7$ GeV, in addition to the other requirements, are rejected. Requiring the dilepton invariant mass ($m_{\ell\ell}$) to be in the range between 76 and 106 GeV largely reduces the contamination from the non-resonant-$\ell\ell$ background, originating from $t\bar{t}$, Wt, WW, and $Z \to \tau\tau$ production. The data sample after the preselection is dominated by the Z + jets and non-resonant-$\ell\ell$ processes. To suppress these backgrounds, a further selection based on E_T^{miss} and event topology is applied.

Candidate events are required to have $E_T^{\mathrm{miss}} > 120$ GeV, which suppresses the Z + jets contamination by several orders of magnitude. The number of residual Z + jets events, which have large fake E_T^{miss}, is further reduced by requiring $S(E_T^{\mathrm{miss}}) > 10$, where $S(E_T^{\mathrm{miss}})$ is the statistical significance of the E_T^{miss} value against the null hypothesis of zero-E_T^{miss} [87]. Additional selection criteria based on angular variables are imposed to further reject the Z + jets and non-resonant-$\ell\ell$ background events. The selection on angular variables is motivated by the desired detector signature, where the $\vec{E}_T^{\mathrm{miss}}$ is back-to-back with the transverse momentum of the dilepton system. The azimuthal angle difference between the dilepton system and $\vec{E}_T^{\mathrm{miss}}$, $\Delta\phi(\vec{p}_T^{\ell\ell}, \vec{E}_T^{\mathrm{miss}})$, must be larger than 2.5 radians, and the selected leptons must be close to each other, with the dis-

tance $\Delta R_{\ell\ell} = \sqrt{(\Delta\phi_{\ell\ell})^2 + (\Delta\eta_{\ell\ell})^2} < 1.8$. Furthermore, the azimuthal angle difference between any of the selected jets with $p_T > 100$ GeV and $\vec{E}_T^{\mathrm{miss}}$ must be larger than 0.4 radians. As a consequence of all the requirements, the Z + jets process only constitutes a small fraction of the total background (about 4%) after the full selection. Finally, events containing one or more b-jets are vetoed to further suppress the $t\bar{t}$ and Wt backgrounds.

The signal region for the VBF production mode (VBF-enriched signal region) is defined for candidate events containing at least two selected jets with $p_T > 30$ GeV, where the two leading jets must have $m_{\mathrm{jj}} > 550$ GeV and $\Delta\eta_{\mathrm{jj}} > 4.4$. The remaining events, failing the requirements for the VBF-enriched signal region, are categorised for the ggF-enriched signal region. The signal acceptance in the ggF-enriched signal region for signal events containing a heavy spin-0 resonance from ggF production is about 30% at $m_H = 400$ GeV and up to 50% at $m_H = 1.4$ TeV. For VBF signal events the signal acceptance in the VBF-enriched signal region is generally lower, ranging from 3% at $m_H = 400$ GeV to 20% at $m_H = 1.6$ TeV.

6.2 Background estimation

In the ggF-enriched signal region, the major backgrounds originate from the ZZ and WZ processes, which account for 60% and 30% of the total background contribution, respectively. The non-resonant-$\ell\ell$ background yields a relative contribution of about 5% to the total background, while the largely suppressed Z + jets background only constitutes a small fraction (4%). Finally, the remaining contributions from other processes (VVV and $t\bar{t}V$), amount in total to less than 1% of the total background. A similar composition of background processes is found in the VBF-enriched signal region, where the total background yield is expected to be smaller than 1% of that in the ggF-enriched signal region, due to the event selection for the VBF phase space. The various background estimates and their uncertainties are described below.

The main background contribution from ZZ production is estimated using a semi-data-driven method. Similarly to the $\ell^+\ell^-\ell'^+\ell'^-$ analysis, the predicted ZZ yield is scaled by a floating normalisation factor, which is determined in the statistical fit to the signal-region data (see Sect. 8.1). The introduction of the data-driven normalisation factor helps constrain the total uncertainty in the ZZ yield, while the theoretical and experimental uncertainties in the transverse mass distribution are evaluated from simulation.

To estimate the background from WZ production in the ggF-enriched signal region, a control region enriched in WZ events, with a purity of over 90%, is defined using the preselection criteria, except that a third lepton with $p_T > 20$ GeV is required. Several further selections such as $S(E_T^{\mathrm{miss}}) > 3$,

a b-jets veto, and $m_T^W > 60$ GeV, where m_T^W is constructed from the third lepton's transverse momentum and the $\vec{E}_T^{\mathrm{miss}}$ vector,[2] are applied to suppress non-WZ contributions. A normalisation factor is calculated in the control region as the number of observed events in data, after subtracting the non-WZ contributions estimated from simulation, divided by the predicted WZ yield. The factor is found to be 1.05 with a total uncertainty of 5%, which is consistent with a recent WZ measurement [88] performed within a broader fiducial phase space. The statistical uncertainty of the data in the control region leads to a 0.8% uncertainty in the WZ estimate in the signal region. The main systematic uncertainty is evaluated for the ratio of the WZ predictions in the signal and control regions, and covers the experimental uncertainties and the theoretical ones related to the PDFs and the QCD scales. The uncertainty related to the subtraction of the non-WZ contribution in the control region is estimated by applying cross-section uncertainties for all the relevant processes and is found to be negligible. An additional uncertainty is assigned to the WZ prediction in the signal region, to account for the efficiency mismodelling of vetoing a third lepton in $WZ \to \ell\ell\ell\nu$ events. The total uncertainty in the WZ estimate for the ggF-enriched signal region is about 5%. A similar method is adopted to estimate the WZ contribution in the VBF-enriched signal region, except that the control region additionally selects two jets with $p_T > 30$ GeV. The normalisation factor is found to be 0.83 with an uncertainty of 0.27, which is compatible with the results presented in Ref. [89]. The total uncertainty in the WZ estimate for the VBF-enriched signal region is about 30%. The kinematic distributions are estimated from simulation.

To estimate the non-resonant-$\ell\ell$ background, a control region dominated by the non-resonant-$\ell\ell$ processes (with a purity of about 95%) is defined with all the event selection criteria except that the final state is required to contain an opposite-sign $e\mu$ pair. The non-resonant-$\ell\ell$ contribution in the ee ($\mu\mu$) channel is calculated as one half of the observed data yield after subtracting the contribution from the other background processes in the control region, and then corrected for the difference in the lepton reconstruction and identification efficiencies between selecting an $e\mu$ pair and an ee ($\mu\mu$) pair. The lepton efficiency correction is derived as the square root of the ratio of the numbers of $\mu\mu$ and ee events in data after the preselection. The choice of deriving the correction after preselection minimises the resulting statistical uncertainty. The total uncertainty in the non-resonant-$\ell\ell$ estimate in the ggF-enriched signal region is about 9%, including the statistical uncertainty of the data in the control region and the method bias estimated from simulation. The estimation of the non-resonant-$\ell\ell$ background in

the VBF-enriched signal region relies on a similar methodology, except that the control region is defined with a jet selection that is looser than in the signal region. The non-resonant-$\ell\ell$ estimate obtained with the looser selection is then scaled by a simulation-based transfer factor to derive the final estimate in the VBF-enriched signal region. The transfer factor is subject to experimental and theoretical uncertainties, and the relative uncertainty in the final estimate in the VBF-enriched signal region is 70%. The kinematic distributions for the non-resonant-$\ell\ell$ background in the signal region are predicted with simulation, and the assigned systematic uncertainty covers the experimental uncertainty in the simulated shape as well as the difference between data and simulation in the control region.

The Z + jets background contribution is estimated from simulation and scaled by a normalisation factor derived in a control region enriched in Z + jets events. The control region is defined with all event selection criteria except that $S(E_T^{\mathrm{miss}})$ must be less than 9 and no requirements on the azimuthal angle difference between jets with $p_T > 100$ GeV and $\vec{E}_T^{\mathrm{miss}}$ are made. The normalisation factor is found to be close to one. Apart from the statistical uncertainty in the control sample, the experimental and theoretical uncertainties are evaluated for the ratio of the number of simulated events in the signal region to that in the control region. The total uncertainty in the Z + jets estimate is about 40%. The kinematic distributions for the Z + jets background are modelled with simulation. Finally, backgrounds from the VVV and $t\bar{t}V$ processes, which contribute less than 1% of the total background, are estimated from simulation.

6.3 Signal and background modelling

The modelling of the transverse mass m_T distribution for signal and background is based on templates derived from fully simulated events and afterwards used to fit the data. In the case of a narrow resonance, simulated events generated for fixed mass hypotheses as described in Sect. 3 are used as the inputs in the moment-morphing technique [90] to obtain the m_T distribution for any other mass hypothesis.

The extraction of the interference terms for the LWA case is performed in the same way as in the $\ell^+\ell^-\ell'^+\ell'^-$ final state, as described in Sect. 5.3. In the case of the $\ell^+\ell^-\nu\bar{\nu}$ final state a correction factor, extracted as a function of m_{ZZ}, is used to reweight the interference distributions obtained at particle level to account for reconstruction effects. The final expected LWA m_T distribution is obtained from the combination of the interference distributions with simulated m_T distributions, which are interpolated between the simulated mass points with a weighting technique using the Higgs propagator, a method similar to that used for the interference.

---

[2] $m_T^W = \sqrt{2 p_T^\ell E_T^{\mathrm{miss}} [1 - \cos \Delta\phi(\vec{p}_T^\ell, \vec{E}_T^{\mathrm{miss}})]}$.

7 Systematic uncertainties

The systematic uncertainties can be categorised into experimental and theoretical uncertainties. The first category includes the uncertainties resulting from the integrated luminosity, the trigger efficiencies, the momentum scale and resolution of tracks, the reconstruction and identification of leptons and jets, and their energy scale and resolution calibrations. Systematic uncertainties associated with data-driven methods are also in this category, but described in their corresponding sections: Sect. 5.2 for $\ell^+\ell^-\ell'^+\ell'^-$ final state and Sect. 6.2 for $\ell^+\ell^-\nu\bar{\nu}$ final state. The second category includes the uncertainties in the theoretical descriptions of the signal and background simulations.

These systematic uncertainties evaluated separately for signal and background in each category affect signal acceptances and background yields as well as the probability density distributions of the discriminating variables. They are provided as the inputs for the statistical interpretations described in Sect. 9, in which the impact of these uncertainties on the expected signal yields are also presented.

7.1 Experimental uncertainties

The uncertainty in the combined 2015–2018 integrated luminosity is 1.7% [91], obtained using the LUCID-2 detector [92] for the primary luminosity measurements.

The lepton identification and reconstruction efficiency and energy/momentum scale and resolution are derived from data using $J/\psi \to \ell\ell$ and $Z \to \ell\ell$ decay events. The uncertainties in the reconstruction performance are computed following the method described in Ref. [64] for muons and Ref. [63] for electrons. In general, their impact on the signal and background yields is less than 1% in the $\ell^+\ell^-\nu\bar{\nu}$ final state, and up to 1.5% in the $\ell^+\ell^-\ell'^+\ell'^-$ final state. In addition, the lepton isolation uncertainty is estimated to be less than 1% in both final states.

The uncertainties in the jet energy scale and resolution have several sources, including uncertainties in the absolute and relative *in situ* calibration, the correction for pile-up, the flavour composition and response [93]. Each source is treated as an independent component. They vary from 4.5% for jets with transverse momentum $p_T = 20$ GeV, decreasing to 1% for jets with $p_T = 100$–1500 GeV and increasing again to 3% for jets with higher p_T. They are the dominant uncertainties in the VBF-enriched categories for ggF signal production and SM ZZ production in both final states.

Uncertainties in the lepton and jet energy scales are propagated to the uncertainty in the E_T^{miss} [94]. Additionally, the uncertainties from the momentum scale and resolution of the tracks that are not associated with any identified lepton or jet contribute 8% and 3%, respectively, to the uncertainty in the E_T^{miss} value.

The efficiency of the lepton triggers in events with reconstructed leptons is nearly 100%, and hence the related uncertainties are negligible. The uncertainties associated with the pile-up reweighting are also taken into account; their impact on the signal and background yields is about 1% for both final states.

These experimental uncertainties are common to the two final states; therefore, they are fully correlated between the two final states.

7.2 Theoretical uncertainties

For the simulation-based estimates, the theoretical uncertainties stemming from parton distribution functions (PDFs), missing higher-order QCD corrections, and parton showering are considered.

The PDF uncertainty is evaluated by taking the envelope of variations among alternative PDF choices and the estimate from its internal PDF error sets, following the PDF4LHC recommendation [95]. The missing higher-order QCD corrections are estimated by halving or doubling the factorisation and renormalisation scales independently, among which the largest effect is taken as the systematic uncertainty. The parton-showering uncertainty is assessed by varying the PYTHIA configurations, such as the parameter values of the AZNLO tune, the multi-parton models and the final-state radiation models.

For different signal hypotheses, the impact of these theoretical uncertainties on the signal acceptance and the spectrum of the discriminating variables is evaluated. In total, the theoretical uncertainty in the signal acceptance varies from less than 1% in the low mass region to 12% in the high mass region of the $\ell^+\ell^-\nu\bar{\nu}$ final state, and from less than 1% in the low mass region to up to 20% in the high mass region of the $\ell^+\ell^-\ell'^+\ell'^-$ final state.

For the continuum ZZ background, a common floating normalisation factor is introduced to scale the number of events for the $q\bar{q} \to ZZ$ and $gg \to ZZ$ processes, while the relative yields of the two processes are estimated from the simulations. Therefore, in addition to the spectrum of the discriminating variables in the ZZ background, the theoretical uncertainties are also propagated to the simulation-based estimation of the relative yields. Moreover, the uncertainty associated with the NLO EW corrections, calculated in Refs. [45,46,48], are also taken into account, affecting the discriminating variables by less than 1% in the low mass region and up to 10% in the high mass region for both final states.

Because the $\ell^+\ell^-\ell'^+\ell'^-$ and $\ell^+\ell^-\nu\bar{\nu}$ searches are sensitive to different energy scales, these theoretical uncertainties are assumed to be completely uncorrelated between the two analyses. A fully correlated scenario is also examined and the differences between the two scenarios in terms of the expected limits on various signal hypotheses are negligible.

8 Results

The statistical procedure used to extract the results is described in Sect. 8.1 and the results are presented in Sect. 8.2.

8.1 Statistical procedure and impact of systematic uncertainties

The statistical treatment of the data interpretation follows the procedure for the Higgs-boson search combination in 7 TeV data [96,97]. The test statistic used for limit setting is the profile likelihood ratio $\Lambda(\alpha, \boldsymbol{\theta})$, which depends on one or more parameters of interest α, additional normalisation factors and extra nuisance parameters $\boldsymbol{\theta}$. The parameter of interest is the cross section times branching ratio of the heavy resonance decaying into the two final states. The normalisation factors, which were not used in the previous publication [18], are introduced separately for each final state to scale the expected number of the SM ZZ background events in each category and are determined by a likelihood fit to the data. This allows the systematic uncertainty to be reduced by removing both the theoretical and luminosity uncertainties contributing to the normalisation uncertainty. In the $\ell^+\ell^-\ell'^+\ell'^-$ final state, three floating normalisation factors are introduced for the VBF-enriched, ggF-MVA-high and ggF-MVA-low categories. They are referred to as $\mu_{ZZ}^{\text{VBF-MVA}}$, $\mu_{ZZ}^{\text{ggF-MVA-high}}$ and $\mu_{ZZ}^{\text{ggF-MVA-low}}$, respectively. The use of three ZZ normalisation factors for the $\ell^+\ell^-\ell'^+\ell'^-$ final state is motivated by the different phase spaces defined for the respective signal regions. Only one floating normalisation factor μ_{ZZ} is introduced in the $\ell^+\ell^-\nu\bar{\nu}$ final state, due to the limited size of the data sample and the worse signal-to-background ratio in the respective VBF-enriched signal region.

The nuisance parameters represent the estimates of the systematic uncertainties and each of them is constrained by a Gaussian distribution. For each category of each final state, a discriminating variable is used to further separate signal from background. The number of signal events is extracted from a simultaneous fit to the discriminating variable, $m_{4\ell}$ in the $\ell^+\ell^-\ell'^+\ell'^-$ analysis and m_{T} in the $\ell^+\ell^-\nu\bar{\nu}$ analysis, in the event categories described in Sects. 5 and 6.

The impact of a systematic uncertainty on the result depends on the production mode and the mass hypothesis. For the ggF production mode, at lower masses the ZZ parameterisation for the $\ell^+\ell^-\ell'^+\ell'^-$ final state and the systematic uncertainty of the Z + jets background for the $\ell^+\ell^-\nu\bar{\nu}$ final state dominate, and at higher masses the uncertainties in the NLO EW correction and parton showering become important, as also seen in VBF production. For the VBF production mode, the dominant uncertainties come from the theoretical modelling of the discriminating variables of the ZZ events in the VBF category. At lower masses, jet-energy-scale uncertainties are also important. Table 1 shows the impact of the leading systematic uncertainties on the predicted signal event yield when the cross section times branching ratio is set to the expected upper limit (shown in Fig. 4), for ggF and VBF production modes. The statistical uncertainty of the data sample dominates in both of the present searches, and the systematic uncertainties impact the searches to a much lesser extent.

8.2 General results

The total number of observed events is 3275 in the $\ell^+\ell^-\ell'^+\ell'^-$ final state ($m_{4\ell} > 200$ GeV) and 2794 in the $\ell^+\ell^-\nu\bar{\nu}$ final state. The expected background yields are obtained from a simultaneous likelihood fit of the two final states under the background-only hypothesis. The fitted normalisation factors for the SM ZZ background are summarised in Table 2.

The number of observed candidate events with mass above 200 GeV together with the expected background yields for each of the five categories of the $\ell^+\ell^-\ell'^+\ell'^-$ analysis as described in Sect. 5.1.2 are presented in Table 3. The $m_{4\ell}$ spectrum in each category is shown in Fig. 2 for illustration, since the backgrounds are determined from a combined unbinned likelihood fit to the data under the background-only hypothesis. Table 4 contains the number of observed events along with the obtained background yields for the $\ell^+\ell^-\nu\bar{\nu}$ analysis and Fig. 3 shows the m_{T} distribution for the electron and muon channels in the ggF-enriched and VBF-enriched categories.

The two previous excesses around 240 GeV and 700 GeV that were observed in the publication [18] using 2015 and 2016 data are not confirmed using the full Run 2 dataset as explained below. The maximum deviation of the data from the background-only hypothesis is evaluated in the context of a NWA signal from the ggF production or from the VBF production separately. For the ggF production, the maximum deviation is for a signal mass hypothesis around 240 GeV, with a local significance of 2.0 standard deviations and a global significance of 0.5 standard deviation. For the VBF production, the maximum deviation is for a signal mass hypothesis around 620 GeV, with a local significance of 2.4 standard deviations and a global significance of 0.9 standard deviation.

9 Interpretations

Since no significant excess with respect to the background predictions is found, results obtained from the combination of the $\ell^+\ell^-\ell'^+\ell'^-$ and $\ell^+\ell^-\nu\bar{\nu}$ final states are interpreted in terms of exclusion limits for different signal hypotheses as presented below.

Table 1 Impact of the leading systematic uncertainties, the data statistical uncertainties and the total uncertainties on the predicted signal event yield with the cross section times branching ratio being set to the expected upper limit, expressed as a percentage of the signal yield for the ggF (left) and VBF (right) production modes at $m_H = 300, 600, 1000,$ and 1500 GeV

ggF production		VBF production	
Systematic source	Impact [%]	Systematic source	Impact (%)
$m_H = 300$ GeV			
ZZ parameterisation ($\ell^+\ell^-\ell'^+\ell'^-$)	4.5	Jet flavor composition	3.0
$Z +$ jets modelling ($\ell^+\ell^-\nu\bar{\nu}$)	2.3	$q\bar{q} \to ZZ$ QCD scale (VBF-enriched category, $\ell^+\ell^-\ell'^+\ell'^-$)	2.8
Parton showering of ggF ($\ell^+\ell^-\ell'^+\ell'^-$)	2.2	ZZ parameterisation ($\ell^+\ell^-\ell'^+\ell'^-$)	2.3
$e\mu$ statistical uncertainty $\ell^+\ell^-\nu\bar{\nu}$	2.0	Jet energy scale(*in-su* calibration)	1.8
Data stat. uncertainty	53	Data stat. uncertainty	58
Total uncertainty	55	Total uncertainty	60
$m_H = 600$ GeV			
Electroweak corrections for $q\bar{q} \to ZZ$ ($\ell^+\ell^-\nu\bar{\nu}$)	4.9	QCD scale of $q\bar{q} \to ZZ$ ($\ell^+\ell^-\nu\bar{\nu}$)	7.6
QCD scale of $q\bar{q} \to ZZ$ ($\ell^+\ell^-\nu\bar{\nu}$)	2.5	Jet energy resolution	5.4
$Z +$ jets modelling ($\ell^+\ell^-\nu\bar{\nu}$)	2.5	Parton showering ($\ell^+\ell^-\nu\bar{\nu}$)	3.3
PDF of $q\bar{q} \to ZZ$ ($\ell^+\ell^-\ell'^+\ell'^-$)	2.2	Electroweak corrections for $q\bar{q} \to ZZ$ ($\ell^+\ell^-\nu\bar{\nu}$)	3.0
Data stat. uncertainty	54	Data stat. uncertainty	61
Total uncertainty	57	Total uncertainty	63
$m_H = 1000$ GeV			
Electroweak corrections for $q\bar{q} \to ZZ$ ($\ell^+\ell^-\nu\bar{\nu}$)	9.3	Parton showering ($\ell^+\ell^-\nu\bar{\nu}$)	6.8
Parton showering ($\ell^+\ell^-\nu\bar{\nu}$)	5.2	Electroweak corrections for $q\bar{q} \to ZZ$ ($\ell^+\ell^-\nu\bar{\nu}$)	4.7
QCD scale of $q\bar{q} \to ZZ$ ($\ell^+\ell^-\nu\bar{\nu}$)	4.8	QCD scale of $q\bar{q} \to ZZ$ ($\ell^+\ell^-\nu\bar{\nu}$)	2.4
$Z +$ jets modelling ($\ell^+\ell^-\nu\bar{\nu}$)	2.4	Jet flavor composition	2.4
Data stat. uncertainty	57	Data stat. uncertainty	58
Total uncertainty	59	Total uncertainty	59
$m_H = 1500$ GeV			
Parton showering ($\ell^+\ell^-\nu\bar{\nu}$)	9.6	Parton showering ($\ell^+\ell^-\nu\bar{\nu}$)	9.0
Electroweak corrections for $q\bar{q} \to ZZ$ ($\ell^+\ell^-\nu\bar{\nu}$)	6.8	Electroweak corrections for $q\bar{q} \to ZZ$ ($\ell^+\ell^-\nu\bar{\nu}$)	4.6
PDF of $q\bar{q} \to ZZ$ ($\ell^+\ell^-\nu\bar{\nu}$)	5.4	PDF of $q\bar{q} \to ZZ$ ($\ell^+\ell^-\nu\bar{\nu}$)	3.4
QCD scale of $q\bar{q} \to ZZ$ ($\ell^+\ell^-\nu\bar{\nu}$)	4.6	QCD scale of $q\bar{q} \to ZZ$ ($\ell^+\ell^-\nu\bar{\nu}$)	2.8
Data stat. uncertainty	57	Data stat. uncertainty	55
Total uncertainty	59	Total uncertainty	57

Table 2 The ZZ normalisation factors together with their total (statistical+systematic) uncertainties in each category of the two final states, which scale the number of ZZ events estimated from the simulations, obtained from a simultaneous likelihood fit of the two final states under the background-only hypothesis. For the $\ell^+\ell^-\ell'^+\ell'^-$ final state, the MVA-based categorisation is used

Final state	Normalisation factor	Fitted value
$\ell^+\ell^-\ell'^+\ell'^-$	$\mu_{ZZ}^{\text{VBF-MVA}}$	0.9 ± 0.3
	$\mu_{ZZ}^{\text{ggF-MVA-high}}$	1.07 ± 0.05
	$\mu_{ZZ}^{\text{ggF-MVA-low}}$	1.12 ± 0.03
$\ell^+\ell^-\nu\bar{\nu}$	μ_{ZZ}	1.04 ± 0.06

9.1 Spin-0 resonances

9.1.1 Spin-0 resonances with NWA

Upper limits on the cross section times branching ratio ($\sigma \times B(H \to ZZ)$) for a heavy resonance are obtained from the combination of the two final states, as a function of m_H with the CL$_s$ procedure [98] in the asymptotic approximation. The results were verified to be correct within about 4% using pseudo-experiments. It is assumed that an additional heavy scalar would be produced mainly via the ggF and VBF processes but that the ratio of the two production mechanisms might depend on the model considered. For this reason, fits for the ggF and VBF processes are done separately, and in each case the other process is allowed to float in the fit as an additional free parameter. Figure 4 presents the observed

Table 3 Expected and observed numbers of events in the $\ell^+\ell^-\ell'^+\ell'^-$ final state for $m_{4\ell} > 200$ GeV, together with their uncertainties, for the VBF-MVA-enriched, ggF-MVA-high and ggF-MVA-low categories. The expected numbers of events, as well as their uncertain-

ties, are obtained from a combined likelihood fit to the data under the background-only hypothesis. The uncertainties of the ZZ normalisation factors, presented in Table 2, are also taken into account

Process	VBF-enriched	ggF-MVA-high			ggF-MVA-low
		4μ channel	$2e2\mu$ channel	$4e$ channel	
$q\bar{q} \rightarrow ZZ$	11 ± 4	232 ± 10	389 ± 17	154 ± 7	2008 ± 47
$gg \rightarrow ZZ$	3 ± 2	37 ± 6	64 ± 10	26 ± 4	247 ± 19
ZZ (EW)	4.1 ± 0.4	4.5 ± 0.2	7.5 ± 0.4	3 ± 0.2	14.3 ± 0.7
$Z + \text{jets}, t\bar{t}$	0.08 ± 0.02	0.6 ± 0.1	1.7 ± 0.4	0.8 ± 0.1	8.8 ± 2.1
$t\bar{t}V, VVV$	0.96 ± 0.1	9.8 ± 0.2	17.5 ± 0.4	7.7 ± 0.2	21.9 ± 0.5
Total background	19 ± 5	284 ± 12	480 ± 20	192 ± 8	2300 ± 51
Observed	19	271	493	191	2301

(a)   **(b)**   **(c)**

(d)   **(e)**
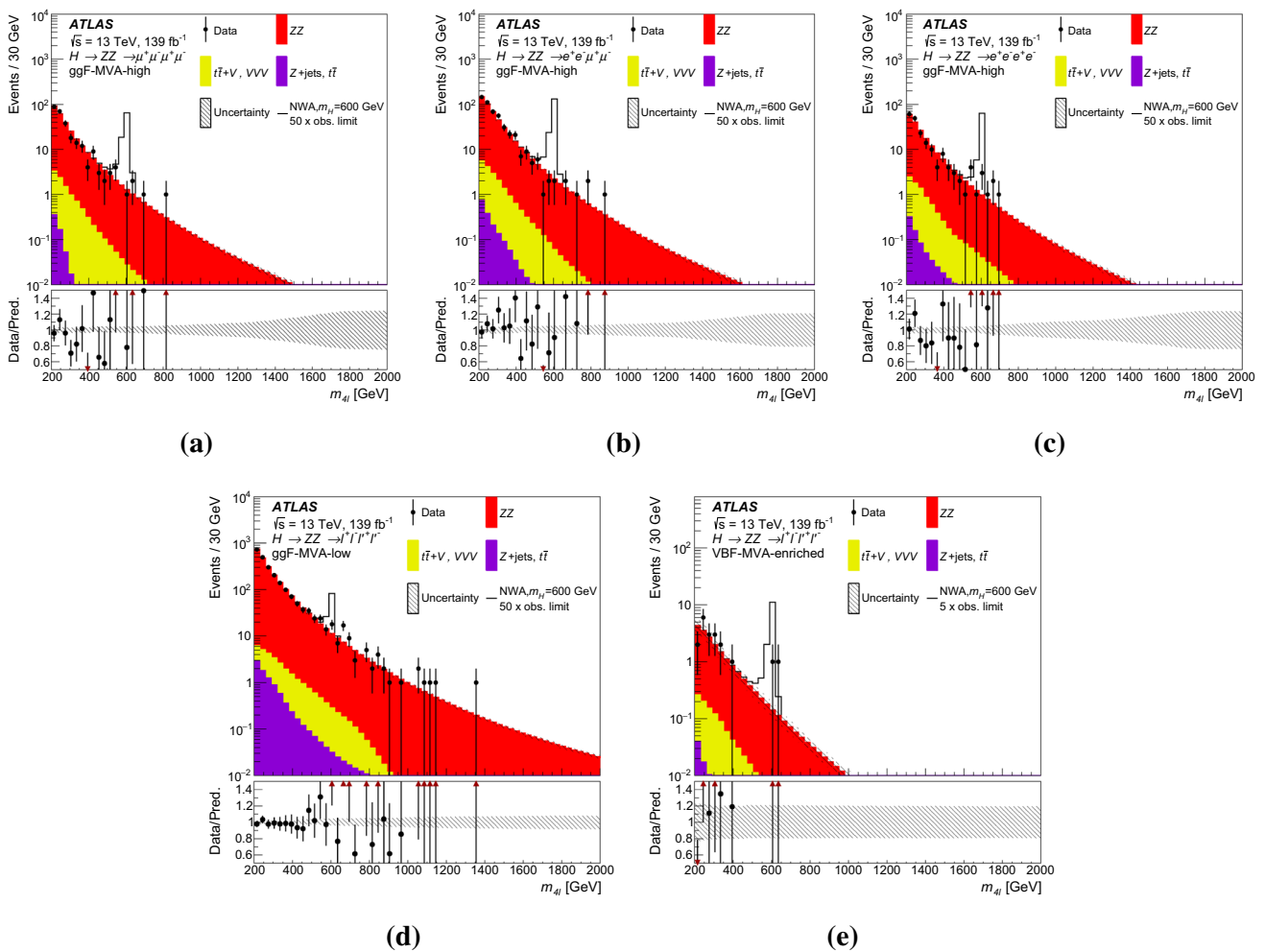
Fig. 2 Distributions of the four-lepton invariant mass $m_{4\ell}$ in the $\ell^+\ell^-\ell'^+\ell'^-$ search for the ggF-MVA-high categories ($\mu^+\mu^-\mu^+\mu^-$ (**a**), $e^+e^-\mu^+\mu^-$ (**b**), and $e^+e^-e^+e^-$ (**c**) final states), for the ggF-MVA-low category (**d**), and for the VBF-MVA-enriched category (**e**). The backgrounds are determined from a combined likelihood fit to the data under the background-only hypothesis. The simulated $m_H = 600$ GeV signal is normalised to a cross section corresponding to 50 (5) times

the observed limit given in Sect. 9.1.1 for the ggF (VBF) production mode. The error bars on the data points indicate the statistical uncertainty, while the systematic uncertainty in the prediction is shown by the hatched band. The lower panels show the ratio of data to prediction. The red arrows indicate data points that are outside the displayed range

Table 4 Expected and observed numbers of events together with their uncertainties in the $\ell^+\ell^-\nu\bar{\nu}$ final state, for the ggF- and VBF-enriched categories. The expected numbers of events, as well as their uncertainties, are obtained from a likelihood fit to the data under the background-only hypothesis. The uncertainties of the ZZ normalisation factors, presented in Table 2, are also taken into account

Process	ggF-enriched		VBF-enriched	
	e^+e^- channel	$\mu^+\mu^-$ channel	e^+e^- channel	$\mu^+\mu^-$ channel
$q\bar{q} \to ZZ$	695 ± 39	795 ± 44	2.8 ± 0.2	3.3 ± 0.2
$gg \to ZZ$	87 ± 28	97 ± 31	1 ± 0.4	1 ± 0.4
ZZ (EW)	6.6 ± 0.5	7 ± 0.5	0.8 ± 0.1	0.9 ± 0.1
WZ	400 ± 13	443 ± 12	2.4 ± 0.5	3 ± 1.3
$Z + \text{jets}$	39 ± 12	56 ± 21	0.2 ± 0.2	0.3 ± 0.3
Non-resonant-$\ell\ell$	66 ± 6	77 ± 7	0.2 ± 0.2	0.3 ± 0.2
$t\bar{t}V, VVV$	5.9 ± 0.4	5.9 ± 0.4	0.08 ± 0.02	0.04 ± 0.01
Total backgrounds	1299 ± 52	1480 ± 59	7.4 ± 0.7	8.4 ± 1.4
Observed	1280	1498	7	9

and expected limits at 95% CL on the $\sigma \times B(H \to ZZ)$ of a narrow scalar resonance for the ggF (left) and VBF (right) production modes, as well as the expected limits from the $\ell^+\ell^-\ell'^+\ell'^-$ and $\ell^+\ell^-\nu\bar{\nu}$ searches. This result is valid for models in which the width is less than 0.5% of m_H. When combining the two final states, the 95% CL upper limits range from 215 fb at $m_H = 240$ GeV to 2.0 fb at $m_H = 1900$ GeV for the ggF production mode and from 87 fb at $m_H = 255$ GeV to 1.5 fb at $m_H = 1800$ GeV for the VBF production mode. Compared with the expected limits projected to the luminosity of 139 fb^{-1} from the previous publication [18], the current expected limits are decreased by a factor ranging from 20 to 28% for the ggF production mode and from 27 to 43% for the VBF production mode, depending on the mass hypothesis.

9.1.2 Spin-0 resonances with LWA

In the case of the LWA, upper limits on the cross section for the ggF process times branching ratio ($\sigma_{\text{ggF}} \times B(H \to ZZ)$) are set for different widths of the heavy scalar. Figure 5 shows the limits for a width of 1%, 5%, 10% and 15% of m_H respectively. The limits are set for masses of m_H higher than 400 GeV. The choice of 400 GeV as the lower boundary is to avoid any major instability in the parametrization of the mass spectra for the LWA signals and the interference effects, especially when the signal pole mass gets smaller. The interpretation has only been carried out for the ggF process, as it is the leading channel to study the impact of non-trivial width on the search.

9.1.3 Two-Higgs-doublet model

A search in the context of a CP-conserving 2HDM is also presented. This model has five physical Higgs bosons after electroweak symmetry breaking: two CP-even, one CP-odd, and two charged. The model considered here has seven free

parameters: the Higgs boson masses, the ratio of the vacuum expectation values of the two Higgs doublets (tan β), the mixing angle between the CP-even Higgs bosons (α), and the potential parameter m_{12}^2 that mixes the two Higgs doublets. The two Higgs doublets Φ_1 and Φ_2 can couple to leptons and up- and down-type quarks in several ways. In the Type-I model, Φ_2 couples to all quarks and leptons, whereas for Type-II, Φ_1 couples to down-type quarks and leptons and Φ_2 couples to up-type quarks. The 'lepton-specific' model is similar to Type-I except for the fact that the leptons couple to Φ_1, instead of Φ_2; the 'flipped' model is similar to Type-II except that the leptons couple to Φ_2, instead of Φ_1. In all these models, the coupling of the heavier CP-even Higgs boson to vector bosons is proportional to $\cos(\beta - \alpha)$. In the limit $\cos(\beta - \alpha) \to 0$, the light CP-even Higgs boson is indistinguishable from a SM Higgs boson with the same mass. In the context of $H \to ZZ$ decays there is no direct coupling of the Higgs boson to leptons, so only the Type-I and II interpretations are presented. In addition, our interpretations assume other Higgs bosons are heavy enough so that the heavy CP-even Higgs boson will not decay to them.

Figure 6 shows exclusion limits in the tan β versus $\cos(\beta - \alpha)$ plane for Type-I and Type-II 2HDMs, for a heavy Higgs boson with mass $m_H = 220$ GeV. This m_H value is chosen so that the assumption of a narrow Higgs boson is valid over most of the parameter space, and the experimental sensitivity is maximal. At this low mass, only the $\ell^+\ell^-\ell'^+\ell'^-$ final state contributes to this result. The range of $\cos(\beta - \alpha)$ and tan β explored is limited to the region where the assumption of a heavy narrow Higgs boson with negligible interference is valid. When calculating the limits at a given choice of $\cos(\beta - \alpha)$ and tan β, the relative rates of ggF and VBF production in the fit are set to the prediction of the 2HDM for that parameter choice. Figure 7 shows exclusion limits as a function of the heavy Higgs boson mass m_H and the parameter tan β for $\cos(\beta - \alpha) = -0.1$, which is chosen so that the light Higgs boson properties are still compatible with
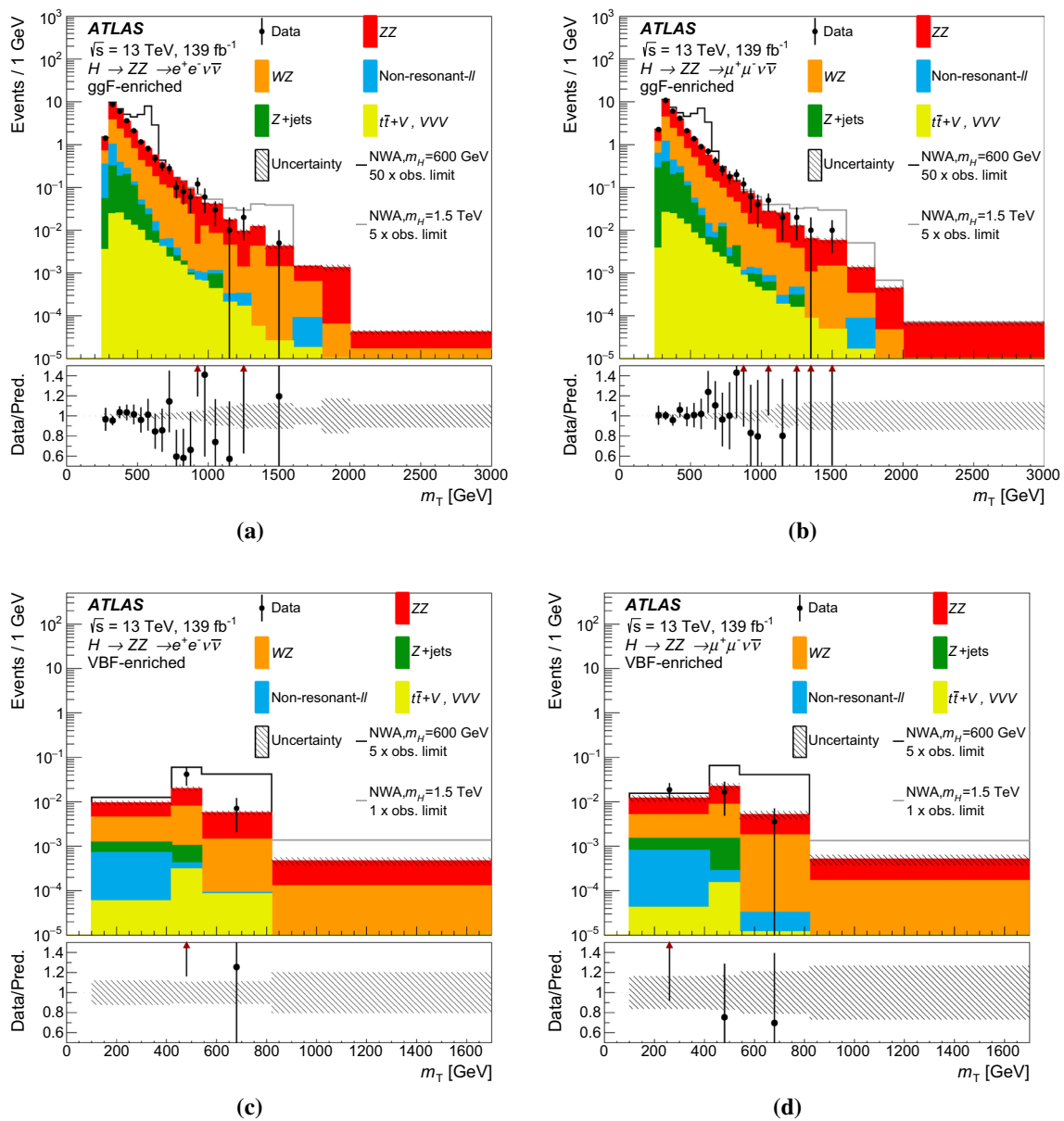
Fig. 3 The m_T distribution in the $\ell^+\ell^-\nu\bar{\nu}$ search for **a**, **b** the ggF categories and **c**, **d** the VBF categories. Events beyond the upper limit of the histogram are included in the last bin of the distribution. The backgrounds are determined from a combined likelihood fit to data under the background-only hypothesis. The simulated $m_H = 600$ GeV (1.5 TeV) signals are normalised to a cross section corresponding to 50 (5) times the observed limit given in Sect. 9.1.1 for the ggF production mode and

to 5 (1) times the observed limit for the VBF production mode. The error bars on the data points indicate the statistical uncertainty and markers are drawn at the bin centre. The systematic uncertainty in the prediction is shown by the hatched band. The lower panels show the ratio of data to prediction. The red arrows indicate data points that are outside the displayed range

the recent measurements of the SM Higgs boson properties [99]. The white regions in the exclusion plots indicate regions of parameter space which are not excluded by the present analysis. In these regions the cross section predicted by the 2HDM is below the observed cross-section limit. In comparison with the previous publication, the excluded regions are significantly expanded. For example, in the $\tan\beta$ versus m_H plane for the Type-II 2HDM the excluded region in $\tan\beta$ is more than 60% larger for $200 < m_H < 400$ GeV.

9.2 Spin-2 resonances

The results are also interpreted as a search for a Kaluza–Klein graviton excitation, G_{KK}, in the context of the bulk RS model with $k/\overline{M}_{Pl} = 1$. The limits on $\sigma \times B(G_{KK} \to ZZ)$ at 95% CL as a function of the KK graviton mass, $m(G_{KK})$, are shown in Fig. 8 together with the predicted G_{KK} cross section. A spin-2 graviton is excluded up to a mass of 1830 GeV.
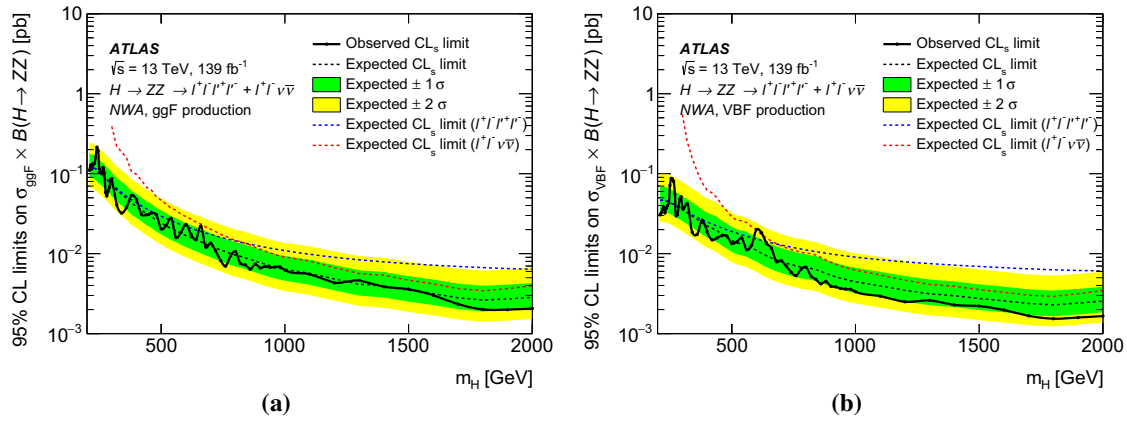
Fig. 4 The upper limits at 95% CL on the cross section times branching ratio as a function of the heavy resonance mass m_H for **a** the ggF production mode ($\sigma_{\text{ggF}} \times B(H \to ZZ)$) and **b** for the VBF production mode ($\sigma_{\text{VBF}} \times B(H \to ZZ)$) in the case of the NWA. The black line indicates the observed limit. The green and yellow bands represent the $\pm 1\sigma$ and $\pm 2\sigma$ uncertainties in the expected limits. The dashed coloured lines indicate the expected limits obtained from the individual searches
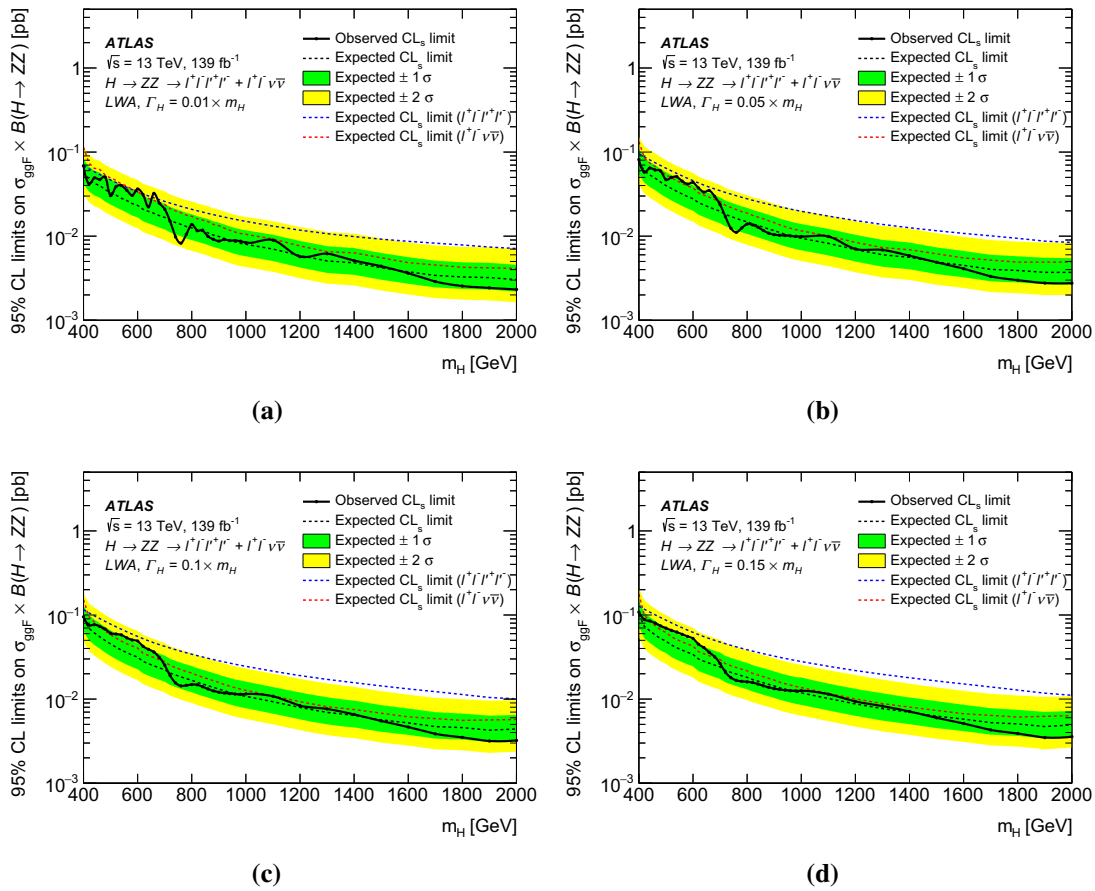
Fig. 5 The upper limits at 95% CL on the cross section for the ggF production mode times branching ratio ($\sigma_{\text{ggF}} \times B(H \to ZZ)$) as a function of m_H for an additional heavy scalar assuming a width of **a** 1%, **b** 5%, **c** 10% and **d** 15%, of m_H. The black line indicates the observed limit. The green and yellow bands represent the $\pm 1\sigma$ and $\pm 2\sigma$ uncertainties in the expected limits. The dashed coloured lines indicate the expected limits obtained from the individual searches
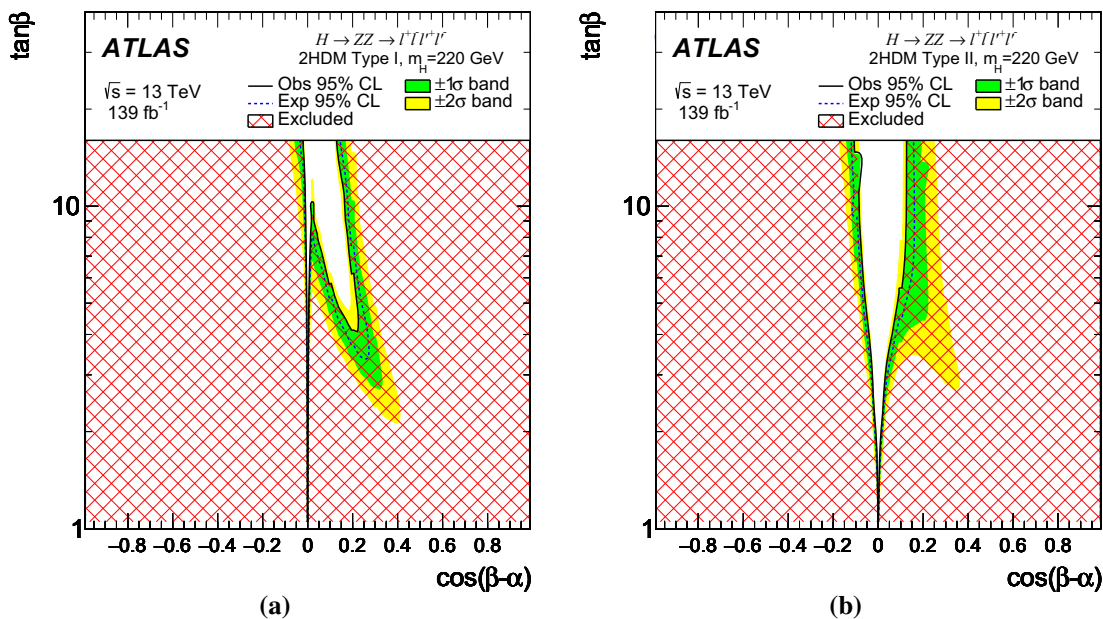
Fig. 6 The exclusion contour in the 2HDM **a** type-I and **b** type-II models for $m_H = 220$ GeV shown as a function of the parameters $\cos(\beta - \alpha)$ and $\tan\beta$. The green and yellow bands represent the $\pm 1\sigma$ and $\pm 2\sigma$ uncertainties in the expected limits. The hatched area shows the observed exclusion
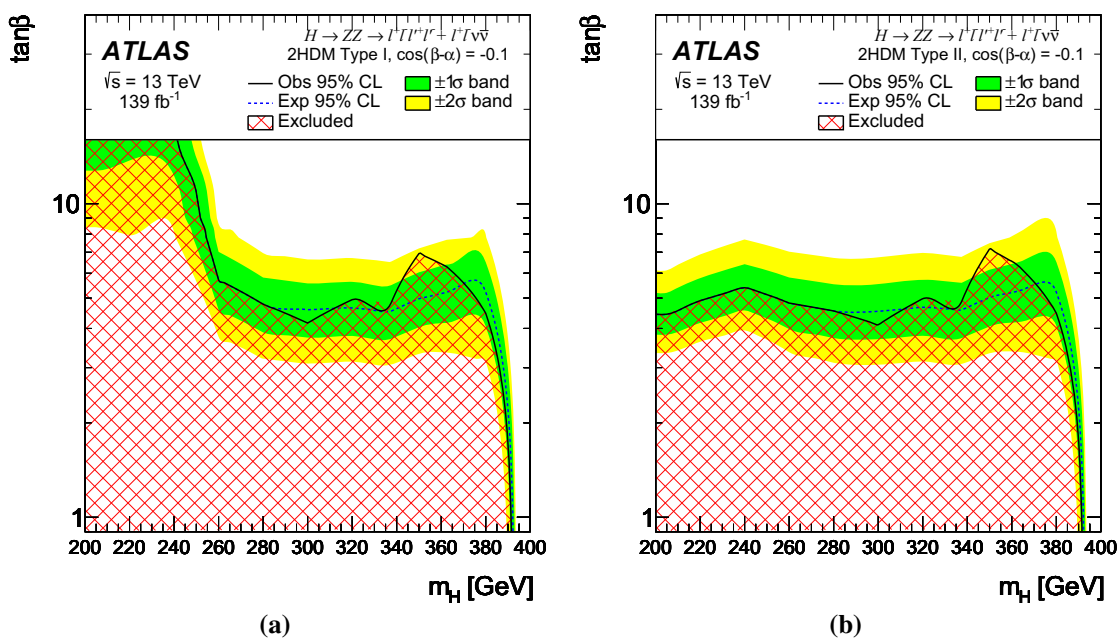
Fig. 7 The exclusion contour in the 2HDM **a** type-I and **b** type-II models for $\cos(\beta - \alpha) = -0.1$, shown as a function of the heavy scalar mass m_H and the parameter $\tan\beta$. The green and yellow bands represent the $\pm 1\sigma$ and $\pm 2\sigma$ uncertainties in the expected limits. The hatched area shows the observed exclusion

10 Summary

A search is conducted for heavy resonances decaying into a pair of Z bosons which subsequently decay into $\ell^+\ell^-\ell'^+\ell'^-$ or $\ell^+\ell^-\nu\bar{\nu}$ final states. The search uses proton–proton collision data collected with the ATLAS detector from 2015 to 2018 at the Large Hadron Collider at a centre-of-mass energy of 13 TeV corresponding to the full Run 2 integrated luminosity of 139 fb^{-1}. No significant excess is observed with respect to the predicted SM background; therefore, the results are interpreted as upper limits on the production cross section of spin-0 resonances or a spin-2 resonance. The mass
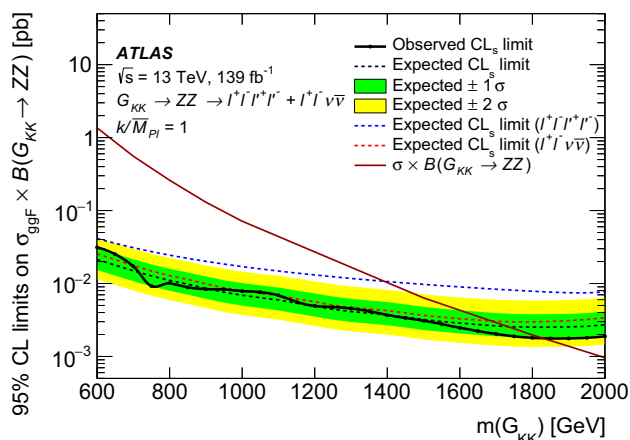
Fig. 8 The upper limits at 95% CL on cross section times branching ratio $\sigma \times B(G_{KK} \to ZZ)$ for a KK graviton produced with $k/\overline{M}_{Pl} = 1$. The black line indicates the observed limit. The green and yellow bands give the $\pm 1\sigma$ and $\pm 2\sigma$ uncertainties in the expected limits. The predicted production cross section times branching ratio as a function of the G_{KK} mass $m(G_{KK})$ is shown by the red solid line

range of the hypothetical resonances considered is between 200 GeV and 2000 GeV depending on the final state and the model considered. The spin-0 resonance is assumed to be a heavy scalar, whose dominant production modes are gluon–gluon fusion and vector-boson fusion, and it is studied in the narrow-width approximation and with the large-width assumption. In the case of the narrow-width approximation, upper limits on the production rate of a heavy scalar decaying into two Z bosons (the production cross-section times the corresponding decay branching fraction) are set separately for ggF and VBF production modes. Combining the two final states, 95% CL upper limits range from 215 fb at $m_H = 240$ GeV to 2.0 fb at $m_H = 1900$ GeV for the gluon–gluon fusion production mode and from 87 fb at $m_H = 255$ GeV to 1.5 fb at $m_H = 1800$ GeV for the vector-boson fusion production mode. The results are also interpreted in the context of Type-I and Type-II two-Higgs-doublet models, with exclusion contours given in the $\tan \beta$ versus $\cos(\beta - \alpha)$ (for $m_H = 220$ GeV) and $\tan \beta$ versus m_H planes. This m_H value is chosen so that the assumption of a narrow Higgs boson is valid over most of the parameter space and the experimental sensitivity is maximal. The limits on the production rate of a large-width scalar are obtained for widths of 1%, 5%, 10% and 15% of the mass of the resonance, with the interference between the heavy scalar and the SM Higgs boson as well as between the heavy scalar and the $gg \to ZZ$ continuum taken into account. In the framework of the Randall–Sundrum model with one warped extra dimension a graviton excitation spin-2 resonance with $m(G_{KK}) < 1830$ GeV is excluded at 95% CL.

Appendix

The results based on the cut-based categorisation as described in Sect. 5.1.3 are presented here. The number of observed candidate events with mass above 200 GeV together with the expected background yields for each of the four categories of the $\ell^+\ell^-\ell'^+\ell'^-$ analysis as described in Sect. 5.1.3 is presented in Table 5. The obtained ZZ normalisation factors

are summarised in Table 6, and the $m_{4\ell}$ spectrum in each category is shown in Fig. 9. The upper limits at 95% CL on the cross section times branching ratio as a function of the heavy resonance mass in the case of the NWA is presented in Fig. 10.

Table 5 $\ell^+\ell^-\ell'^+\ell'^-$ search: expected and observed numbers of events for $m_{4\ell} > 200$ GeV, together with their uncertainties, for the VBF-CBA-enriched and ggF-CBA-enriched categories using the cut-based categorisation. The expected numbers of events, as well as their uncertainties, are obtained from a combined likelihood fit to the data under the background-only hypothesis. The uncertainties of the ZZ normalisation factors, presented in Table 6, are also taken into account

Process	VBF-CBA-enriched	ggF-CBA-enriched		
		4μ channel	$2e2\mu$ channel	$4e$ channel
$q\bar{q} \to ZZ$	48 ± 8	860 ± 18	1360 ± 28	515 ± 11
$gg \to ZZ$	13 ± 4	114 ± 9	189 ± 14	73 ± 6
ZZ (EW)	10.9 ± 0.9	6.9 ± 0.3	11.1 ± 0.4	4.4 ± 0.2
$Z + \text{jets}/t\bar{t}/WZ$	0.3 ± 0.1	2.1 ± 0.4	6.7 ± 1.6	3.1 ± 0.4
Other backgrounds	3 ± 0.2	16.3 ± 0.4	26.8 ± 0.6	11.8 ± 0.3
Total background	75 ± 9	999 ± 20	1594 ± 31	607 ± 13
Observed	75	932	1656	612

Table 6 The ZZ normalisation factors in each category of the two final states, which scale the number of ZZ events estimated from the MC simulations, obtained from a simultaneous likelihood fit of the two final states under the background-only hypothesis. For the $\ell^+\ell^-\ell'^+\ell'^-$ final state, the cut-based categorisation is used

Analysis	Normalisation factor	Fitted value
$\ell^+\ell^-\ell'^+\ell'^-$	$\mu_{ZZ}^{\text{VBF-CBA}}$	1.1 ± 0.2
	μ_{ZZ}^{ggF}	1.10 ± 0.02
$\ell^+\ell^-\nu\bar{\nu}$	μ_{ZZ}	1.04 ± 0.06

(a)

(b)

(c)

(d)
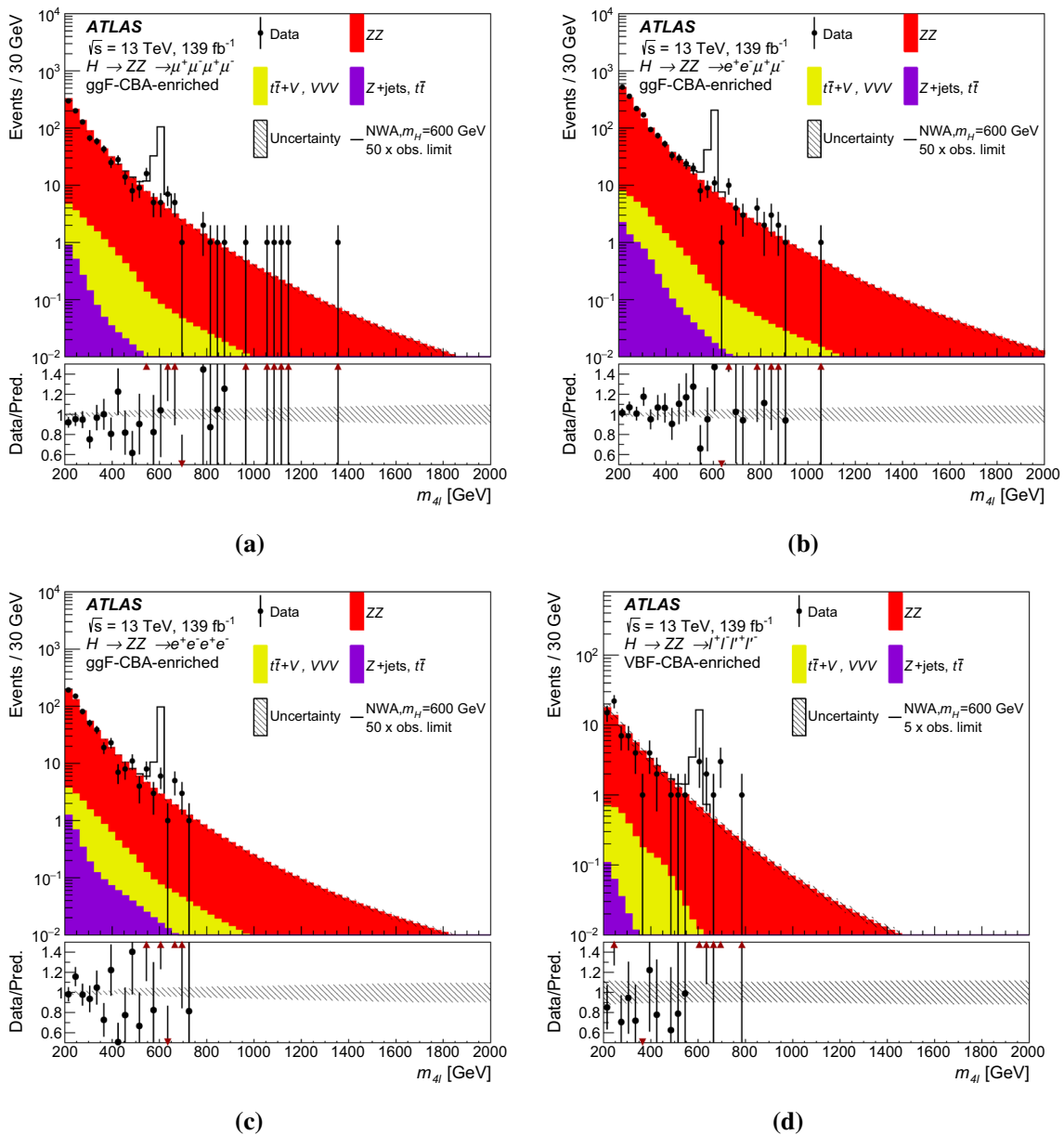
Fig. 9 Distribution of the four-lepton invariant mass $m_{4\ell}$ in the $\ell^+\ell^-\ell'^+\ell'^-$ search for **a**, **b**, **c** the ggF-CBA-enriched categories and **d** the VBF-CBA-enriched category. The backgrounds are determined from a combined likelihood fit to the data under the background-only hypothesis. The simulated $m_H = 600$ GeV signal is normalised to a cross section corresponding to 50 (5) times the observed limit given in Sect. 9.1.1 for the ggF (VBF) production mode. The error bars on the data points indicate the statistical uncertainty, while the systematic uncertainty in the prediction is shown by the hatched band. The lower panels show the ratio of data to prediction

(a)

(b)
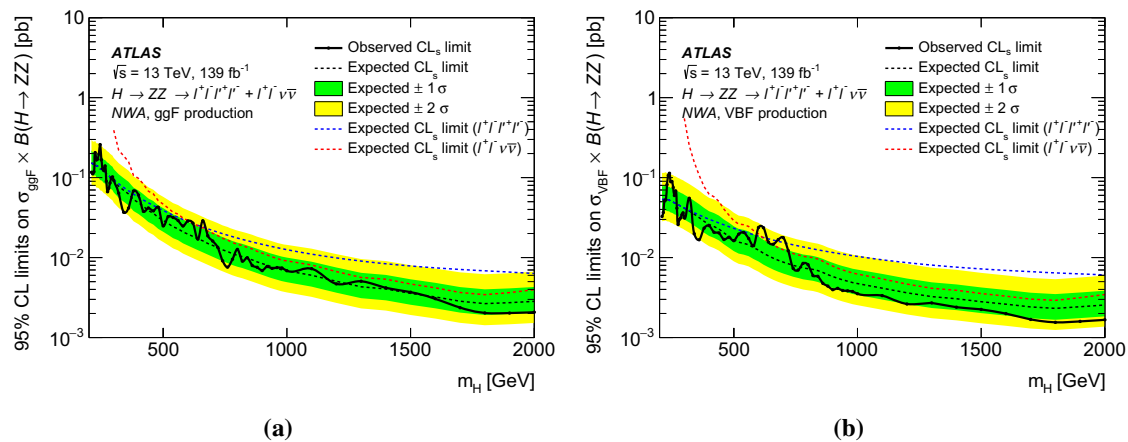
Fig. 10 The upper limits at 95% CL on the cross section times branching ratio as a function of the heavy resonance mass m_H for **a** the ggF production mode ($\sigma_{ggF} \times B(H \to ZZ)$) and **b** for the VBF production mode ($\sigma_{VBF} \times B(H \to ZZ)$) in the case of the NWA. For the

$\ell^+\ell^-\ell'^+\ell'^-$ state the cut-based categorisation is used. The green and yellow bands represent the $\pm 1\sigma$ and $\pm 2\sigma$ uncertainties in the expected limits. The dashed coloured lines indicate the expected limits obtained from the individual searches

References

1. ATLAS Collaboration, Observation of a new particle in the search for the Standard Model Higgs boson with the ATLAS detector at the LHC. Phys. Lett. B **716**, 1 (2012). arXiv:1207.7214 [hep-ex]
2. CMS Collaboration, Observation of a new boson at a mass of 125 GeV with the CMS experiment at the LHC. Phys. Lett. B **716**, 30 (2012). arXiv:1207.7235 [hep-ex]
3. ATLAS Collaboration, Measurements of the Higgs boson production and decay rates and coupling strengths using pp collision data at $\sqrt{s} = 7$ and 8 TeV in the ATLAS experiment. Eur. Phys. J. C **76**, 6 (2016). arXiv:1507.04548 [hep-ex]
4. CMS Collaboration, Precise determination of the mass of the Higgs boson and tests of compatibility of its couplings with the standard model predictions using proton collisions at 7 and 8 TeV. Eur. Phys. J. C **75**, 212 (2015). arXiv:1412.8662 [hep-ex]
5. ATLAS Collaboration, Evidence for the spin-0 nature of the Higgs boson using ATLAS data. Phys. Lett. B **726**, 120 (2013). arXiv:1307.1432 [hep-ex]
6. ATLAS Collaboration, Combined measurements of Higgs boson production and decay using up to 80 fr^{-1} of proton–proton collision data at $\sqrt{s} = 13$ TeV collected with the ATLAS experiment. Phys. Rev. D **101**, 012002 (2020). arXiv:1909.02845 [hep-ex]
7. CMS collaboration, Combined measurements of Higgs boson couplings in proton–proton collisions at $\sqrt{s} = 13$ TeV. Eur. Phys. J. C **79**, 421 (2019). arXiv:1809.10733 [hep-ex]
8. S. Glashow, Partial-symmetries of weak interactions. Nucl. Phys. **22**, 579 (1961)
9. S. Weinberg, A Model of Leptons. Phys. Rev. Lett. **19**, 1264 (1967)
10. A. Salam, Weak and electromagnetic interactions. Conf. Proc. C **680519**, 367 (1968)
11. F. Englert, R. Brout, Broken symmetry and the mass of gauge vector mesons. Phys. Rev. Lett. **13**, 321 (1964)
12. P.W. Higgs, Broken symmetries and the masses of gauge bosons. Phys. Rev. Lett. **13**, 508 (1964)
13. G.S. Guralnik, C.R. Hagen, T.W.B. Kibble, Global conservation laws and massless particles. Phys. Rev. Lett. **13**, 585 (1964)
14. G. Branco et al., Theory and phenomenology of two-Higgs-doublet models. Phys. Rep. **516**, 1 (2012). arXiv:1106.0034 [hep-ph]
15. M. Tanabashi et al., Review of particle physics. Phys. Rev. D **98**, 030001 (2018)
16. L. Randall, R. Sundrum, A large mass hierarchy from a small extra dimension. Phys. Rev. Lett. **83**, 3370 (1999). arXiv:hep-ph/9905221
17. H. Davoudiasl, J.L. Hewett, T.G. Rizzo, Bulk gauge fields in the Randall–Sundrum model. Phys. Lett. B **473**, 43 (2000). arXiv:hep-ph/9911262
18. ATLAS Collaboration, Search for heavy ZZ resonances in the $l^+l^-l^+l^-$ and $l^+l^-\nu\bar{\nu}$ final states using proton–proton collisions at $\sqrt{s} = 13$ TeV with the ATLAS detector. Eur. Phys. J. C **78**, 293 (2018). arXiv:1712.06386 [hep-ex]
19. CMS Collaboration, Search for a new scalar resonance decaying to a pair of Z bosons in proton–proton collisions at $\sqrt{s} = 13$ TeV. JHEP **06**, 127 (2018) (**Erratum: JHEP 03, 128 (2019)**). arXiv:1804.01939 [hep-ex]
20. ATLAS Collaboration, The ATLAS Experiment at the CERN Large Hadron Collider. JINST **3**, S08003 (2008)
21. ATLAS Collaboration, ATLAS Intertable B-Layer Technical Design Report. CERN-LHCC-2010-013, ATLAS-TDR-19, (2010). https://cds.cern.ch/record/1291633, ATLAS Insertable B-Layer Technical Design Report Addendum, ATLAS-TDR-19-ADD-l, 2012, https://cds.cern.ch/record/1451888
22. ATLAS Collaboration, Performance of the ATLAS Trigger System in 2015. Eur. Phys. J. C **77**, 317 (2017). arXiv:1611.09661 [hep-ex]
23. ATLAS Collaboration, ATLAS data quality operations and performance for 2015–2018 data-taking. JINST **15**, P04003 (2020). arXiv:1911.04632 [physics.ins-det]
24. ATLAS Collaboration, The ATLAS simulation infrastructure. Eur. Phys. J. C **70**, 823 (2010). arXiv:1005.4568 [physics.ins-det]
25. S. Agostinelli et al., GEANT4: a simulation toolkit. Nucl. Instrum. Methods A **506**, 250 (2003)
26. T. Sjöstrand, S. Mrenna, P.Z. Skands, A brief introduction to PYTHIA 8.1. Comput. Phys. Commun. **178**, 852 (2008). arXiv:0710.3820 [hep-ph]
27. ATLAS Collaboration, Summary of ATLAS Pythia 8 tunes, ATL-PHYS-PUB-2012-003, (2012). https://cds.cern.ch/record/1474107

28. A.D. Martin, W.J. Stirling, R.S. Thorne, G. Watt, Parton distributions for the LHC. Eur. Phys. J. C **63**, 189 (2009). arXiv:0901.0002 [hep-ph]

29. P. Nason, G. Zanderighi, W^+W^-, WZ and ZZ production in the POWHEG-BOX-V2. Eur. Phys. J. C **74**, 2702 (2014). arXiv:1311.1365 [hep-ph]

30. T. Sjöstrand et al., An introduction to PYTHIA 8.2. Comput. Phys. Commun. **191**, 159 (2015). arXiv: 1410.3012 [hep-ph]

31. ATLAS Collaboration, Measurement of the $Z/\gamma*$ boson transverse momentum distribution in pp collisions at $\sqrt{s} = 7$ TeV with the ATLAS detector. JHEP **09** 145 (2014). arXiv:1406.3660 [hep-ex]

32. D.J. Lange, The EvtGen particle decay simulation package. Nucl. Instrum. Methods A **462**, 152 (2001)

33. H.-L. Lai et al., New parton distributions for collider physics. Phys. Rev. D **82**, 074024 (2010). arXiv:1007.2241 [hep-ph]

34. J. Alwall et al., The automated computation of tree-level and next-to-leading order differential cross sections, and their matching to parton shower simulations. JHEP **07**, 079 (2014). arXiv:1405.0301 [hep-ph]

35. ATLAS Collaboration, ATLAS Pythia 8 tunes to 7 TeV data, ATL-PHYS-PUB-2014-021 (2014). https://cds.cern.ch/record/1966419

36. K. Agashe, H. Davoudiasl, G. Perez, A. Soni, Warped gravitons at the CERN LHC and beyond. Phys. Rev. D **76**, 036006 (2007)

37. R.D. Ball et al., Parton distributions for the LHC Run II. JHEP **04**, 040 (2015). arXiv:1410.8849 [hep-ph]

38. E. Bothmann et al., Event generation with Sherpa 2.2. SciPost Phys. **7**, 034 (2019). arXiv:1905.09127 [hep-ph]

39. T. Gleisberg, S. Höche, Comix, a new matrix element generator. JHEP **12**, 039 (2008). arXiv:0808.3674 [hep-ph]

40. F. Buccioni et al., OpenLoops 2. Eur. Phys. J. C **79**, 866 (2019). arXiv:1907.13071 [hep-ph]

41. F. Cascioli, P. Maieröfer, S. Pozzorini, Scattering amplitudes with open loops. Phys. Rev. Lett. **108**, 111601 (2012). arXiv:1111.5206 [hep-ph]

42. A. Denner, S. Dittmaier, L. Hofer, Collier: a fortran-based complex one-loop library in extended regularizations. Comput. Phys. Commun. **212**, 220 (2017). arXiv:1604.06792 [hep-ph]

43. S. Schumann, F. Krauss, A Parton shower algorithm based on Catani–Seymour dipole factorisation. JHEP **03**, 038 (2008). arXiv:0709.1027 [hep-ph]

44. S. Höche, F. Krauss, M. Schönherr, F. Siegert, QCD matrix elements + parton showers. The NLO case. JHEP **04**, 027 (2013). arXiv:1207.5030 [hep-ph]

45. B. Biedermann, A. Denner, S. Dittmaier, L. Hofer, B. Jäger, Electroweak corrections to pp $\rightarrow \mu^+\mu^-e^+e^- + X$ at the LHC: a Higgs Boson background study. Phys. Rev. Lett. **116**, 161803 (2016). arXiv:1601.07787 [hep-ph]

46. B. Biedermann, A. Denner, S. Dittmaier, L. Hofer, B. Jäger, Next-to-leading-order electroweak corrections to the production of four charged leptons at the LHC. JHEP **01**, 033 (2017). arXiv:1611.05338 [hep-ph]

47. S. Kallweit, J.M. Lindert, P. Maierhofer, S. Pozzorini, M. Schönherr, NLO electroweak automation and precise predictions for W + multijet production at the LHC. JHEP **04**, 012 (2015). arXiv:1412.5157 [hep-ph]

48. S. Kallweit, J. Lindert, S. Pozzorini, M. Schonherr, NLO QCD + EW predictions for $2l2\nu$ diboson signatures at the LHC. JHEP **11**, 120 (2017). arXiv:1705.00598 [hep-ph]

49. M. Schönherr, An automated subtraction of NLO EW infrared divergences. Eur. Phys. J. C **78**, 119 (2018). arXiv:1712.07975 [hep-ph]

50. M. Grazzini, S. Kallweit, J.M. Lindert, S. Pozzorini, M. Wiesemann, NNLO QCD + NLO EW with Matrix + OpenLoops: precise predictions for vector-boson pair production. JHEP **02**, 087 (2020). arXiv:1912.00068 [hep-ph]

51. F. Caola, K. Melnikov, R. Röntsch, L. Tancredi, QCD corrections to ZZ production in gluon fusion at the LHC. Phys. Rev. D **92**, 094028 (2015). arXiv:1509.06734 [hep-ph]

52. J.M. Campbell, R.K. Ellis, M. Czakon, S. Kirchner, Two loop correction to interference in gg $\rightarrow$ ZZ. JHEP **08**, 011 (2016). arXiv:1605.01380 [hep-ph]

53. S. Alioli, F. Caola, G. Luisoni, R. Röntsch, ZZ production in gluon fusion at NLO matched to parton-shower. Phys. Rev. D **95**, 034042 (2017). arXiv:1609.09719 [hep-ph]

54. K. Melnikov, M. Dowling, Production of two Z-bosons in gluon fusion in the heavy top quark approximation. Phys. Lett. B **744**, 43 (2015). arXiv:1503.01274 [hep-ph]

55. C.S. Li, H.T. Li, D.Y. Shao, J. Wang, Soft gluon resummation in the signal-background interference process of $gg(\rightarrow h^*) \rightarrow ZZ$. JHEP **08**, 065 (2015). arXiv:1504.02388 [hep-ph]

56. R. Gavin, Y. Li, F. Petriello, S. Quackenbush, FEWZ 2.0: a code for hadronic Z production at next-to-next-to-leading order. Comput. Phys. Commun. **182**, 2388 (2011). arXiv:1011.3540 [hep-ph]

57. S. Frixione, V. Hirschi, D. Pagani, H.-S. Shao, M. Zaro, Electroweak and QCD corrections to top-pair hadroproduction in association with heavy bosons. JHEP **06**, 184 (2015). arXiv:1504.03446 [hep-ph]

58. J.M. Campbell, R.K. Ellis, C. Williams, Vector boson pair production at the LHC. JHEP **07**, 18 (2011). arXiv:1105.0020 [hep-ph]

59. N. Kauer, G. Passarino, Inadequacy of zero-width approximation for a light Higgs boson signal. JHEP **08**, 116 (2012). arXiv:1206.4803 [hep-ph]

60. N. Kauer, Interference effects for $H \rightarrow WW/ZZ \rightarrow l\bar{\nu}_l\bar{l}\nu_l$ searches in gluon fusion at the LHC. JHEP **12**, 082 (2013). arXiv:1310.7011 [hep-ph]

61. ATLAS Collaboration, Electron and photon performance measurements with the ATLAS detector using the 2015-2017 LHC proton–proton collision data. JINST **14**, P12006 (2019). arXiv:1908.00005 [hep-ex]

62. ATLAS Collaboration, Improved electron reconstruction in ATLAS using the Gaussian Sum Filter-based model for bremsstrahlung. ATLAS-CONF-2012-047 (2012). https://cds.cern.ch/record/1449796

63. ATLAS Collaboration, Electron reconstruction and identification in the ATLAS experiment using the 2015 and 2016 LHC proton–proton collision data at $\sqrt{s} = 13\,TeV$. Eur. Phys. J. C **79**, 639 (2019). arXiv:1902.04655 [hep-ex]

64. ATLAS Collaboration, Muon reconstruction performance of the ATLAS detector in proton–proton collision data at $\sqrt{s} = 13\,TeV$. Eur. Phys. J. C **76**, 292 (2016). arXiv:1603.05598 [hep-ex]

65. ATLAS Collaboration, Jet reconstruction and performance using particle flow with the ATLAS Detector. Eur. Phys. J. C **77**, 466 (2017). arXiv:1703.10485 [hep-ex]

66. ATLAS Collaboration, Topological cell clustering in the ATLAS calorimeters and its performance in LHC Run 1. Eur. Phys. J. C **77**, 490 (2017). arXiv:1603.02934 [hep-ex]

67. M. Cacciari, G.P. Salam, G. Soyez, The anti-k_t jet clustering algorithm. JHEP **04**, 063 (2008). arXiv:0802.1189 [hep-ph]

68. ATLAS Collaboration, Jet energy scale measurements and their systematic uncertainties in proton–proton collisions at $\sqrt{s} = 13\,TeV$ with the ATLAS detector. Phys. Rev. D **96**, 072002 (2017). arXiv:1703.09665 [hep-ex]

69. ATLAS Collaboration, Tagging and suppression of pileup jets with the ATLAS detector, tech. rep. ATLAS-CONF-2014-018, CERN (2014). https://cds.cern.ch/record/1700870

70. ATLAS Collaboration, *Performance of pile-up mitigation techniques for jets in pp collisions at $\sqrt{s} = 8\,TeV$ using the ATLAS detector,* Eur. Phys. J. C 76, 581 (2016). arXiv: 1510.03823 [hep-ex]

71. ATLAS Collaboration, ATLAS b-jet identification performance and efficiency measurement with $t\bar{t}$ events in pp collisions at $\sqrt{s}=$ 13 TeV. Eur. Phys. J. C **79**, 970 (2019). arXiv:1907.05120 [hep-ex]

72. ATLAS Collaboration, *Performance of missing transverse momentum reconstruction with the ATLAS detector using proton-proton collisions at $\sqrt{s}=13TeV$* , Eur. Phys. J. C 78, 903 (2018), arXiv:1802.08168 [hep-ex]

73. ATLAS Collaboration, *2015 start-up trigger menu and initial performance assessment of the ATLAS trigger using Run-2 data,* ATL-DAQ-PUB-2016-001, (2016), URL: https://cds.cern.ch/record/2136007

74. ATLAS Collaboration, *Trigger Menu in 2016,* ATL-DAQ-PUB-2017-001, (2017), URL: https://cds.cern.ch/record/2242069

75. ATLAS Collaboration, *Search for an additional, heavy Higgs boson in the $H \to ZZ$ decay channel at $\sqrt{s}=8$ TeV in pp collision data with the ATLAS detector,* Eur. Phys. J. C 76, 45 (2016), arXiv:1507.05930 [hep-ex]

76. ATLAS Collaboration, *Measurement of the Higgs boson mass from the $H \to \gamma\gamma$ and $H \to ZZ^* \to 4l$ channels in pp collisions at center-of-mass energies of 7 and 8 TeV with the ATLAS detector,* Phys. Rev. D 90, 052004 (2014), arXiv:1406.3827 [hep-ex]

77. ATLAS Collaboration, Higgs boson production cross-section measurements and their EFT interpretation in the $4l$ decay channel at $\sqrt{s}=$ 13 TeV with the ATLAS detector, (2020), arXiv:2004.03447 [hep-ex]

78. M. Abadi et al., *TensorFlow: Large-Scale Machine Learning on Heterogeneous Systems,* (2015), URL: https://www.tensorflow.org/

79. ATLAS Collaboration, *Measurement of inclusive and differential cross sections in the $H \to ZZ^* \to 4l$ At decay channel in pp collisions at $\sqrt{s}=$ 13 TeV with the ATLAS detector,* JHEP 10, 132 (2017), arXiv:1708.02810 [hep-ex]

80. ATLAS Collaboration, *Measurement of the Higgs boson coupling properties in the $H \to ZZ^* \to 4l$ decay channel at $\sqrt{s}=13$ TeV with the ATLAS detector,* JHEP 03, 095 (2018), arXiv:1712.02304 [hep-ex]

81. M. Pivk, F.R. Le Diberder, SPlot: A Statistical tool to unfold data distributions. Nucl. Instrum. Meth. A **555**, 356 (2005). arXiv:physics/0402083 [physics.data-an]

82. M. Oreglia, *A Study of the Reactions $\psi' \to \gamma\gamma\psi$* , (1980), URL: https://www.slac.Stanford.edu/cgi-wrap/getdoc/slac-r-236.pdf

83. J. Gaiser, *Charmonium Spectroscopy From Radiative Decays of the J/ψ and ψ',* (1982), URL: https://www.slac.Stanford.edu/cgi-wrap/getdoc/slac-r-255.pdf

84. S. Goria, G. Passarino, D. Rosco, The Higgs-boson lineshape. Nucl. Phys. B **864**, 530 (2012). arXiv:1112.5517 [hep-ph]

85. J. Bijnens, P. Eerola, M. Maul, A. Mansson, T. Sjostrand, QCD signatures of narrow graviton resonances in hadron colliders. Phys. Lett. B **503**, 341 (2001). arXiv:hep-ph/0101316

86. N. Kauer, C. O'Brien, Heavy Higgs signal-background interference in $gg \to VV$ in the Standard Model plus real singlet. Eur. Phys. J. C **75**, 374 (2015). arXiv:1502.04113 [hep-ph]

87. ATLAS Collaboration, *Object-based missing transverse momentum significance in the ATLAS Detector,* ATLAS-CONF-2018-038, (2018), URL: https://cds.cern.ch/record/2630948

88. ATLAS Collaboration, *Measurement of $W^{\pm}Z$ production cross sections and gauge boson polarisation in pp collisions at $\sqrt{s}=13$ TeV with the ATLAS detector,* Eur. Phys. J. C 79, 535 (2019), arXiv:1902.05759 [hep-ex]

89. ATLAS Collaboration, *Observation of electroweak $W^{\pm}Z$ boson pair production in association with two jets in pp collisions at $\sqrt{s}=13$ TeV with the ATLAS detector,* Phys. Lett. B 793, 469 (2019), arXiv:1812.09740 [hep-ex]

90. M. Baak, S. Gadatsch, R. Harrington, W. Verkerke, Interpolation between multi-dimensional histograms using a new non-linear moment morphing method. Nucl. Instrum. Meth. A **771**, 39 (2015). arXiv:1410.7388 [physics.data-an]

91. ATLAS Collaboration, *Luminosity determination in pp collisions at $\sqrt{s}=13$ TeV using the ATLAS detector at the LHC,* ATLAS-CONF-2019-021, (2019), URL: https://cds.cern.ch/record/2677054

92. G. Avoni et al., The new LUCID-2 detector for luminosity measurement and monitoring in ATLAS. JINST **13**, P07017 (2018)

93. ATLAS Collaboration, *Jet energy scale measurements and their systematic uncertainties in proton-proton collisions at $\sqrt{s}=13$ TeV with the ATLAS detector,* Phys. Rev. D **96**, 072002 (2017), arXiv:1703.09665 [hep-ex]

94. ATLAS Collaboration, *Performance of missing transverse momentum reconstruction with the ATLAS detector using proton-proton collisions at $\sqrt{s}=13$ TeV,* Eur. Phys. J. C **78**, 903 (2018), arXiv:1802.08168 [hep-ex]

95. J. Butterworth et al., PDF4LHC recommendations for LHC Run II. J. Phys. G **43**, 023001 (2016). arXiv:1510.03865 [hep-ph]

96. ATLAS and CMS Collaboration, *Procedure for the LHC Higgs boson search combination in summer 2011,* ATL-PHYS-PUB-2011-011, CMS-NOTE-2011-005, (2011), URL: https://cds.cern.ch/record/1375842

97. ATLAS Collaboration, *Combined search for the Standard Model Higgs boson in pp collisions at $\sqrt{s}=7$ TeV with the ATLAS detector,* Phys. Rev. D **86**, 032003 (2012), arXiv:1207 . 0319 [hep-ex]

98. A.L. Read, Presentation of search results: the CLs technique. J. Phys. G **28**, 2693 (2002)

99. ATLAS Collaboration, *Combined measurements of Higgs boson production and decay using up to 80 fb^{-1} of proton-proton collision data at $\sqrt{s}=13$ TeV collected with the ATLAS experiment,* Phys. Rev. D **101**, 012002 (2020), arXiv:1909.02845 [hep-ex]

100. *ATLAS Computing Acknowledgements,* tech. rep. ATL-SOFT-PUB-2020-001, CERN, (2020), URL: https://cds.cern.ch/record/2717821

Springer

ATLAS Collaboration

G. Aad[102], B. Abbott[128], D. C. Abbott[103], A. Abed Abud[36], K. Abeling[53], D. K. Abhayasinghe[94], S. H. Abidi[167], O. S. AbouZeid[40], N. L. Abraham[156], H. Abramowicz[161], H. Abreu[160], Y. Abulaiti[6], B. S. Acharya[67a,67b,n], B. Achkar[53], L. Adam[100], C. Adam Bourdarios[5], L. Adamczyk[84a], L. Adamek[167], J. Adelman[121], A. Adiguzel[12c,ac], S. Adorni[54], T. Adye[143], A. A. Affolder[145], Y. Afik[160], C. Agapopoulou[65], M. N. Agaras[38], A. Aggarwal[119], C. Agheorghiesei[27c], J. A. Aguilar-Saavedra[139a,139f,ab], A. Ahmad[36], F. Ahmadov[80], W. S. Ahmed[104], X. Ai[18], G. Aielli[74a,74b], S. Akatsuka[86], M. Akbiyik[100], T. P. A. Åkesson[97], E. Akilli[54], A. V. Akimov[111], K. Al Khoury[65], G. L. Alberghi[23a,23b], J. Albert[176], M. J. Alconada Verzini[161], S. Alderweireldt[36], M. Aleksa[36], I. N. Aleksandrov[80], C. Alexa[27b], T. Alexopoulos[10], A. Alfonsi[120], F. Alfonsi[23a,23b], M. Alhroob[128], B. Ali[141], S. Ali[158], M. Aliev[166], G. Alimonti[69a], C. Allaire[36], B. M. M. Allbrooke[156], B. W. Allen[131], P. P. Allport[21], A. Aloisio[70a,70b], F. Alonso[89], C. Alpigiani[148], E. Alunno Camelia[74a,74b], M. Alvarez Estevez[99], M. G. Alviggi[70a,70b], Y. Amaral Coutinho[81b], A. Ambler[104], L. Ambroz[134], C. Amelung[36], D. Amidei[106], S. P. Amor Dos Santos[139a], S. Amoroso[46], C. S. Amrouche[54], F. An[79], C. Anastopoulos[149], N. Andari[144], T. Andeen[11], J. K. Anders[20], S. Y. Andrean[45a,45b], A. Andreazza[69a,69b], V. Andrei[61a], C. R. Anelli[176], S. Angelidakis[9], A. Angerami[39], A. V. Anisenkov[122a,122b], A. Annovi[72a], C. Antel[54], M. T. Anthony[149], E. Antipov[129], M. Antonelli[51], D. J. A. Antrim[18], F. Anulli[73a], M. Aoki[82], J. A. Aparisi Pozo[174], M. A. Aparo[156], L. Aperio Bella[46], N. Aranzabal[36], V. Araujo Ferraz[81a], R. Araujo Pereira[81b], C. Arcangeletti[51], A. T. H. Arce[49], J-F. Arguin[110], S. Argyropoulos[52], J.-H. Arling[46], A. J. Armbruster[36], A. Armstrong[171], O. Arnaez[167], H. Arnold[120], Z. P. Arrubarrena Tame[114], G. Artoni[134], H. Asada[117], K. Asai[126], S. Asai[163], T. Asawatavonvanich[165], N. Asbah[59], E. M. Asimakopoulou[172], L. Asquith[156], J. Assahsah[35e], K. Assamagan[29], R. Astalos[28a], R. J. Atkin[33a], M. Atkinson[173], N. B. Atlay[19], H. Atmani[65], P. A. Atmasiddha[106], K. Augsten[141], V. A. Austrup[182], G. Avolio[36], M. K. Ayoub[15a], G. Azuelos[110,aj], D. Babal[28a], H. Bachacou[144], K. Bachas[162], F. Backman[45a,45b], P. Bagnaia[73a,73b], M. Bahmani[85], H. Bahrasemani[152], A. J. Bailey[174], V. R. Bailey[173], J. T. Baines[143], C. Bakalis[10], O. K. Baker[183], P. J. Bakker[120], E. Bakos[16], D. Bakshi Gupta[8], S. Balaji[157], R. Balasubramanian[120], E. M. Baldin[122a,122b], P. Balek[180], F. Balli[144], W. K. Balunas[134], J. Balz[100], E. Banas[85], M. Bandieramonte[138], A. Bandyopadhyay[19], Sw. Banerjee[181,i], L. Barak[161], W. M. Barbe[38], E. L. Barberio[105], D. Barberis[55a,55b], M. Barbero[102], G. Barbour[95], T. Barillari[115], M-S. Barisits[36], J. Barkeloo[131], T. Barklow[153], R. Barnea[160], B. M. Barnett[143], R. M. Barnett[18], Z. Barnovska-Blenessy[60a], A. Baroncelli[60a], G. Barone[29], A. J. Barr[134], L. Barranco Navarro[45a,45b], F. Barreiro[99], J. Barreiro Guimarães da Costa[15a], U. Barron[161], S. Barsov[137], F. Bartels[61a], R. Bartoldus[153], G. Bartolini[102], A. E. Barton[90], P. Bartos[28a], A. Basalaev[46], A. Basan[100], A. Bassalat[65,ag], M. J. Basso[167], R. L. Bates[57], S. Batlamous[35f], J. R. Batley[32], B. Batool[151], M. Battaglia[145], M. Bauce[73a,73b], F. Bauer[144,*], P. Bauer[24], H. S. Bawa[31], A. Bayirli[12c], J. B. Beacham[49], T. Beau[135], P. H. Beauchemin[170], F. Becherer[52], P. Bechtle[24], H. C. Beck[53], H. P. Beck[20,p], K. Becker[178], C. Becot[46], A. Beddall[12d], A. J. Beddall[12a], V. A. Bednyakov[80], M. Bedognetti[120], C. P. Bee[155], T. A. Beermann[182], M. Begalli[81b], M. Begel[29], A. Behera[155], J. K. Behr[46], F. Beisiegel[24], M. Belfkir[5], A. S. Bell[95], G. Bella[161], L. Bellagamba[23b], A. Bellerive[34], P. Bellos[9], K. Beloborodov[122a,122b], K. Belotskiy[112], N. L. Belyaev[112], D. Benchekroun[35a], N. Benekos[10], Y. Benhammou[161], D. P. Benjamin[6], M. Benoit[29], J. R. Bensinger[26], S. Bentvelsen[120], L. Beresford[134], M. Beretta[51], D. Berge[19], E. Bergeaas Kuutmann[172], N. Berger[5], B. Bergmann[141], L. J. Bergsten[26], J. Beringer[18], S. Berlendis[7], G. Bernardi[135], C. Bernius[153], F. U. Bernlochner[24], T. Berry[94], P. Berta[100], A. Berthold[48], I. A. Bertram[90], O. Bessidskaia Bylund[182], N. Besson[144], S. Bethke[115], A. Betti[42], A. J. Bevan[93], J. Beyer[115], S. Bhatta[155], D. S. Bhattacharya[177], P. Bhattarai[26], V. S. Bhopatkar[6], R. Bi[138], R. M. Bianchi[138], O. Biebel[114], D. Biedermann[19], R. Bielski[36], K. Bierwagen[100], N. V. Biesuz[72a,72b], M. Biglietti[75a], T. R. V. Billoud[141], M. Bindi[53], A. Bingul[12d], C. Bini[73a,73b], S. Biondi[23a,23b], C. J. Birch-sykes[101], M. Birman[180], T. Bisanz[36], J. P. Biswal[3], D. Biswas[181,i], A. Bitadze[101], C. Bittrich[48], K. Bjørke[133], T. Blazek[28a], I. Bloch[46], C. Blocker[26], A. Blue[57], U. Blumenschein[93], G. J. Bobbink[120], V. S. Bobrovnikov[122a,122b], S. S. Bocchetta[97], D. Bogavac[14], A. G. Bogdanchikov[122a,122b], C. Bohm[45a], V. Boisvert[94], P. Bokan[172,53], T. Bold[84a], A. E. Bolz[61b], M. Bomben[135], M. Bona[93], J. S. Bonilla[131], M. Boonekamp[144], C. D. Booth[94], A. G. Borbély[57], H. M. Borecka-Bielska[91], L. S. Borgna[95], A. Borisov[123], G. Borissov[90], D. Bortoletto[134], D. Boscherini[23b], M. Bosman[14], J. D. Bossio Sola[104], K. Bouaouda[35a], J. Boudreau[138], E. V. Bouhova-Thacker[90], D. Boumediene[38], A. Boveia[127], J. Boyd[36],

D. Boye[33c], I. R. Boyko[80], A. J. Bozson[94], J. Bracinik[21], N. Brahimi[60c,60d], G. Brandt[182], O. Brandt[32], F. Braren[46], B. Brau[103], J. E. Brau[131], W. D. Breaden Madden[57], K. Brendlinger[46], R. Brener[160], L. Brenner[36], R. Brenner[172], S. Bressler[180], B. Brickwedde[100], D. L. Briglin[21], D. Britton[57], D. Britzger[115], I. Brock[24], R. Brock[107], G. Brooijmans[39], W. K. Brooks[146d], E. Brost[29], P. A. Bruckman de Renstrom[85], B. Brüers[46], D. Bruncko[28b], A. Bruni[23b], G. Bruni[23b], M. Bruschi[23b], N. Bruscino[73a,73b], L. Bryngemark[153], T. Buanes[17], Q. Buat[155], P. Buchholz[151], A. G. Buckley[57], I. A. Budagov[80], M. K. Bugge[133], O. Bulekov[112], B. A. Bullard[59], T. J. Burch[121], S. Burdin[91], C. D. Burgard[120], A. M. Burger[129], B. Burghgrave[8], J. T. P. Burr[46], C. D. Burton[11], J. C. Burzynski[103], V. Büscher[100], E. Buschmann[53], P. J. Bussey[57], J. M. Butler[25], C. M. Buttar[57], J. M. Butterworth[95], P. Butti[36], W. Buttinger[143], C. J. Buxo Vazquez[107], A. Buzatu[158], A. R. Buzykaev[122a,122b], G. Cabras[23a,23b], S. Cabrera Urbán[174], D. Caforio[56], H. Cai[138], V. M. M. Cairo[153], O. Cakir[4a], N. Calace[36], P. Calafiura[18], G. Calderini[135], P. Calfayan[66], G. Callea[57], L. P. Caloba[81b], A. Caltabiano[74a,74b], S. Calvente Lopez[99], D. Calvet[38], S. Calvet[38], T. P. Calvet[102], M. Calvetti[72a,72b], R. Camacho Toro[135], S. Camarda[36], D. Camarero Munoz[99], P. Camarri[74a,74b], M. T. Camerlingo[75a,75b], D. Cameron[133], C. Camincher[36], S. Campana[36], M. Campanelli[95], A. Camplani[40], V. Canale[70a,70b], A. Canesse[104], M. Cano Bret[78], J. Cantero[129], T. Cao[161], Y. Cao[173], M. Capua[41a,41b], R. Cardarelli[74a], F. Cardillo[174], G. Carducci[41a,41b], I. Carli[142], T. Carli[36], G. Carlino[70a], B. T. Carlson[138], E. M. Carlson[168a,176], L. Carminati[69a,69b], R. M. D. Carney[153], S. Caron[119], E. Carquin[146d], S. Carrá[46], G. Carratta[23a,23b], J. W. S. Carter[167], T. M. Carter[50], M. P. Casado[14,f], A. F. Casha[167], E. G. Castiglia[183], F. L. Castillo[174], L. Castillo Garcia[14], V. Castillo Gimenez[174], N. F. Castro[139a,139e], A. Catinaccio[36], J. R. Catmore[133], A. Cattai[36], V. Cavaliere[29], V. Cavasinni[72a,72b], E. Celebi[12b], F. Celli[134], K. Cerny[130], A. S. Cerqueira[81a], A. Cerri[156], L. Cerrito[74a,74b], F. Cerutti[18], A. Cervelli[23a,23b], S. A. Cetin[12b], Z. Chadi[35a], D. Chakraborty[121], J. Chan[181], W. S. Chan[120], W. Y. Chan[91], J. D. Chapman[32], B. Chargeishvili[159b], D. G. Charlton[21], T. P. Charman[93], M. Chatterjee[20], C. C. Chau[34], S. Che[127], S. Chekanov[6], S. V. Chekulaev[168a], G. A. Chelkov[80,ae], B. Chen[79], C. Chen[60a], C. H. Chen[79], H. Chen[15c], H. Chen[29], J. Chen[60a], J. Chen[39], J. Chen[26], S. Chen[136], S. J. Chen[15c], X. Chen[15b], Y. Chen[60a], Y-H. Chen[46], H. C. Cheng[63a], H. J. Cheng[15a], A. Cheplakov[80], E. Cheremushkina[123], R. Cherkaoui El Moursli[35f], E. Cheu[7], K. Cheung[64], T. J. A. Chevalérias[144], L. Chevalier[144], V. Chiarella[51], G. Chiarelli[72a], G. Chiodini[68a], A. S. Chisholm[21], A. Chitan[27b], I. Chiu[163], Y. H. Chiu[176], M. V. Chizhov[80], K. Choi[11], A. R. Chomont[73a,73b], Y. Chou[103], Y. S. Chow[120], L. D. Christopher[33e], M. C. Chu[63a], X. Chu[15a,15d], J. Chudoba[140], J. J. Chwastowski[85], L. Chytka[130], D. Cieri[115], K. M. Ciesla[85], V. Cindro[92], I. A. Cioară[27b], A. Ciocio[18], F. Cirotto[70a,70b], Z. H. Citron[180,j], M. Citterio[69a], D. A. Ciubotaru[27b], B. M. Ciungu[167], A. Clark[54], P. J. Clark[50], S. E. Clawson[101], C. Clement[45a,45b], Y. Coadou[102], M. Cobal[67a,67c], A. Coccaro[55b], J. Cochran[79], R. Coelho Lopes De Sa[103], H. Cohen[161], A. E. C. Coimbra[36], B. Cole[39], A. P. Colijn[120], J. Collot[58], P. Conde Muiño[139a,139h], S. H. Connell[33c], I. A. Connelly[57], S. Constantinescu[27b], F. Conventi[70a,ak], A. M. Cooper-Sarkar[134], F. Cormier[175], K. J. R. Cormier[167], L. D. Corpe[95], M. Corradi[73a,73b], E. E. Corrigan[97], F. Corriveau[104,z], M. J. Costa[174], F. Costanza[5], D. Costanzo[149], G. Cowan[94], J. W. Cowley[32], J. Crane[101], K. Cranmer[125], R. A. Creager[136], S. Crépé-Renaudin[58], F. Crescioli[135], M. Cristinziani[24], V. Croft[170], G. Crosetti[41a,41b], A. Cueto[5], T. Cuhadar Donszelmann[171], H. Cui[15a,15d], A. R. Cukierman[153], W. R. Cunningham[57], S. Czekierda[85], P. Czodrowski[36], M. M. Czurylo[61b], M. J. Da Cunha Sargedas De Sousa[60b], J. V. Da Fonseca Pinto[81b], C. Da Via[101], W. Dabrowski[84a], F. Dachs[36], T. Dado[47], S. Dahbi[33e], T. Dai[106], C. Dallapiccola[103], M. Dam[40], G. D'amen[29], V. D'Amico[75a,75b], J. Damp[100], J. R. Dandoy[136], M. F. Daneri[30], M. Danninger[152], V. Dao[36], G. Darbo[55b], O. Dartsi[5], A. Dattagupta[131], T. Daubney[46], S. D'Auria[69a,69b], C. David[168b], T. Davidek[142], D. R. Davis[49], I. Dawson[149], K. De[8], R. De Asmundis[70a], M. De Beurs[120], S. De Castro[23a,23b], N. De Groot[119], P. de Jong[120], H. De la Torre[107], A. De Maria[15c], D. De Pedis[73a], A. De Salvo[73a], U. De Sanctis[74a,74b], M. De Santis[74a,74b], A. De Santo[156], J. B. De Vivie De Regie[65], D. V. Dedovich[80], A. M. Deiana[42], J. Del Peso[99], Y. Delabat Diaz[46], D. Delgove[65], F. Deliot[144], C. M. Delitzsch[7], M. Della Pietra[70a,70b], D. Della Volpe[54], A. Dell'Acqua[36], L. Dell'Asta[74a,74b], M. Delmastro[5], C. Delporte[65], P. A. Delsart[58], S. Demers[183], M. Demichev[80], G. Demontigny[110], S. P. Denisov[123], L. D'Eramo[121], D. Derendarz[85], J. E. Derkaoui[35e], F. Derue[135], P. Dervan[91], K. Desch[24], K. Dette[167], C. Deutsch[24], M. R. Devesa[30], P. O. Deviveiros[36], F. A. Di Bello[73a,73b], A. Di Ciaccio[74a,74b], L. Di Ciaccio[5], W. K. Di Clemente[136], C. Di Donato[70a,70b], A. Di Girolamo[36], G. Di Gregorio[72a,72b], A. Di Luca[76a,76b], B. Di Micco[75a,75b], R. Di Nardo[75a,75b], K. F. Di Petrillo[59], R. Di Sipio[167], C. Diaconu[102], F. A. Dias[120], T. Dias Do Vale[139a], M. A. Diaz[146a], F. G. Diaz Capriles[24],

J. Dickinson[18], M. Didenko[166], E. B. Diehl[106], J. Dietrich[19], S. Díez Cornell[46], C. Diez Pardos[151], A. Dimitrievska[18], W. Ding[15b], J. Dingfelder[24], S. J. Dittmeier[61b], F. Dittus[36], F. Djama[102], T. Djobava[159b], J. I. Djuvsland[17], M. A. B. Do Vale[147], M. Dobre[27b], D. Dodsworth[26], C. Doglioni[97], J. Dolejsi[142], Z. Dolezal[142], M. Donadelli[81c], B. Dong[60c], J. Donini[38], A. D'onofrio[15c], M. D'Onofrio[91], J. Dopke[143], A. Doria[70a], M. T. Dova[89], A. T. Doyle[57], E. Drechsler[152], E. Dreyer[152], T. Dreyer[53], A. S. Drobac[170], D. Du[60b], T. A. du Pree[120], Y. Duan[60d], F. Dubinin[111], M. Dubovsky[28a], A. Dubreuil[54], E. Duchovni[180], G. Duckeck[114], O. A. Ducu[36,27b], D. Duda[115], A. Dudarev[36], A. C. Dudder[100], E. M. Duffield[18], M. D'uffizi[101], L. Duflot[65], M. Dührssen[36], C. Dülsen[182], M. Dumancic[180], A. E. Dumitriu[27b], M. Dunford[61a], S. Dungs[47], A. Duperrin[102], H. Duran Yildiz[4a], M. Düren[56], A. Durglishvili[159b], D. Duschinger[48], B. Dutta[46], D. Duvnjak[1], G. I. Dyckes[136], M. Dyndal[36], S. Dysch[101], B. S. Dziedzic[85], M. G. Eggleston[49], T. Eifert[8], G. Eigen[17], K. Einsweiler[18], T. Ekelof[172], H. El Jarrari[35f], V. Ellajosyula[172], M. Ellert[172], F. Ellinghaus[182], A. A. Elliot[93], N. Ellis[36], J. Elmsheuser[29], M. Elsing[36], D. Emeliyanov[143], A. Emerman[39], Y. Enari[163], M. B. Epland[49], J. Erdmann[47], A. Ereditato[20], P. A. Erland[85], M. Errenst[182], M. Escalier[65], C. Escobar[174], O. Estrada Pastor[174], E. Etzion[161], G. Evans[139a], H. Evans[66], M. O. Evans[156], A. Ezhilov[137], F. Fabbri[57], L. Fabbri[23a,23b], V. Fabiani[119], G. Facini[178], R. M. Fakhrutdinov[123], S. Falciano[73a], P. J. Falke[24], S. Falke[36], J. Faltova[142], Y. Fang[15a], Y. Fang[15a], G. Fanourakis[44], M. Fanti[69a,69b], M. Faraj[67a,67c], A. Farbin[8], A. Farilla[75a], E. M. Farina[71a,71b], T. Farooque[107], S. M. Farrington[50], P. Farthouat[36], F. Fassi[35f], P. Fassnacht[36], D. Fassouliotis[9], M. Faucci Giannelli[50], W. J. Fawcett[32], L. Fayard[65], O. L. Fedin[137,o], W. Fedorko[175], A. Fehr[20], M. Feickert[173], L. Feligioni[102], A. Fell[149], C. Feng[60b], M. Feng[49], M. J. Fenton[171], A. B. Fenyuk[123], S. W. Ferguson[43], J. Ferrando[46], A. Ferrari[172], P. Ferrari[120], R. Ferrari[71a], D. E. Ferreira de Lima[61b], A. Ferrer[174], D. Ferrere[54], C. Ferretti[106], F. Fiedler[100], A. Filipčič[92], F. Filthaut[119], K. D. Finelli[25], M. C. N. Fiolhais[139a,139c,a], L. Fiorini[174], F. Fischer[114], J. Fischer[100], W. C. Fisher[107], T. Fitschen[21], I. Fleck[151], P. Fleischmann[106], T. Flick[182], B. M. Flierl[114], L. Flores[136], L. R. Flores Castillo[63a], F. M. Follega[76a,76b], N. Fomin[17], J. H. Foo[167], G. T. Forcolin[76a,76b], B. C. Forland[66], A. Formica[144], F. A. Förster[14], A. C. Forti[101], E. Fortin[102], M. G. Foti[134], D. Fournier[65], H. Fox[90], P. Francavilla[72a,72b], S. Francescato[73a,73b], M. Franchini[23a,23b], S. Franchino[61a], D. Francis[36], L. Franco[5], L. Franconi[20], M. Franklin[59], G. Frattari[73a,73b], A. N. Fray[93], P. M. Freeman[21], B. Freund[110], W. S. Freund[81b], E. M. Freundlich[47], D. C. Frizzell[128], D. Froidevaux[36], J. A. Frost[134], M. Fujimoto[126], C. Fukunaga[164], E. Fullana Torregrosa[174], T. Fusayasu[116], J. Fuster[174], A. Gabrielli[23a,23b], A. Gabrielli[36], S. Gadatsch[54], P. Gadow[115], G. Gagliardi[55b,55a], L. G. Gagnon[110], G. E. Gallardo[134], E. J. Gallas[134], B. J. Gallop[143], R. Gamboa Goni[93], K. K. Gan[127], S. Ganguly[180], J. Gao[60a], Y. Gao[50], Y. S. Gao[31,l], F. M. Garay Walls[146a], C. García[174], J. E. García Navarro[174], J. A. García Pascual[15a], C. Garcia-Argos[52], M. Garcia-Sciveres[18], R. W. Gardner[37], N. Garelli[153], S. Gargiulo[52], C. A. Garner[167], V. Garonne[133], S. J. Gasiorowski[148], P. Gaspar[81b], A. Gaudiello[55b,55a], G. Gaudio[71a], P. Gauzzi[73a,73b], I. L. Gavrilenko[111], A. Gavrilyuk[124], C. Gay[175], G. Gaycken[46], E. N. Gazis[10], A. A. Geanta[27b], C. M. Gee[145], C. N. P. Gee[143], J. Geisen[97], M. Geisen[100], C. Gemme[55b], M. H. Genest[58], C. Geng[106], S. Gentile[73a,73b], S. George[94], T. Geralis[44], L. O. Gerlach[53], P. Gessinger-Befurt[100], G. Gessner[47], M. Ghasemi Bostanabad[176], M. Ghneimat[151], A. Ghosh[65], A. Ghosh[78], B. Giacobbe[23b], S. Giagu[73a,73b], N. Giangiacomi[167], P. Giannetti[72a], A. Giannini[70a,70b], G. Giannini[14], S. M. Gibson[94], M. Gignac[145], D. T. Gil[84b], B. J. Gilbert[39], D. Gillberg[34], G. Gilles[182], N. E. K. Gillwald[46], D. M. Gingrich[3,aj], M. P. Giordani[67a,67c], P. F. Giraud[144], G. Giugliarelli[67a,67c], D. Giugni[69a], F. Giuli[74a,74b], S. Gkaitatzis[162], I. Gkialas[9,g], E. L. Gkougkousis[14], P. Gkountoumis[10], L. K. Gladilin[113], C. Glasman[99], J. Glatzer[14], P. C. F. Glaysher[46], A. Glazov[46], G. R. Gledhill[131], I. Gnesi[41b,b], M. Goblirsch-Kolb[26], D. Godin[110], S. Goldfarb[105], T. Golling[54], D. Golubkov[123], A. Gomes[139a,139b], R. Goncalves Gama[53], R. Gonçalo[139a,139c], G. Gonella[131], L. Gonella[21], A. Gongadze[80], F. Gonnella[21], J. L. Gonski[39], S. González de la Hoz[174], S. Gonzalez Fernandez[14], R. Gonzalez Lopez[91], C. Gonzalez Renteria[18], R. Gonzalez Suarez[172], S. Gonzalez-Sevilla[54], G. R. Gonzalvo Rodriguez[174], L. Goossens[36], N. A. Gorasia[21], P. A. Gorbounov[124], H. A. Gordon[29], B. Gorini[36], E. Gorini[68a,68b], A. Gorišek[92], A. T. Goshaw[49], M. I. Gostkin[80], C. A. Gottardo[119], M. Gouighri[35b], A. G. Goussiou[148], N. Govender[33c], C. Goy[5], I. Grabowska-Bold[84a], E. C. Graham[91], J. Gramling[171], E. Gramstad[133], S. Grancagnolo[19], M. Grandi[156], V. Gratchev[137], P. M. Gravila[27f], F. G. Gravili[68a,68b], C. Gray[57], H. M. Gray[18], C. Grefe[24], K. Gregersen[97], I. M. Gregor[46], P. Grenier[153], K. Grevtsov[46], C. Grieco[14], N. A. Grieser[128], A. A. Grillo[145], K. Grimm[31,k], S. Grinstein[14,v], J.-F. Grivaz[65], S. Groh[100], E. Gross[180],

J. Grosse-Knetter[53] , Z. J. Grout[95] , C. Grud[106] , A. Grummer[118] , J. C. Grundy[134] , L. Guan[106] , W. Guan[181] , C. Gubbels[175] , J. Guenther[77] , A. Guerguichon[65] , J. G. R. Guerrero Rojas[174] , F. Guescini[115] , D. Guest[77] , R. Gugel[100] , A. Guida[46] , T. Guillemin[5] , S. Guindon[36] , J. Guo[60c] , W. Guo[106] , Y. Guo[60a] , Z. Guo[102] , R. Gupta[46] , S. Gurbuz[12c] , G. Gustavino[128] , M. Guth[52] , P. Gutierrez[128] , C. Gutschow[95] , C. Guyot[144] , C. Gwenlan[134] , C. B. Gwilliam[91] , E. S. Haaland[133] , A. Haas[125] , C. Haber[18] , H. K. Hadavand[8] , A. Hadef[100] , M. Haleem[177] , J. Haley[129] , J. J. Hall[149] , G. Halladjian[107] , G. D. Hallewell[102] , K. Hamano[176] , H. Hamdaoui[35f] , M. Hamer[24] , G. N. Hamity[50] , K. Han[60a] , L. Han[15c] , L. Han[60a] , S. Han[18] , Y. F. Han[167] , K. Hanagaki[82,t] , M. Hance[145] , D. M. Handl[114] , M. D. Hank[37] , R. Hankache[135] , E. Hansen[97] , J. B. Hansen[40] , J. D. Hansen[40] , M. C. Hansen[24] , P. H. Hansen[40] , E. C. Hanson[101] , K. Hara[169] , T. Harenberg[182] , S. Harkusha[108] , P. F. Harrison[178] , N. M. Hartman[153] , N. M. Hartmann[114] , Y. Hasegawa[150] , A. Hasib[50] , S. Hassani[144] , S. Haug[20] , R. Hauser[107] , M. Havranek[141] , C. M. Hawkes[21] , R. J. Hawkings[36] , S. Hayashida[117] , D. Hayden[107] , C. Hayes[106] , R. L. Hayes[175] , C. P. Hays[134] , J. M. Hays[93] , H. S. Hayward[91] , S. J. Haywood[143] , F. He[60a] , Y. He[165] , M. P. Heath[50] , V. Hedberg[97] , A. L. Heggelund[133] , N. D. Hehir[93] , C. Heidegger[52] , K. K. Heidegger[52] , W. D. Heidorn[79] , J. Heilman[34] , S. Heim[46] , T. Heim[18] , B. Heinemann[46,ah] , J. G. Heinlein[136] , J. J. Heinrich[131] , L. Heinrich[36] , J. Hejbal[140] , L. Helary[46] , A. Held[125] , S. Hellesund[133] , C. M. Helling[145] , S. Hellman[45a,45b] , C. Helsens[36] , R. C. W. Henderson[90] , L. Henkelmann[32] , A. M. Henriques Correia[36] , H. Herde[26] , Y. Hernández Jiménez[33e] , H. Herr[100] , M. G. Herrmann[114] , T. Herrmann[48] , G. Herten[52] , R. Hertenberger[114] , L. Hervas[36] , G. G. Hesketh[95] , N. P. Hessey[168a] , H. Hibi[83] , S. Higashino[82] , E. Higón-Rodriguez[174] , K. Hildebrand[37] , J. C. Hill[32] , K. K. Hill[29] , K. H. Hiller[46] , S. J. Hillier[21] , M. Hils[48] , I. Hinchliffe[18] , F. Hinterkeuser[24] , M. Hirose[132] , S. Hirose[169] , D. Hirschbuehl[182] , B. Hiti[92] , O. Hladik[140] , J. Hobbs[155] , R. Hobincu[27e] , N. Hod[180] , M. C. Hodgkinson[149] , A. Hoecker[36] , D. Hohn[52] , D. Hohov[65] , T. Holm[24] , T. R. Holmes[37] , M. Holzbock[115] , L. B. A. H. Hommels[32] , T. M. Hong[138] , J. C. Honig[52] , A. Hönle[115] , B. H. Hooberman[173] , W. H. Hopkins[6] , Y. Horii[117] , P. Horn[48] , L. A. Horyn[37] , S. Hou[158] , A. Hoummada[35a] , J. Howarth[57] , J. Hoya[89] , M. Hrabovsky[130] , J. Hrivnac[65] , A. Hrynevich[109] , T. Hryn'ova[5] , P. J. Hsu[64] , S.-C. Hsu[148] , Q. Hu[39] , S. Hu[60c] , Y. F. Hu[15a,15d,al] , D. P. Huang[95] , X. Huang[15c] , Y. Huang[60a] , Y. Huang[15a] , Z. Hubacek[141] , F. Hubaut[102] , M. Huebner[24] , F. Huegging[24] , T. B. Huffman[134] , M. Huhtinen[36] , R. Hulsken[58] , R. F. H. Hunter[34] , N. Huseynov[80,aa] , J. Huston[107] , J. Huth[59] , R. Hyneman[153] , S. Hyrych[28a] , G. Iacobucci[54] , G. Iakovidis[29] , I. Ibragimov[151] , L. Iconomidou-Fayard[65] , P. Iengo[36] , R. Ignazzi[40] , R. Iguchi[163] , T. Iizawa[54] , Y. Ikegami[82] , M. Ikeno[82] , N. Ilic[119,167,z] , F. Iltzsche[48] , H. Imam[35a] , G. Introzzi[71a,71b] , M. Iodice[75a] , K. Iordanidou[168a] , V. Ippolito[73a,73b] , M. F. Isacson[172] , M. Ishino[163] , W. Islam[129] , C. Issever[19,46] , S. Istin[160] , J. M. Iturbe Ponce[63a] , R. Iuppa[76a,76b] , A. Ivina[180] , J. M. Izen[43] , V. Izzo[70a] , P. Jacka[140] , P. Jackson[1] , R. M. Jacobs[46] , B. P. Jaeger[152] , V. Jain[2] , G. Jäkel[182] , K. B. Jakobi[100] , K. Jakobs[52] , T. Jakoubek[180] , J. Jamieson[57] , K. W. Janas[84a] , R. Jansky[54] , M. Janus[53] , P. A. Janus[84a] , G. Jarlskog[97] , A. E. Jaspan[91] , N. Javadov[80,aa] , T. Javůrek[36] , M. Javurkova[103] , F. Jeanneau[144] , L. Jeanty[131] , J. Jejelava[159a] , P. Jenni[52,c] , N. Jeong[46] , S. Jézéquel[5] , J. Jia[155] , Z. Jia[15c] , H. Jiang[79] , Y. Jiang[60a] , Z. Jiang[153] , S. Jiggins[52] , F. A. Jimenez Morales[38] , J. Jimenez Pena[115] , S. Jin[15c] , A. Jinaru[27b] , O. Jinnouchi[165] , H. Jivan[33e] , P. Johansson[149] , K. A. Johns[7] , C. A. Johnson[66] , E. Jones[178] , R. W. L. Jones[90] , S. D. Jones[156] , T. J. Jones[91] , J. Jovicevic[36] , X. Ju[18] , J. J. Junggeburth[115] , A. Juste Rozas[14,v] , A. Kaczmarska[85] , M. Kado[73a,73b] , H. Kagan[127] , M. Kagan[153] , A. Kahn[39] , C. Kahra[100] , T. Kaji[179] , E. Kajomovitz[160] , C. W. Kalderon[29] , A. Kaluza[100] , A. Kamenshchikov[123] , M. Kaneda[163] , N. J. Kang[145] , S. Kang[79] , Y. Kano[117] , J. Kanzaki[82] , L. S. Kaplan[181] , D. Kar[33e] , K. Karava[134] , M. J. Kareem[168b] , I. Karkanias[162] , S. N. Karpov[80] , Z. M. Karpova[80] , V. Kartvelishvili[90] , A. N. Karyukhin[123] , E. Kasimi[162] , A. Kastanas[45a,45b] , C. Kato[60d] , J. Katzy[46] , K. Kawade[150] , K. Kawagoe[88] , T. Kawaguchi[117] , T. Kawamoto[144] , G. Kawamura[53] , E. F. Kay[176] , F. I. Kaya[170] , S. Kazakos[14] , V. F. Kazanin[122a,122b] , J. M. Keaveney[33a] , R. Keeler[176] , J. S. Keller[34] , E. Kellermann[97] , D. Kelsey[156] , J. J. Kempster[21] , J. Kendrick[21] , K. E. Kennedy[39] , O. Kepka[140] , S. Kersten[182] , B. P. Kerševan[92] , S. Ketabchi Haghighat[167] , F. Khalil-Zada[13] , M. Khandoga[144] , A. Khanov[129] , A. G. Kharlamov[122a,122b] , T. Kharlamova[122a,122b] , E. E. Khoda[175] , T. J. Khoo[77] , G. Khoriauli[177] , E. Khramov[80] , J. Khubua[159b] , S. Kido[83] , M. Kiehn[36] , E. Kim[165] , Y. K. Kim[37] , N. Kimura[95] , A. Kirchhoff[53] , D. Kirchmeier[48] , J. Kirk[143] , A. E. Kiryunin[115] , T. Kishimoto[163] , D. P. Kisliuk[167] , V. Kitali[46] , C. Kitsaki[10] , O. Kivernyk[24] , T. Klapdor-Kleingrothaus[52] , M. Klassen[61a] , C. Klein[34] , M. H. Klein[106] , M. Klein[91] , U. Klein[91] , K. Kleinknecht[100] , P. Klimek[36] , A. Klimentov[29] , F. Klimpel[36] , T. Klingl[24] , T. Klioutchnikova[36] , F. F. Klitzner[114] , P. Kluit[120] , S. Kluth[115] , E. Kneringer[77] , E. B. F. G. Knoops[102] , A. Knue[52] , D. Kobayashi[88] , M. Kobel[48] , M. Kocian[153] , T. Kodama[163] , P. Kodys[142] , D. M. Koeck[156] ,

P. T. Koenig[24], T. Koffas[34], N. M. Köhler[36], M. Kolb[144], I. Koletsou[5], T. Komarek[130], T. Kondo[82], K. Köneke[52], A. X. Y. Kong[1], A. C. König[119], T. Kono[126], V. Konstantinides[95], N. Konstantinidis[95], B. Konya[97], R. Kopeliansky[66], S. Koperny[84a], K. Korcyl[85], K. Kordas[162], G. Koren[161], A. Korn[95], I. Korolkov[14], E. V. Korolkova[149], N. Korotkova[113], O. Kortner[115], S. Kortner[115], V. V. Kostyukhin[149,166], A. Kotsokechagia[65], A. Kotwal[49], A. Koulouris[10], A. Kourkoumeli-Charalampidi[71a,71b], C. Kourkoumelis[9], E. Kourlitis[6], V. Kouskoura[29], R. Kowalewski[176], W. Kozanecki[101], A. S. Kozhin[123], V. A. Kramarenko[113], G. Kramberger[92], D. Krasnopevtsev[60a], M. W. Krasny[135], A. Krasznahorkay[36], D. Krauss[115], J. A. Kremer[100], J. Kretzschmar[91], K. Kreul[19], P. Krieger[167], F. Krieter[114], S. Krishnamurthy[103], A. Krishnan[61b], M. Krivos[142], K. Krizka[18], K. Kroeninger[47], H. Kroha[115], J. Kroll[140], J. Kroll[136], K. S. Krowpman[107], U. Kruchonak[80], H. Krüger[24], N. Krumnack[79], M. C. Kruse[49], J. A. Krzysiak[85], A. Kubota[165], O. Kuchinskaia[166], S. Kuday[4b], D. Kuechler[46], J. T. Kuechler[46], S. Kuehn[36], T. Kuhl[46], V. Kukhtin[80], Y. Kulchitsky[108,ad], S. Kuleshov[146b], Y. P. Kulinich[173], M. Kuna[58], A. Kupco[140], T. Kupfer[47], O. Kuprash[52], H. Kurashige[83], L. L. Kurchaninov[168a], Y. A. Kurochkin[108], A. Kurova[112], M. G. Kurth[15a,15d], E. S. Kuwertz[36], M. Kuze[165], A. K. Kvam[148], J. Kvita[130], T. Kwan[104], C. Lacasta[174], F. Lacava[73a,73b], D. P. J. Lack[101], H. Lacker[19], D. Lacour[135], E. Ladygin[80], R. Lafaye[5], B. Laforge[135], T. Lagouri[146c], S. Lai[53], I. K. Lakomiec[84a], J. E. Lambert[128], S. Lammers[66], W. Lampl[7], C. Lampoudis[162], E. Lançon[29], U. Landgraf[52], M. P. J. Landon[93], V. S. Lang[52], J. C. Lange[53], R. J. Langenberg[103], A. J. Lankford[171], F. Lanni[29], K. Lantzsch[24], A. Lanza[71a], A. Lapertosa[55b,55a], J. F. Laporte[144], T. Lari[69a], F. Lasagni Manghi[23a,23b], M. Lassnig[36], V. Latonova[140], T. S. Lau[63a], A. Laudrain[100], A. Laurier[34], M. Lavorgna[70a,70b], S. D. Lawlor[94], M. Lazzaroni[69a,69b], B. Le[101], E. Le Guirriec[102], A. Lebedev[79], M. LeBlanc[7], T. LeCompte[6], F. Ledroit-Guillon[58], A. C. A. Lee[95], C. A. Lee[29], G. R. Lee[17], L. Lee[59], S. C. Lee[158], S. Lee[79], B. Lefebvre[168a], H. P. Lefebvre[94], M. Lefebvre[176], C. Leggett[18], K. Lehmann[152], N. Lehmann[20], G. Lehmann Miotto[36], W. A. Leight[46], A. Leisos[162,u], M. A. L. Leite[81c], C. E. Leitgeb[114], R. Leitner[142], K. J. C. Leney[42], T. Lenz[24], S. Leone[72a], C. Leonidopoulos[50], A. Leopold[135], C. Leroy[110], R. Les[107], C. G. Lester[32], M. Levchenko[137], J. Levêque[5], D. Levin[106], L. J. Levinson[180], D. J. Lewis[21], B. Li[15b], B. Li[106], C-Q. Li[60c,60d], F. Li[60c], H. Li[60a], H. Li[60b], J. Li[60c], K. Li[148], L. Li[60c], M. Li[15a,15d], Q. Y. Li[60a], S. Li[60c,60d], X. Li[46], Y. Li[46], Z. Li[60b], Z. Li[134], Z. Li[104], Z. Li[91], Z. Liang[15a], M. Liberatore[46], B. Liberti[74a], K. Lie[63c], S. Lim[29], C. Y. Lin[32], K. Lin[107], R. A. Linck[66], R. E. Lindley[7], J. H. Lindon[21], A. Linss[46], A. L. Lionti[54], E. Lipeles[136], A. Lipniacka[17], T. M. Liss[173,ai], A. Lister[175], J. D. Little[8], B. Liu[79], B. X. Liu[152], H. B. Liu[29], J. B. Liu[60a], J. K. K. Liu[37], K. Liu[60d,60c], M. Liu[60a], M. Y. Liu[60a], P. Liu[15a], X. Liu[60a], Y. Liu[46], Y. Liu[15a,15d], Y. L. Liu[106], Y. W. Liu[60a], M. Livan[71a,71b], A. Lleres[58], J. Llorente Merino[152], S. L. Lloyd[93], C. Y. Lo[63b], E. M. Lobodzinska[46], P. Loch[7], S. Loffredo[74a,74b], T. Lohse[19], K. Lohwasser[149], M. Lokajicek[140], J. D. Long[173], R. E. Long[90], I. Longarini[73a,73b], L. Longo[36], I. Lopez Paz[101], A. Lopez Solis[149], J. Lorenz[114], N. Lorenzo Martinez[5], A. M. Lory[114], A. Lösle[52], X. Lou[45a,45b], X. Lou[15a], A. Lounis[65], J. Love[6], P. A. Love[90], J. J. Lozano Bahilo[174], M. Lu[60a], Y. J. Lu[64], H. J. Lubatti[148], C. Luci[73a,73b], F. L. Lucio Alves[15c], A. Lucotte[58], F. Luehring[66], I. Luise[155], L. Luminari[73a], B. Lund-Jensen[154], N. A. Luongo[131], M. S. Lutz[161], D. Lynn[29], H. Lyons[91], R. Lysak[140], E. Lytken[97], F. Lyu[15a], V. Lyubushkin[80], T. Lyubushkina[80], H. Ma[29], L. L. Ma[60b], Y. Ma[95], D. M. Mac Donell[176], G. Maccarrone[51], C. M. Macdonald[149], J. C. MacDonald[149], J. Machado Miguens[136], R. Madar[38], W. F. Mader[48], M. Madugoda Ralalage Don[129], N. Madysa[48], J. Maeda[83], T. Maeno[29], M. Maerker[48], V. Magerl[52], N. Magini[79], J. Magro[67a,67c,q], D. J. Mahon[39], C. Maidantchik[81b], A. Maio[139a,139b,139d], K. Maj[84a], O. Majersky[28a], S. Majewski[131], Y. Makida[82], N. Makovec[65], B. Malaescu[135], Pa. Malecki[85], V. P. Maleev[137], F. Malek[58], D. Malito[41a,41b], U. Mallik[78], C. Malone[32], S. Maltezos[10], S. Malyukov[80], J. Mamuzic[174], G. Mancini[51], J. P. Mandalia[93], I. Mandić[92], L. Manhaes de Andrade Filho[81a], I. M. Maniatis[162], J. Manjarres Ramos[48], K. H. Mankinen[97], A. Mann[114], A. Manousos[77], B. Mansoulie[144], I. Manthos[162], S. Manzoni[120], A. Marantis[162], G. Marceca[30], L. Marchese[134], G. Marchiori[135], M. Marcisovsky[140], L. Marcoccia[74a,74b], C. Marcon[97], M. Marjanovic[128], Z. Marshall[18], M. U. F. Martensson[172], S. Marti-Garcia[174], C. B. Martin[127], T. A. Martin[178], V. J. Martin[50], B. Martin dit Latour[17], L. Martinelli[75a,75b], M. Martinez[14,v], P. Martinez Agullo[174], V. I. Martinez Outschoorn[103], S. Martin-Haugh[143], V. S. Martoiu[27b], A. C. Martyniuk[95], A. Marzin[36], S. R. Maschek[115], L. Masetti[100], T. Mashimo[163], R. Mashinistov[111], J. Masik[101], A. L. Maslennikov[122a,122b], L. Massa[23a,23b], P. Massarotti[70a,70b], P. Mastrandrea[72a,72b], A. Mastroberardino[41a,41b], T. Masubuchi[163], D. Matakias[29], A. Matic[114], N. Matsuzawa[163], P. Mättig[24], J. Maurer[27b], B. Maček[92], D. A. Maximov[122a,122b],

R. Mazini[158], I. Maznas[162], S. M. Mazza[145], J. P. Mc Gowan[104], S. P. Mc Kee[106], T. G. McCarthy[115], W. P. McCormack[18], E. F. McDonald[105], A. E. McDougall[120], J. A. Mcfayden[18], G. Mchedlidze[159b], M. A. McKay[42], K. D. McLean[176], S. J. McMahon[143], P. C. McNamara[105], C. J. McNicol[178], R. A. McPherson[176,z], J. E. Mdhluli[33e], Z. A. Meadows[103], S. Meehan[36], T. Megy[38], S. Mehlhase[114], A. Mehta[91], B. Meirose[43], D. Melini[160], B. R. Mellado Garcia[33e], J. D. Mellenthin[53], M. Melo[28a], F. Meloni[46], A. Melzer[24], E. D. Mendes Gouveia[139a,139e], A. M. Mendes Jacques Da Costa[21], H. Y. Meng[167], L. Meng[36], X. T. Meng[106], S. Menke[115], E. Meoni[41a,41b], S. Mergelmeyer[19], S. A. M. Merkt[138], C. Merlassino[134], P. Mermod[54], L. Merola[70a,70b], C. Meroni[69a], G. Merz[106], O. Meshkov[113,111], J. K. R. Meshreki[151], J. Metcalfe[6], A. S. Mete[6], C. Meyer[66], J-P. Meyer[144], M. Michetti[19], R. P. Middleton[143], L. Mijović[50], G. Mikenberg[180], M. Mikestikova[140], M. Mikuž[92], H. Mildner[149], A. Milic[167], C. D. Milke[42], D. W. Miller[37], L. S. Miller[34], A. Milov[180], D. A. Milstead[45a,45b], A. A. Minaenko[123], I. A. Minashvili[159b], L. Mince[57], A. I. Mincer[125], B. Mindur[84a], M. Mineev[80], Y. Minegishi[163], Y. Mino[86], L. M. Mir[14], M. Mironova[134], T. Mitani[179], J. Mitrevski[114], V. A. Mitsou[174], M. Mittal[60c], O. Miu[167], A. Miucci[20], P. S. Miyagawa[93], A. Mizukami[82], J. U. Mjörnmark[97], T. Mkrtchyan[61a], M. Mlynarikova[121], T. Moa[45a,45b], S. Mobius[53], K. Mochizuki[110], P. Moder[46], P. Mogg[114], S. Mohapatra[39], R. Moles-Valls[24], K. Mönig[46], E. Monnier[102], A. Montalbano[152], J. Montejo Berlingen[36], M. Montella[95], F. Monticelli[89], S. Monzani[69a], N. Morange[65], A. L. Moreira De Carvalho[139a], D. Moreno[22a], M. Moreno Llácer[174], C. Moreno Martinez[14], P. Morettini[55b], M. Morgenstern[160], S. Morgenstern[48], D. Mori[152], M. Morii[59], M. Morinaga[179], V. Morisbak[133], A. K. Morley[36], G. Mornacchi[36], A. P. Morris[95], L. Morvaj[36], P. Moschovakos[36], B. Moser[120], M. Mosidze[159b], T. Moskalets[144], P. Moskvitina[119], J. Moss[31,m], E. J. W. Moyse[103], S. Muanza[102], J. Mueller[138], R. S. P. Mueller[114], D. Muenstermann[90], G. A. Mullier[97], D. P. Mungo[69a,69b], J. L. Munoz Martinez[14], F. J. Munoz Sanchez[101], P. Murin[28b], W. J. Murray[178,143], A. Murrone[69a,69b], J. M. Muse[128], M. Muškinja[18], C. Mwewa[33a], A. G. Myagkov[123,ae], A. A. Myers[138], G. Myers[66], J. Myers[131], M. Myska[141], B. P. Nachman[18], O. Nackenhorst[47], A. Nag Nag[48], K. Nagai[134], K. Nagano[82], Y. Nagasaka[62], J. L. Nagle[29], E. Nagy[102], A. M. Nairz[36], Y. Nakahama[117], K. Nakamura[82], T. Nakamura[163], H. Nanjo[132], F. Napolitano[61a], R. F. Naranjo Garcia[46], R. Narayan[42], I. Naryshkin[137], M. Naseri[34], T. Naumann[46], G. Navarro[22a], P. Y. Nechaeva[111], F. Nechansky[46], T. J. Neep[21], A. Negri[71a,71b], M. Negrini[23b], C. Nellist[119], C. Nelson[104], M. E. Nelson[45a,45b], S. Nemecek[140], M. Nessi[36,e], M. S. Neubauer[173], F. Neuhaus[100], M. Neumann[182], R. Newhouse[175], P. R. Newman[21], C. W. Ng[138], Y. S. Ng[19], Y. W. Y. Ng[171], B. Ngair[35f], H. D. N. Nguyen[102], T. Nguyen Manh[110], E. Nibigira[38], R. B. Nickerson[134], R. Nicolaidou[144], D. S. Nielsen[40], J. Nielsen[145], M. Niemeyer[53], N. Nikiforou[11], V. Nikolaenko[123,ae], I. Nikolic-Audit[135], K. Nikolopoulos[21], P. Nilsson[29], H. R. Nindhito[54], A. Nisati[73a], N. Nishu[60c], R. Nisius[115], I. Nitsche[47], T. Nitta[179], T. Nobe[163], D. L. Noel[32], Y. Noguchi[86], I. Nomidis[135], M. A. Nomura[29], M. Nordberg[36], J. Novak[92], T. Novak[92], O. Novgorodova[48], R. Novotny[118], L. Nozka[130], K. Ntekas[171], E. Nurse[95], F. G. Oakham[34,aj], J. Ocariz[135], A. Ochi[83], I. Ochoa[139a], J. P. Ochoa-Ricoux[146a], K. O'Connor[26], S. Oda[88], S. Odaka[82], S. Oerdek[53], A. Ogrodnik[84a], A. Oh[101], C. C. Ohm[154], H. Oide[165], R. Oishi[163], M. L. Ojeda[167], H. Okawa[169], Y. Okazaki[86], M. W. O'Keefe[91], Y. Okumura[163], A. Olariu[27b], L. F. Oleiro Seabra[139a], S. A. Olivares Pino[146a], D. Oliveira Damazio[29], J. L. Oliver[1], M. J. R. Olsson[171], A. Olszewski[85], J. Olszowska[85], Ö. O. Öncel[24], D. C. O'Neil[152], A. P. O'neill[134], A. Onofre[139a,139e], P. U. E. Onyisi[11], H. Oppen[133], R. G. Oreamuno Madriz[121], M. J. Oreglia[37], G. E. Orellana[89], D. Orestano[75a,75b], N. Orlando[14], R. S. Orr[167], V. O'Shea[57], R. Ospanov[60a], G. Otero y Garzon[30], H. Otono[88], P. S. Ott[61a], G. J. Ottino[18], M. Ouchrif[35e], J. Ouellette[29], F. Ould-Saada[133], A. Ouraou[144,*], Q. Ouyang[15a], M. Owen[57], R. E. Owen[143], V. E. Ozcan[12c], N. Ozturk[8], J. Pacalt[130], H. A. Pacey[32], K. Pachal[49], A. Pacheco Pages[14], C. Padilla Aranda[14], S. Pagan Griso[18], G. Palacino[66], S. Palazzo[50], S. Palestini[36], M. Palka[84b], P. Palni[84a], C. E. Pandini[54], J. G. Panduro Vazquez[94], P. Pani[46], G. Panizzo[67a,67c], L. Paolozzi[54], C. Papadatos[110], K. Papageorgiou[9,g], S. Parajuli[42], A. Paramonov[6], C. Paraskevopoulos[10], D. Paredes Hernandez[63b], S. R. Paredes Saenz[134], B. Parida[180], T. H. Park[167], A. J. Parker[31], M. A. Parker[32], F. Parodi[55a,55b], E. W. Parrish[121], J. A. Parsons[39], U. Parzefall[52], L. Pascual Dominguez[135], V. R. Pascuzzi[18], J. M. P. Pasner[145], F. Pasquali[120], E. Pasqualucci[73a], S. Passaggio[55b], F. Pastore[94], P. Pasuwan[45a,45b], S. Pataraia[100], J. R. Pater[101], A. Pathak[181,i], J. Patton[91], T. Pauly[36], J. Pearkes[153], M. Pedersen[133], L. Pedraza Diaz[119], R. Pedro[139a], T. Peiffer[53], S. V. Peleganchuk[122a,122b], O. Penc[140], C. Peng[63b], H. Peng[60a], B. S. Peralva[81a], M. M. Perego[65], A. P. Pereira Peixoto[139a], L. Pereira Sanchez[45a,45b], D. V. Perepelitsa[29], E. Perez Codina[168a], L. Perini[69a,69b], H. Pernegger[36], S. Perrella[36], A. Perrevoort[120],

K. Peters[46], R. F. Y. Peters[101], B. A. Petersen[36], T. C. Petersen[40], E. Petit[102], V. Petousis[141], C. Petridou[162], F. Petrucci[75a,75b], M. Pettee[183], N. E. Pettersson[103], K. Petukhova[142], A. Peyaud[144], R. Pezoa[146d], L. Pezzotti[71a,71b], T. Pham[105], P. W. Phillips[143], M. W. Phipps[173], G. Piacquadio[155], E. Pianori[18], A. Picazio[103], R. H. Pickles[101], R. Piegaia[30], D. Pietreanu[27b], J. E. Pilcher[37], A. D. Pilkington[101], M. Pinamonti[67a,67c], J. L. Pinfold[3], C. Pitman Donaldson[95], M. Pitt[161], L. Pizzimento[74a,74b], A. Pizzini[120], M. -A. Pleier[29], V. Plesanovs[52], V. Pleskot[142], E. Plotnikova[80], P. Podberezko[122a,122b], R. Poettgen[97], R. Poggi[54], L. Poggioli[135], I. Pogrebnyak[107], D. Pohl[24], I. Pokharel[53], G. Polesello[71a], A. Poley[152,168a], A. Policicchio[73a,73b], R. Polifka[142], A. Polini[23b], C. S. Pollard[46], V. Polychronakos[29], D. Ponomarenko[112], L. Pontecorvo[36], S. Popa[27a], G. A. Popeneciu[27d], L. Portales[5], D. M. Portillo Quintero[58], S. Pospisil[141], K. Potamianos[46], I. N. Potrap[80], C. J. Potter[32], H. Potti[11], T. Poulsen[97], J. Poveda[174], T. D. Powell[149], G. Pownall[46], M. E. Pozo Astigarraga[36], A. Prades Ibanez[174], P. Pralavorio[102], M. M. Prapa[44], S. Prell[79], D. Price[101], M. Primavera[68a], M. L. Proffitt[148], N. Proklova[112], K. Prokofiev[63c], F. Prokoshin[80], S. Protopopescu[29], J. Proudfoot[6], M. Przybycien[84a], D. Pudzha[137], A. Puri[173], P. Puzo[65], D. Pyatiizbyantseva[112], J. Qian[106], Y. Qin[101], A. Quadt[53], M. Queitsch-Maitland[36], G. Rabanal Bolanos[59], M. Racko[28a], F. Ragusa[69a,69b], G. Rahal[98], J. A. Raine[54], S. Rajagopalan[29], A. Ramirez Morales[93], K. Ran[15a,15d], D. F. Rassloff[61a], D. M. Rauch[46], F. Rauscher[114], S. Rave[100], B. Ravina[57], I. Ravinovich[180], J. H. Rawling[101], M. Raymond[36], A. L. Read[133], N. P. Readioff[149], M. Reale[68a,68b], D. M. Rebuzzi[71a,71b], G. Redlinger[29], K. Reeves[43], D. Reikher[161], A. Reiss[100], A. Rej[151], C. Rembser[36], A. Renardi[46], M. Renda[27b], M. B. Rendel[115], A. G. Rennie[57], S. Resconi[69a], E. D. Resseguie[18], S. Rettie[95], B. Reynolds[127], E. Reynolds[21], O. L. Rezanova[122a,122b], P. Reznicek[142], E. Ricci[76a,76b], R. Richter[115], S. Richter[46], E. Richter-Was[84b], M. Ridel[135], P. Rieck[115], O. Rifki[46], M. Rijssenbeek[155], A. Rimoldi[71a,71b], M. Rimoldi[46], L. Rinaldi[23b], T. T. Rinn[173], G. Ripellino[154], I. Riu[14], P. Rivadeneira[46], J. C. Rivera Vergara[176], F. Rizatdinova[129], E. Rizvi[93], C. Rizzi[36], S. H. Robertson[104,z], M. Robin[46], D. Robinson[32], C. M. Robles Gajardo[146d], M. Robles Manzano[100], A. Robson[57], A. Rocchi[74a,74b], C. Roda[72a,72b], S. Rodriguez Bosca[174], A. Rodriguez Rodriguez[52], A. M. Rodríguez Vera[168b], S. Roe[36], J. Roggel[182], O. Røhne[133], R. Röhrig[115], R. A. Rojas[146d], B. Roland[52], C. P. A. Roland[66], J. Roloff[29], A. Romaniouk[112], M. Romano[23a,23b], N. Rompotis[91], M. Ronzani[125], L. Roos[135], S. Rosati[73a], G. Rosin[103], B. J. Rosser[136], E. Rossi[46], E. Rossi[75a,75b], E. Rossi[70a,70b], L. P. Rossi[55b], L. Rossini[46], R. Rosten[14], M. Rotaru[27b], B. Rottler[52], D. Rousseau[65], G. Rovelli[71a,71b], A. Roy[11], D. Roy[33e], A. Rozanov[102], Y. Rozen[160], X. Ruan[33e], T. A. Ruggeri[1], F. Rühr[52], A. Ruiz-Martinez[174], A. Rummler[36], Z. Rurikova[52], N. A. Rusakovich[80], H. L. Russell[104], L. Rustige[38,47], J. P. Rutherfoord[7], E. M. Rüttinger[149], M. Rybar[142], G. Rybkin[65], E. B. Rye[133], A. Ryzhov[123], J. A. Sabater Iglesias[46], P. Sabatini[174], L. Sabetta[73a,73b], S. Sacerdoti[65], H. F-W. Sadrozinski[145], R. Sadykov[80], F. Safai Tehrani[73a], B. Safarzadeh Samani[156], M. Safdari[153], P. Saha[121], S. Saha[104], M. Sahinsoy[115], A. Sahu[182], M. Saimpert[36], M. Saito[163], T. Saito[163], H. Sakamoto[163], D. Salamani[54], G. Salamanna[75a,75b], A. Salnikov[153], J. Salt[174], A. Salvador Salas[14], D. Salvatore[41a,41b], F. Salvatore[156], A. Salvucci[63a], A. Salzburger[36], J. Samarati[36], D. Sammel[52], D. Sampsonidis[162], D. Sampsonidou[60d,60c], J. Sánchez[174], A. Sanchez Pineda[67a,36,67c], H. Sandaker[133], C. O. Sander[46], I. G. Sanderswood[90], M. Sandhoff[182], C. Sandoval[22b], D. P. C. Sankey[143], M. Sannino[55a,55b], Y. Sano[117], A. Sansoni[51], C. Santoni[38], H. Santos[139a,139b], S. N. Santpur[18], A. Santra[174], K. A. Saoucha[149], A. Sapronov[80], J. G. Saraiva[139a,139d], O. Sasaki[82], K. Sato[169], F. Sauerburger[52], E. Sauvan[5], P. Savard[167,aj], R. Sawada[163], C. Sawyer[143], L. Sawyer[96], I. Sayago Galvan[174], C. Sbarra[23b], A. Sbrizzi[67a,67c], T. Scanlon[95], J. Schaarschmidt[148], P. Schacht[115], D. Schaefer[37], L. Schaefer[136], U. Schäfer[100], A. C. Schaffer[65], D. Schaile[114], R. D. Schamberger[155], E. Schanet[114], C. Scharf[19], N. Scharmberg[101], V. A. Schegelsky[137], D. Scheirich[142], F. Schenck[19], M. Schernau[171], C. Schiavi[55a,55b], L. K. Schildgen[24], Z. M. Schillaci[26], E. J. Schioppa[68a,68b], M. Schioppa[41a,41b], K. E. Schleicher[52], S. Schlenker[36], K. R. Schmidt-Sommerfeld[115], K. Schmieden[100], C. Schmitt[100], S. Schmitt[46], L. Schoeffel[144], A. Schoening[61b], P. G. Scholer[52], E. Schopf[134], M. Schott[100], J. F. P. Schouwenberg[119], J. Schovancova[36], S. Schramm[54], F. Schroeder[182], A. Schulte[100], H-C. Schultz-Coulon[61a], M. Schumacher[52], B. A. Schumm[145], Ph. Schune[144], A. Schwartzman[153], T. A. Schwarz[106], Ph. Schwemling[144], R. Schwienhorst[107], A. Sciandra[145], G. Sciolla[26], F. Scuri[72a], F. Scutti[105], L. M. Scyboz[115], C. D. Sebastiani[91], K. Sedlaczek[47], P. Seema[19], S. C. Seidel[118], A. Seiden[145], B. D. Seidlitz[29], T. Seiss[37], C. Seitz[46], J. M. Seixas[81b], G. Sekhniaidze[70a], S. J. Sekula[42], N. Semprini-Cesari[23a,23b], S. Sen[49], C. Serfon[29], L. Serin[65], L. Serkin[67a,67b], M. Sessa[60a], H. Severini[128], S. Sevova[153], F. Sforza[55a,55b], A. Sfyrla[54], E. Shabalina[53], J. D. Shahinian[136], N. W. Shaikh[45a,45b],

D. Shaked Renous[180], L. Y. Shan[15a], M. Shapiro[18], A. Sharma[36], A. S. Sharma[1], P. B. Shatalov[124],
K. Shaw[156], S. M. Shaw[101], M. Shehade[180], Y. Shen[128], A. D. Sherman[25], P. Sherwood[95], L. Shi[95],
C. O. Shimmin[183], Y. Shimogama[179], M. Shimojima[116], J. D. Shinner[94], I. P. J. Shipsey[134], S. Shirabe[165],
M. Shiyakova[80,x], J. Shlomi[180], A. Shmeleva[111], M. J. Shochet[37], J. Shojaii[105], D. R. Shope[154], S. Shrestha[127],
E. M. Shrif[33e], M. J. Shroff[176], E. Shulga[180], P. Sicho[140], A. M. Sickles[173], E. Sideras Haddad[33e],
O. Sidiropoulou[36], A. Sidoti[23a,23b], F. Siegert[48], Dj. Sijacki[16], M. Jr. Silva[181], M. V. Silva Oliveira[36],
S. B. Silverstein[45a], S. Simion[65], R. Simoniello[100], C. J. Simpson-allsop[21], S. Simsek[12b], P. Sinervo[167],
V. Sinetckii[113], S. Singh[152], S. Sinha[33e], M. Sioli[23a,23b], I. Siral[131], S. Yu. Sivoklokov[113], J. Sjölin[45a,45b],
A. Skaf[53], E. Skorda[97], P. Skubic[128], M. Slawinska[85], K. Sliwa[170], V. Smakhtin[180], B. H. Smart[143],
J. Smiesko[28b], N. Smirnov[112], S. Yu. Smirnov[112], Y. Smirnov[112], L. N. Smirnova[113,r], O. Smirnova[97],
E. A. Smith[37], H. A. Smith[134], M. Smizanska[90], K. Smolek[141], A. Smykiewicz[85], A. A. Snesarev[111],
H. L. Snoek[120], I. M. Snyder[131], S. Snyder[29], R. Sobie[176,z], A. Soffer[161], A. Søgaard[50], F. Sohns[53],
C. A. Solans Sanchez[36], E. Yu. Soldatov[112], U. Soldevila[174], A. A. Solodkov[123], A. Soloshenko[80],
O. V. Solovyanov[123], V. Solovyev[137], P. Sommer[149], H. Son[170], A. Sonay[14], W. Song[143], W. Y. Song[168b],
A. Sopczak[141], A. L. Sopio[95], F. Sopkova[28b], S. Sottocornola[71a,71b], R. Soualah[67a,67c], A. M. Soukharev[122a,122b],
D. South[46], S. Spagnolo[68a,68b], M. Spalla[115], M. Spangenberg[178], F. Spanò[94], D. Sperlich[52],
T. M. Spieker[61a], G. Spigo[36], M. Spina[156], D. P. Spiteri[57], M. Spousta[142], A. Stabile[69a,69b],
B. L. Stamas[121], R. Stamen[61a], M. Stamenkovic[120], A. Stampekis[21], E. Stanecka[85], B. Stanislaus[134],
M. M. Stanitzki[46], M. Stankaityte[134], B. Stapf[120], E. A. Starchenko[123], G. H. Stark[145], J. Stark[58],
P. Staroba[140], P. Starovoitov[61a], S. Stärz[104], R. Staszewski[85], G. Stavropoulos[44], M. Stegler[46], P. Steinberg[29],
A. L. Steinhebel[131], B. Stelzer[152,168a], H. J. Stelzer[138], O. Stelzer-Chilton[168a], H. Stenzel[56], T. J. Stevenson[156],
G. A. Stewart[36], M. C. Stockton[36], G. Stoicea[27b], M. Stolarski[139a], S. Stonjek[115], A. Straessner[48],
J. Strandberg[154], S. Strandberg[45a,45b], M. Strauss[128], T. Strebler[102], P. Strizenec[28b], R. Ströhmer[177],
D. M. Strom[131], R. Stroynowski[42], A. Strubig[45a,45b], S. A. Stucci[29], B. Stugu[17], J. Stupak[128], N. A. Styles[46],
D. Su[153], W. Su[60c,60d,148], X. Su[60a], N. B. Suarez[138], V. V. Sulin[111], M. J. Sullivan[91], D. M. S. Sultan[54],
S. Sultansoy[4c], T. Sumida[86], S. Sun[106], X. Sun[101], C. J. E. Suster[157], M. R. Sutton[156], S. Suzuki[82],
M. Svatos[140], M. Swiatlowski[168a], S. P. Swift[2], T. Swirski[177], A. Sydorenko[100], I. Sykora[28a], M. Sykora[142],
T. Sykora[142], D. Ta[100], K. Tackmann[46,w], J. Taenzer[161], A. Taffard[171], R. Tafirout[168a], E. Tagiev[123],
R. H. M. Taibah[135], R. Takashima[87], K. Takeda[83], T. Takeshita[150], E. P. Takeva[50], Y. Takubo[82], M. Talby[102],
A. A. Talyshev[122a,122b], K. C. Tam[63b], N. M. Tamir[161], J. Tanaka[163], R. Tanaka[65], S. Tapia Araya[173],
S. Tapprogge[100], A. Tarek Abouelfadl Mohamed[107], S. Tarem[160], K. Tariq[60b], G. Tarna[27b,d], G. F. Tartarelli[69a],
P. Tas[142], M. Tasevsky[140], E. Tassi[41a,41b], G. Tateno[163], A. Tavares Delgado[139a], Y. Tayalati[35f], A. J. Taylor[50],
G. N. Taylor[105], W. Taylor[168b], H. Teagle[91], A. S. Tee[90], R. Teixeira De Lima[153], P. Teixeira-Dias[94],
H. Ten Kate[36], J. J. Teoh[120], K. Terashi[163], J. Terron[99], S. Terzo[14], M. Testa[51], R. J. Teuscher[167,z],
N. Themistokleous[50], T. Theveneaux-Pelzer[19], D. W. Thomas[94], J. P. Thomas[21], E. A. Thompson[46],
P. D. Thompson[21], E. Thomson[136], E. J. Thorpe[93], V. O. Tikhomirov[111,af], Yu. A. Tikhonov[122a,122b],
S. Timoshenko[112], P. Tipton[183], S. Tisserant[102], K. Todome[23a,23b], S. Todorova-Nova[142], S. Todt[48],
J. Tojo[88], S. Tokár[28a], K. Tokushuku[82], E. Tolley[127], R. Tombs[32], K. G. Tomiwa[33e], M. Tomoto[82,117],
L. Tompkins[153], P. Tornambe[103], E. Torrence[131], H. Torres[48], E. Torró Pastor[174], M. Toscani[30], C. Tosciri[134],
J. Toth[102,y], D. R. Tovey[149], A. Traeet[17], C. J. Treado[125], T. Trefzger[177], F. Tresoldi[156], A. Tricoli[29],
I. M. Trigger[168a], S. Trincaz-Duvoid[135], D. A. Trischuk[175], W. Trischuk[167], B. Trocmé[58], A. Trofymov[65],
C. Troncon[69a], F. Trovato[156], L. Truong[33c], M. Trzebinski[85], A. Trzupek[85], F. Tsai[46], P. V. Tsiareshka[108,ad],
A. Tsirigotis[162,u], V. Tsiskaridze[155], E. G. Tskhadadze[159a], M. Tsopoulou[162], I. I. Tsukerman[124], V. Tsulaia[18],
S. Tsuno[82], D. Tsybychev[155], Y. Tu[63b], A. Tudorache[27b], V. Tudorache[27b], A. N. Tuna[36], S. Turchikhin[80],
D. Turgeman[180], I. Turk Cakir[4b,s], R. J. Turner[21], R. Turra[69a], P. M. Tuts[39], S. Tzamarias[162], E. Tzovara[100],
K. Uchida[163], F. Ukegawa[169], G. Unal[36], M. Unal[11], A. Undrus[29], G. Unel[171], F. C. Ungaro[105],
Y. Unno[82], K. Uno[163], J. Urban[28b], P. Urquijo[105], G. Usai[8], Z. Uysal[12d], V. Vacek[141], B. Vachon[104],
K. O. H. Vadla[133], T. Vafeiadis[36], A. Vaidya[95], C. Valderanis[114], E. Valdes Santurio[45a,45b], M. Valente[168a],
S. Valentinetti[23a,23b], A. Valero[174], L. Valéry[46], R. A. Vallance[21], A. Vallier[36], J. A. Valls Ferrer[174],
T. R. Van Daalen[14], P. Van Gemmeren[6], S. Van Stroud[95], I. Van Vulpen[120], M. Vanadia[74a,74b], W. Vandelli[36],
M. Vandenbroucke[144], E. R. Vandewall[129], D. Vannicola[73a,73b], R. Vari[73a], E. W. Varnes[7], C. Varni[55a,55b],
T. Varol[158], D. Varouchas[65], K. E. Varvell[157], M. E. Vasile[27b], G. A. Vasquez[176], F. Vazeille[38],
D. Vazquez Furelos[14], T. Vazquez Schroeder[36], J. Veatch[53], V. Vecchio[101], M. J. Veen[120], L. M. Veloce[167],

F. Veloso[139a,139c], S. Veneziano[73a], A. Ventura[68a,68b], A. Verbytskyi[115], V. Vercesi[71a], M. Verducci[72a,72b], C. M. Vergel Infante[79], C. Vergis[24], W. Verkerke[120], A. T. Vermeulen[120], J. C. Vermeulen[120], C. Vernieri[153], P. J. Verschuuren[94], M. C. Vetterli[152,aj], N. Viaux Maira[146d], T. Vickey[149], O. E. Vickey Boeriu[149], G. H. A. Viehhauser[134], L. Vigani[61b], M. Villa[23a,23b], M. Villaplana Perez[174], E. M. Villhauer[50], E. Vilucchi[51], M. G. Vincter[34], G. S. Virdee[21], A. Vishwakarma[50], C. Vittori[23a,23b], I. Vivarelli[156], M. Vogel[182], P. Vokac[141], J. Von Ahnen[46], S. E. von Buddenbrock[33e], E. Von Toerne[24], V. Vorobel[142], K. Vorobev[112], M. Vos[174], J. H. Vossebeld[91], M. Vozak[101], N. Vranjes[16], M. Vranjes Milosavljevic[16], V. Vrba[141,*], M. Vreeswijk[120], N. K. Vu[102], R. Vuillermet[36], I. Vukotic[37], S. Wada[169], P. Wagner[24], W. Wagner[182], J. Wagner-Kuhr[114], S. Wahdan[182], H. Wahlberg[89], R. Wakasa[169], V. M. Walbrecht[115], J. Walder[143], R. Walker[114], S. D. Walker[94], W. Walkowiak[151], V. Wallangen[45a,45b], A. M. Wang[59], A. Z. Wang[181], C. Wang[60a], C. Wang[60c], H. Wang[18], H. Wang[3], J. Wang[63a], P. Wang[42], Q. Wang[128], R.-J. Wang[100], R. Wang[60a], R. Wang[6], S. M. Wang[158], W. T. Wang[60a], W. Wang[15c], W. X. Wang[60a], Y. Wang[60a], Z. Wang[106], C. Wanotayaroj[46], A. Warburton[104], C. P. Ward[32], R. J. Ward[21], N. Warrack[57], A. T. Watson[21], M. F. Watson[21], G. Watts[148], B. M. Waugh[95], A. F. Webb[11], C. Weber[29], M. S. Weber[20], S. A. Weber[34], S. M. Weber[61a], Y. Wei[134], A. R. Weidberg[134], J. Weingarten[47], M. Weirich[100], C. Weiser[52], P. S. Wells[36], T. Wenaus[29], B. Wendland[47], T. Wengler[36], S. Wenig[36], N. Wermes[24], M. Wessels[61a], T. D. Weston[20], K. Whalen[131], A. M. Wharton[90], A. S. White[106], A. White[8], M. J. White[1], D. Whiteson[171], B. W. Whitmore[90], W. Wiedenmann[181], C. Wiel[48], M. Wielers[143], N. Wieseotte[100], C. Wiglesworth[40], L. A. M. Wiik-Fuchs[52], H. G. Wilkens[36], L. J. Wilkins[94], D. M. Williams[39], H. H. Williams[136], S. Williams[32], S. Willocq[103], P. J. Windischhofer[134], I. Wingerter-Seez[5], E. Winkels[156], F. Winklmeier[131], B. T. Winter[52], M. Wittgen[153], M. Wobisch[96], A. Wolf[100], R. Wölker[134], J. Wollrath[52], M. W. Wolter[85], H. Wolters[139a,139c], V. W. S. Wong[175], A. F. Wongel[46], N. L. Woods[145], S. D. Worm[46], B. K. Wosiek[85], K. W. Woźniak[85], K. Wraight[57], S. L. Wu[181], X. Wu[54], Y. Wu[60a], J. Wuerzinger[134], T. R. Wyatt[101], B. M. Wynne[50], S. Xella[40], J. Xiang[63c], X. Xiao[106], X. Xie[60a], I. Xiotidis[156], D. Xu[15a], H. Xu[60a], H. Xu[60a], L. Xu[29], R. Xu[136], T. Xu[144], W. Xu[106], Y. Xu[15b], Z. Xu[60b], Z. Xu[153], B. Yabsley[157], S. Yacoob[33a], D. P. Yallup[95], N. Yamaguchi[88], Y. Yamaguchi[165], A. Yamamoto[82], M. Yamatani[163], T. Yamazaki[163], Y. Yamazaki[83], J. Yan[60c], Z. Yan[25], H. J. Yang[60c,60d], H. T. Yang[18], S. Yang[60a], T. Yang[63c], X. Yang[60a], X. Yang[60b,58], Y. Yang[163], Z. Yang[60a], W-M. Yao[18], Y. C. Yap[46], H. Ye[15c], J. Ye[42], S. Ye[29], I. Yeletskikh[80], M. R. Yexley[90], E. Yigitbasi[25], P. Yin[39], K. Yorita[179], K. Yoshihara[79], C. J. S. Young[36], C. Young[153], J. Yu[79], R. Yuan[60b,h], X. Yue[61a], M. Zaazoua[35f], B. Zabinski[85], G. Zacharis[10], E. Zaffaroni[54], J. Zahreddine[135], A. M. Zaitsev[123,ae], T. Zakareishvili[159b], N. Zakharchuk[34], S. Zambito[36], D. Zanzi[36], S. V. Zeißner[47], C. Zeitnitz[182], G. Zemaityte[134], J. C. Zeng[173], O. Zenin[123], T. Ženiš[28a], D. Zerwas[65], M. Zgubič[134], B. Zhang[15c], D. F. Zhang[15b], G. Zhang[15b], J. Zhang[6], K. Zhang[15a], L. Zhang[15c], L. Zhang[60a], M. Zhang[173], R. Zhang[181], S. Zhang[106], X. Zhang[60c], X. Zhang[60b], Y. Zhang[15a,15d], Z. Zhang[63a], Z. Zhang[65], P. Zhao[49], Y. Zhao[145], Z. Zhao[60a], A. Zhemchugov[80], Z. Zheng[106], D. Zhong[173], B. Zhou[106], C. Zhou[181], H. Zhou[7], M. Zhou[155], N. Zhou[60c], Y. Zhou[7], C. G. Zhu[60b], C. Zhu[15a,15d], H. L. Zhu[60a], H. Zhu[15a], J. Zhu[106], Y. Zhu[60a], X. Zhuang[15a], K. Zhukov[111], V. Zhulanov[122a,122b], D. Zieminska[66], N. I. Zimine[80], S. Zimmermann[52,*], Z. Zinonos[115], M. Ziolkowski[151], L. Živković[16], G. Zobernig[181], A. Zoccoli[23a,23b], K. Zoch[53], T. G. Zorbas[149], R. Zou[37], L. Zwalinski[36]

[1] Department of Physics, University of Adelaide, Adelaide, Australia

[2] Physics Department, SUNY Albany, Albany, NY, USA

[3] Department of Physics, University of Alberta, Edmonton, AB, Canada

[4] (a)Department of Physics, Ankara University, Ankara, Turkey; (b)Istanbul Aydin University, Application and Research Center for Advanced Studies, Istanbul, Turkey; (c)Division of Physics, TOBB University of Economics and Technology, Ankara, Turkey

[5] LAPP, Université Grenoble Alpes, Université Savoie Mont Blanc, CNRS/IN2P3, Annecy, France

[6] High Energy Physics Division, Argonne National Laboratory, Argonne, IL, USA

[7] Department of Physics, University of Arizona, Tucson, AZ, USA

[8] Department of Physics, University of Texas at Arlington, Arlington, TX, USA

[9] Physics Department, National and Kapodistrian University of Athens, Athens, Greece

[10] Physics Department, National Technical University of Athens, Zografou, Greece

[11] Department of Physics, University of Texas at Austin, Austin, TX, USA

12 (a)Bahcesehir University, Faculty of Engineering and Natural Sciences, Istanbul, Turkey; (b)Istanbul Bilgi University, Faculty of Engineering and Natural Sciences, Istanbul, Turkey; (c)Department of Physics, Bogazici University, Istanbul, Turkey; (d)Department of Physics Engineering, Gaziantep University, Gaziantep, Turkey

13 Institute of Physics, Azerbaijan Academy of Sciences, Baku, Azerbaijan

14 Institut de Física d'Altes Energies (IFAE), Barcelona Institute of Science and Technology, Barcelona, Spain

15 (a)Institute of High Energy Physics, Chinese Academy of Sciences, Beijing, China; (b)Physics Department, Tsinghua University, Beijing, China; (c)Department of Physics, Nanjing University, Nanjing, China; (d)University of Chinese Academy of Science (UCAS), Beijing, China

16 Institute of Physics, University of Belgrade, Belgrade, Serbia

17 Department for Physics and Technology, University of Bergen, Bergen, Norway

18 Physics Division, Lawrence Berkeley National Laboratory and University of California, Berkeley, CA, USA

19 Institut für Physik, Humboldt Universität zu Berlin, Berlin, Germany

20 Albert Einstein Center for Fundamental Physics and Laboratory for High Energy Physics, University of Bern, Bern, Switzerland

21 School of Physics and Astronomy, University of Birmingham, Birmingham, UK

22 (a)Facultad de Ciencias y Centro de Investigaciónes, Universidad Antonio Nariño, Bogotá, Colombia; (b)Departamento de Física, Universidad Nacional de Colombia, Bogotá, Colombia, Colombia

23 (a)Dipartimento di Fisica, INFN Bologna and Universita' di Bologna, Bologna, Italy; (b)INFN Sezione di Bologna, Bologna, Italy

24 Physikalisches Institut, Universität Bonn, Bonn, Germany

25 Department of Physics, Boston University, Boston, MA, USA

26 Department of Physics, Brandeis University, Waltham, MA, USA

27 (a)Transilvania University of Brasov, Brasov, Romania; (b)Horia Hulubei National Institute of Physics and Nuclear Engineering, Bucharest, Romania; (c)Department of Physics, Alexandru Ioan Cuza University of Iasi, Iasi, Romania; (d)Physics Department, National Institute for Research and Development of Isotopic and Molecular Technologies, Cluj-Napoca, Romania; (e)University Politehnica Bucharest, Bucharest, Romania; (f)West University in Timisoara, Timisoara, Romania

28 (a)Faculty of Mathematics, Physics and Informatics, Comenius University, Bratislava, Slovakia; (b)Department of Subnuclear Physics, Institute of Experimental Physics of the Slovak Academy of Sciences, Kosice, Slovak Republic

29 Physics Department, Brookhaven National Laboratory, Upton, NY, USA

30 Departamento de Física, Universidad de Buenos Aires, Buenos Aires, Argentina

31 California State University, Long Beach, CA, United States of America

32 Cavendish Laboratory, University of Cambridge, Cambridge, UK

33 (a)Department of Physics, University of Cape Town, Cape Town, South Africa; (b)iThemba Labs, Johannesburg, Western Cape, South Africa; (c)Department of Mechanical Engineering Science, University of Johannesburg, Johannesburg, South Africa; (d)University of South Africa, Department of Physics, Pretoria, South Africa; (e)School of Physics, University of the Witwatersrand, Johannesburg, South Africa

34 Department of Physics, Carleton University, Ottawa, ON, Canada

35 (a)Faculté des Sciences Ain Chock, Réseau Universitaire de Physique des Hautes Energies-Université Hassan II, Casablanca, Morocco; (b)Faculté des Sciences, Université Ibn-Tofail, Kenitra, Morocco; (c)Faculté des Sciences Semlalia, Université Cadi Ayyad, LPHEA-Marrakech, Marrakesh, Morocco; (d)Moroccan Foundation for Advanced Science Innovation and Research (MAScIR), Rabat, Morocco; (e)LPMR, Faculté des Sciences, Université Mohamed Premier, Oujda, Morocco; (f)Faculté des sciences, Université Mohammed V, Rabat, Morocco

36 CERN, Geneva, Switzerland

37 Enrico Fermi Institute, University of Chicago, Chicago, IL, USA

38 LPC, Université Clermont Auvergne, CNRS/IN2P3, Clermont-Ferrand, France

39 Nevis Laboratory, Columbia University, Irvington, NY, USA

40 Niels Bohr Institute, University of Copenhagen, Copenhagen, Denmark

41 (a)Dipartimento di Fisica, Università della Calabria, Rende, Italy; (b)INFN Gruppo Collegato di Cosenza, Laboratori Nazionali di Frascati, Italy

42 Physics Department, Southern Methodist University, Dallas, TX, USA

43 Physics Department, University of Texas at Dallas, Richardson, TX, USA

44 National Centre for Scientific Research "Demokritos", Agia Paraskevi, Greece

45 (a)Department of Physics, Stockholm University, Stockholm, Sweden; (b)Oskar Klein Centre, Stockholm, Sweden

46 Deutsches Elektronen-Synchrotron DESY, Hamburg and Zeuthen, Germany

47 Lehrstuhl für Experimentelle Physik IV, Technische Universität Dortmund, Dortmund, Germany

48 Institut für Kern- und Teilchenphysik, Technische Universität Dresden, Dresden, Germany

49 Department of Physics, Duke University, Durham, NC, USA

50 SUPA-School of Physics and Astronomy, University of Edinburgh, Edinburgh, UK

51 INFN e Laboratori Nazionali di Frascati, Frascati, Italy

52 Physikalisches Institut, Albert-Ludwigs-Universität Freiburg, Freiburg, Germany

53 II. Physikalisches Institut, Georg-August-Universität Göttingen, Göttingen, Germany

54 Département de Physique Nucléaire et Corpusculaire, Université de Genève, Geneva, Switzerland

55 (a)Dipartimento di Fisica, Università di Genova, Genoa, Italy; (b)INFN Sezione di Genova, Genoa, Italy

56 II. Physikalisches Institut, Justus-Liebig-Universität Giessen, Giessen, Germany

57 SUPA-School of Physics and Astronomy, University of Glasgow, Glasgow, UK

58 LPSC, Université Grenoble Alpes, CNRS/IN2P3, Grenoble INP, Grenoble, France

59 Laboratory for Particle Physics and Cosmology, Harvard University, Cambridge, MA, USA

60 (a)Department of Modern Physics and State Key Laboratory of Particle Detection and Electronics, University of Science and Technology of China, Hefei, China; (b)Institute of Frontier and Interdisciplinary Science and Key Laboratory of Particle Physics and Particle Irradiation (MOE), Shandong University, Qingdao, China; (c)School of Physics and Astronomy, Shanghai Jiao Tong University, Key Laboratory for Particle Astrophysics and Cosmology (MOE), SKLPPC, Shanghai, China; (d)Tsung-Dao Lee Institute, Shanghai, China

61 (a)Kirchhoff-Institut für Physik, Ruprecht-Karls-Universität Heidelberg, Heidelberg, Germany; (b)Physikalisches Institut, Ruprecht-Karls-Universität Heidelberg, Heidelberg, Germany

62 Faculty of Applied Information Science, Hiroshima Institute of Technology, Hiroshima, Japan

63 (a)Department of Physics, Chinese University of Hong Kong, Shatin N.T., Hong Kong, China; (b)Department of Physics, University of Hong Kong, Pok Fu Lam, Hong Kong; (c)Department of Physics and Institute for Advanced Study, Hong Kong University of Science and Technology, Clear Water Bay, Kowloon, Hong Kong, China

64 Department of Physics, National Tsing Hua University, Hsinchu, Taiwan

65 IJCLab, Université Paris-Saclay, CNRS/IN2P3, 91405, Orsay, France

66 Department of Physics, Indiana University, Bloomington, IN, USA

67 (a)INFN Gruppo Collegato di Udine, Sezione di Trieste, Udine, Italy; (b)ICTP, Trieste, Italy; (c)Dipartimento Politecnico di Ingegneria e Architettura, Università di Udine, Udine, Italy

68 (a)INFN Sezione di Lecce, Lecce, Italy; (b)Dipartimento di Matematica e Fisica, Università del Salento, Lecce, Italy

69 (a)INFN Sezione di Milano, Milan, Italy; (b)Dipartimento di Fisica, Università di Milano, Milan, Italy

70 (a)INFN Sezione di Napoli, Naples, Italy; (b)Dipartimento di Fisica, Università di Napoli, Naples, Italy

71 (a)INFN Sezione di Pavia, Pavia, Italy; (b)Dipartimento di Fisica, Università di Pavia, Pavia, Italy

72 (a)INFN Sezione di Pisa, Pisa, Italy; (b)Dipartimento di Fisica E. Fermi, Università di Pisa, Pisa, Italy

73 (a)INFN Sezione di Roma, Rome, Italy; (b)Dipartimento di Fisica, Sapienza Università di Roma, Rome, Italy

74 (a)INFN Sezione di Roma Tor Vergata, Rome, Italy; (b)Dipartimento di Fisica, Università di Roma Tor Vergata, Rom, Italy

75 (a)INFN Sezione di Roma Tre, Rome, Italy; (b)Dipartimento di Matematica e Fisica, Università Roma Tre, Rome, Italy

76 (a)INFN-TIFPA, Trento, Italy; (b)Università degli Studi di Trento, Trento, Italy

77 Institut für Astro- und Teilchenphysik, Leopold-Franzens-Universität, Innsbruck, Austria

78 University of Iowa, Iowa City, IA, USA

79 Department of Physics and Astronomy, Iowa State University, Ames, IA, USA

80 Joint Institute for Nuclear Research, Dubna, Russia

81 (a)Departamento de Engenharia Elétrica, Universidade Federal de Juiz de Fora (UFJF), Juiz de Fora, Brazil; (b)Universidade Federal do Rio De Janeiro COPPE/EE/IF, Rio de Janeiro, Brazil; (c)Instituto de Física, Universidade de São Paulo, São Paulo, Brazil

82 KEK, High Energy Accelerator Research Organization, Tsukuba, Japan

83 Graduate School of Science, Kobe University, Kobe, Japan

84 (a)AGH University of Science and Technology, Faculty of Physics and Applied Computer Science, Kraków, Poland; (b)Marian Smoluchowski Institute of Physics, Jagiellonian University, Kraków, Poland

85 Institute of Nuclear Physics Polish Academy of Sciences, Kraków, Poland

[86] Faculty of Science, Kyoto University, Kyoto, Japan

[87] Kyoto University of Education, Kyoto, Japan

[88] Research Center for Advanced Particle Physics and Department of Physics, Kyushu University, Fukuoka , Japan

[89] Instituto de Física La Plata, Universidad Nacional de La Plata and CONICET, La Plata, Argentina

[90] Physics Department, Lancaster University, Lancaster, UK

[91] Oliver Lodge Laboratory, University of Liverpool, Liverpool, UK

[92] Department of Experimental Particle Physics, Jožef Stefan Institute and Department of Physics, University of Ljubljana, Ljubljana, Slovenia

[93] School of Physics and Astronomy, Queen Mary University of London, London, UK

[94] Department of Physics, Royal Holloway University of London, Egham, UK

[95] Department of Physics and Astronomy, University College London, London, UK

[96] Louisiana Tech University, Ruston, LA, USA

[97] Fysiska institutionen, Lunds universitet, Lund, Sweden

[98] Centre de Calcul de l'Institut National de Physique Nucléaire et de Physique des Particules (IN2P3), Villeurbanne, France

[99] Departamento de Física Teorica C-15 and CIAFF, Universidad Autónoma de Madrid, Madrid, Spain

[100] Institut für Physik, Universität Mainz, Mainz, Germany

[101] School of Physics and Astronomy, University of Manchester, Manchester, UK

[102] CPPM, Aix-Marseille Université, CNRS/IN2P3, Marseille, France

[103] Department of Physics, University of Massachusetts, Amherst, MA, USA

[104] Department of Physics, McGill University, Montreal, QC, Canada

[105] School of Physics, University of Melbourne, Victoria, Australia

[106] Department of Physics, University of Michigan, Ann Arbor, MI, USA

[107] Department of Physics and Astronomy, Michigan State University, East Lansing, MI, USA

[108] B.I. Stepanov Institute of Physics, National Academy of Sciences of Belarus, Minsk, Belarus

[109] Research Institute for Nuclear Problems of Byelorussian State University, Minsk, Belarus

[110] Group of Particle Physics, University of Montreal, Montreal, QC, Canada

[111] P.N. Lebedev Physical Institute of the Russian Academy of Sciences, Moscow, Russia

[112] National Research Nuclear University MEPhI, Moscow, Russia

[113] D.V. Skobeltsyn Institute of Nuclear Physics, M.V. Lomonosov Moscow State University, Moscow, Russia

[114] Fakultät für Physik, Ludwig-Maximilians-Universität München, Munich, Germany

[115] Max-Planck-Institut für Physik (Werner-Heisenberg-Institut), Munich, Germany

[116] Nagasaki Institute of Applied Science, Nagasaki, Japan

[117] Graduate School of Science and Kobayashi-Maskawa Institute, Nagoya University, Nagoya, Japan

[118] Department of Physics and Astronomy, University of New Mexico, Albuquerque, NM, USA

[119] Institute for Mathematics, Astrophysics and Particle Physics, Radboud University/Nikhef, Nijmegen, The Netherlands

[120] Nikhef National Institute for Subatomic Physics and University of Amsterdam, Amsterdam, The Netherlands

[121] Department of Physics, Northern Illinois University, DeKalb, IL, USA

[122] (a)Budker Institute of Nuclear Physics and NSU, SB RAS, Novosibirsk, Russia; (b)Novosibirsk State University Novosibirsk, Novosibirsk, Russia

[123] Institute for High Energy Physics of the National Research Centre Kurchatov Institute, Protvino, Russia

[124] Institute for Theoretical and Experimental Physics named by A.I. Alikhanov of National Research Centre "Kurchatov Institute", Moscow, Russia

[125] Department of Physics, New York University, New York, NY, USA

[126] Ochanomizu University, Otsuka, Bunkyo-ku, Tokyo, Japan

[127] Ohio State University, Columbus, OH, USA

[128] Homer L. Dodge Department of Physics and Astronomy, University of Oklahoma, Norman, OK, USA

[129] Department of Physics, Oklahoma State University, Stillwater, OK, USA

[130] Palacký University, RCPTM, Joint Laboratory of Optics, Olomouc, Czech Republic

[131] Institute for Fundamental Science, University of Oregon, Eugene, OR, USA

[132] Graduate School of Science, Osaka University, Osaka, Japan

[133] Department of Physics, University of Oslo, Oslo, Norway

[134] Department of Physics, Oxford University, Oxford, UK

[135] LPNHE, Sorbonne Université, Université de Paris, CNRS/IN2P3, Paris, France

[136] Department of Physics, University of Pennsylvania, Philadelphia, PA, USA

[137] Konstantinov Nuclear Physics Institute of National Research Centre "Kurchatov Institute", PNPI, St. Petersburg, Russia

[138] Department of Physics and Astronomy, University of Pittsburgh, Pittsburgh, PA, USA

[139] (a)Laboratório de Instrumentação e Física Experimental de Partículas-LIP, Lisbon, Portugal; (b)Departamento de Física, Faculdade de Ciências, Universidade de Lisboa, Lisbon, Portugal; (c)Departamento de Física, Universidade de Coimbra, Coimbra, Portugal; (d)Centro de Física Nuclear da Universidade de Lisboa, Lisbon, Portugal; (e)Departamento de Física, Universidade do Minho, Braga, Portugal; (f)Departamento de Física Teórica y del Cosmos, Universidad de Granada, Granada, Spain; (g)Dep Física and CEFITEC of Faculdade de Ciências e Tecnologia, Universidade Nova de Lisboa, Caparica, Spain; (h)Instituto Superior Técnico, Universidade de Lisboa, Lisbon, Portugal

[140] Institute of Physics of the Czech Academy of Sciences, Prague, Czech Republic

[141] Czech Technical University in Prague, Prague, Czech Republic

[142] Charles University, Faculty of Mathematics and Physics, Prague, Czech Republic

[143] Particle Physics Department, Rutherford Appleton Laboratory, Didcot, UK

[144] IRFU, CEA, Université Paris-Saclay, Gif-sur-Yvette, France

[145] Santa Cruz Institute for Particle Physics, University of California Santa Cruz, Santa Cruz, CA, USA

[146] (a)Departamento de Física, Pontificia Universidad Católica de Chile, Santiago, Chile; (b)Universidad Andres Bello, Department of Physics, Santiago, Chile; (c)Instituto de Alta Investigación, Universidad de Tarapacá, Arica, Chile; (d)Departamento de Física, Universidad Técnica Federico Santa María, Valparaiso, Chile

[147] Universidade Federal de São João del Rei (UFSJ), São João del Rei, Brazil

[148] Department of Physics, University of Washington, Seattle, WA, USA

[149] Department of Physics and Astronomy, University of Sheffield, Sheffield, UK

[150] Department of Physics, Shinshu University, Nagano, Japan

[151] Department Physik, Universität Siegen, Siegen, Germany

[152] Department of Physics, Simon Fraser University, Burnaby, BC, Canada

[153] SLAC National Accelerator Laboratory, Stanford, CA, USA

[154] Physics Department, Royal Institute of Technology, Stockholm, Sweden

[155] Departments of Physics and Astronomy, Stony Brook University, Stony Brook, NY, USA

[156] Department of Physics and Astronomy, University of Sussex, Brighton, UK

[157] School of Physics, University of Sydney, Sydney, Australia

[158] Institute of Physics, Academia Sinica, Taipei, Taiwan

[159] (a)E. Andronikashvili Institute of Physics, Iv. Javakhishvili Tbilisi State University, Tbilisi, Georgia; (b)High Energy Physics Institute, Tbilisi State University, Tbilisi, Georgia

[160] Department of Physics, Technion, Israel Institute of Technology, Haifa, Israel

[161] Raymond and Beverly Sackler School of Physics and Astronomy, Tel Aviv University, Tel Aviv, Israel

[162] Department of Physics, Aristotle University of Thessaloniki, Thessaloniki, Greece

[163] International Center for Elementary Particle Physics and Department of Physics, University of Tokyo, Tokyo, Japan

[164] Graduate School of Science and Technology, Tokyo Metropolitan University, Tokyo, Japan

[165] Department of Physics, Tokyo Institute of Technology, Tokyo, Japan

[166] Tomsk State University, Tomsk, Russia

[167] Department of Physics, University of Toronto, Toronto, ON, Canada

[168] (a)TRIUMF, Vancouver, BC, Canada; (b)Department of Physics and Astronomy, York University, Toronto, ON, Canada

[169] Division of Physics and Tomonaga Center for the History of the Universe, Faculty of Pure and Applied Sciences, University of Tsukuba, Tsukuba, Japan

[170] Department of Physics and Astronomy, Tufts University, Medford, MA, USA

[171] Department of Physics and Astronomy, University of California Irvine, Irvine, CA, USA

[172] Department of Physics and Astronomy, University of Uppsala, Uppsala, Sweden

[173] Department of Physics, University of Illinois, Urbana, IL, USA

[174] Instituto de Física Corpuscular (IFIC), Centro Mixto Universidad de Valencia-CSIC, Valencia, Spain

[175] Department of Physics, University of British Columbia, Vancouver, BC, Canada

[176] Department of Physics and Astronomy, University of Victoria, Victoria, BC, Canada

[177] Fakultät für Physik und Astronomie, Julius-Maximilians-Universität Würzburg, Würzburg, Germany

[178] Department of Physics, University of Warwick, Coventry, UK

[179] Waseda University, Tokyo, Japan

[180] Department of Particle Physics and Astrophysics, Weizmann Institute of Science, Rehovot, Israel

[181] Department of Physics, University of Wisconsin, Madison, WI, USA

[182] Fakultät für Mathematik und Naturwissenschaften, Fachgruppe Physik, Bergische Universität Wuppertal, Wuppertal, Germany

[183] Department of Physics, Yale University, New Haven, CT, USA

[a] Also at Borough of Manhattan Community College, City University of New York, New York, NY, USA

[b] Centro Studi e Ricerche Enrico Fermi, Rome, Italy

[c] CERN, Geneva, Switzerland

[d] Also at CPPM, Aix-Marseille Université, CNRS/IN2P3, Marseille, France

[e] Also at Département de Physique Nucléaire et Corpusculaire, Université de Genève, Geneva, Switzerland

[f] Departament de Fisica de la Universitat Autonoma de Barcelona, Barcelona, Spain

[g] Also at Department of Financial and Management Engineering, University of the Aegean, Chios, Greece

[h] Also at Department of Physics and Astronomy, Michigan State University, East Lansing, MI, USA

[i] Also at Department of Physics and Astronomy, University of Louisville, Louisville, KY, USA

[j] Also at Department of Physics, Ben Gurion University of the Negev, Beer Sheva, Israel

[k] Also at Department of Physics, California State University, East Bay, USA

[l] Also at Department of Physics, California State University, Fresno, USA

[m] Also at Department of Physics, California State University, Sacramento, USA

[n] Also at Department of Physics, King's College London, London, UK

[o] Also at Department of Physics, St. Petersburg State Polytechnical University, St. Petersburg, Russia

[p] Also at Department of Physics, University of Fribourg, Fribourg, Switzerland

[q] Also at Dipartimento di Matematica, Informatica e Fisica, Università di Udine, Udine, Italy

[r] Also at Faculty of Physics, M.V. Lomonosov Moscow State University, Moscow, Russia

[s] Also at Giresun University, Faculty of Engineering, Giresun, Turkey

[t] Also at Graduate School of Science, Osaka University, Osaka, Japan

[u] Hellenic Open University, Patras, Greece

[v] Also at Institucio Catalana de Recerca i Estudis Avancats, ICREA, Barcelona, Spain

[w] Also at Institut für Experimentalphysik, Universität Hamburg, Hamburg, Germany

[x] Institute for Nuclear Research and Nuclear Energy (INRNE) of the Bulgarian Academy of Sciences, Sofia, Bulgaria

[y] Also at Institute for Particle and Nuclear Physics, Wigner Research Centre for Physics, Budapest, Hungary

[z] Institute of Particle Physics (IPP), Montreal, Canada

[aa] Also at Institute of Physics, Azerbaijan Academy of Sciences, Baku, Azerbaijan

[ab] Also at Instituto de Fisica Teorica, IFT-UAM/CSIC, Madrid, Spain

[ac] Also at Department of Physics, Istanbul University, Istanbul, Turkey

[ad] Joint Institute for Nuclear Research, Dubna, Russia

[ae] Moscow Institute of Physics and Technology State University, Dolgoprudny, Russia

[af] National Research Nuclear University MEPhI, Moscow, Russia

[ag] Also at Physics Department, An-Najah National University, Nablus, Palestine

[ah] Also at Physikalisches Institut, Albert-Ludwigs-Universität Freiburg, Freiburg, Germany

[ai] The City College of New York, New York, NY, USA

[aj] TRIUMF, Vancouver, BC, Canada

[ak] Universita di Napoli Parthenope, Naples, Italy

[al] University of Chinese Academy of Sciences (UCAS), Beijing, China

[*] Deceased